ÉCOLE DE TECHNOLOGIE SUPÉRIEURE
UNIVERSITÉ DU QUÉBEC

THESIS PRESENTED TO
ÉCOLE DE TECHNOLOGIE SUPÉRIEURE

IN PARTIAL FULFILLMENT OF REQUIREMENTS FOR
THE DEGREE OF DOCTOR OF PHILOSOPHY
Ph.D.

BY
Bahaa BALOUT

CENTRIFUGAL CASTING OF ZA8 ZINC ALLOY AND COMPOSITE A356/SiC: STUDY AND MODELING OF PHASES' AND PARTICLES' SEGREGATION

MONTREAL, MAY 6 2010

BOARD OF EXAMINERS

THIS THESIS HAS BEEN EVALUATED

BY THE FOLLOWING BOARD OF EXAMINERS

Mr. Victor Songmene, Thesis Supervisor
Département de génie mécanique à l'École de technologie supérieure

Mr. Robert Hausler, President of the Board of Examiners
Département de génie mécanique à l'École de technologie supérieure

Mr. Vladimir Brailovski, Membre of the Board of Examiners
Département de génie mécanique à l'École de technologie supérieure

Mr. Fawzy-H Samuel, External Examiner
Département des sciences appliquées à l'Université du Québec à Chicoutimi

THIS THESIS WAS PRESENTED AND DEFENDED

BEFORE A BOARD OF EXAMINERS AND PUBLIC

MAY 03, 2010

AT ÉCOLE DE TECHNOLOGIE SUPÉRIEURE

ACKNOWLEDGMENTS

I would first like to profoundly thank my research director, Professor Victor Songmene, for his support during my project. I also thank Professor Jacques Masounave.

I would like also to sincerely thank the staff of the College of Saint-Laurent, particularly teachers Jacek Litwin and Patrick Lesourd, for their support during the experiments.

I thank cordially Mr. Alexandre Vigneault, "Chargé de l'application technologique et informatique" at "École de technologie supérieure," for his cooperation during my research. I also wish to thank technicians Jean-Guy Gagnon and Radu Romanica, who were able to support my work.

I express my acknowledgments also to all teachers and employees of "École de technologie supérieure" for their contributions to keeping this university prosperous and bright.

I would like to express my gratitude to the FQRNT (Fonds Québécois de la Recherche sur la Nature et les Technologies) and to the CQRDA (Centre Québecois de Recherche et de Développement de l'Aluminium) for the interest they manifested toward my work, and for their financial support.

Finally, I express my deep feelings to all my friends, Natasha, my family, and God for giving me the will to do this work.

MISE EN FORME PAR CENTRIFUGATION DE L'ALLIAGE DU ZINC ZA8 ET DU COMPOSITE A356/SiC : ÉTUDE ET MODÉLISATION DE LA SÉGRÉGATION DES PHASES ET DES PARTICULES

Bahaa BALOUT

RÉSUMÉ

La centrifugation est une technologie de mise en forme qui permet de fabriquer des pièces cylindriques et graduées, c'est-à-dire ne possédant pas les mêmes propriétés mécaniques à travers la section. Le besoin de matériaux de bonne qualité avec des propriétés mécaniques spécifiques nous incite à utiliser cette technologie afin de fabriquer plusieurs types des matériaux comme les alliages du zinc et les composites à matrices métalliques gradués renforcés par des particules dures et résistantes à l'usure.

Le but de cette étude est de modéliser la macroségrégation de l'eutectique et les vitesses des fronts de solidification, pendant le moulage par centrifugation de l'alliage du zinc-aluminium ZA8. Cette étude permettra d'améliorer la qualité de la pièce et d'augmenter sa résistance et fiabilité en service. D'ailleur, la ségrégation des particules à travers la matrice pendant le moulage par centrifugation d'un composite à matrice d'aluminium renfrocé par des particules de carbure de silicium (A356/SiC) sera étudiée. Le taux de refroidissement, le déplacement et la ségrégation des particules à travers la section seront modélisés en discrétizant la loi de Stokes dans le temps afin de tenir compte de la variation du rayon de centrifugation et de la viscosité pendant le processus de refroidissement. Cette étude permettra de contrôler le degré de graduation des particules à travers la section afin d'améliorer les propriétés et la résistance à l'usure du composite. Ce composite peut être utilisé pour des applications où le frottement est élevé et la charge est critique (renforts de parties du moteur à explosion, des cylindres de systèmes pneumatiques).

Les résultats obtenus montrent que la zone de la macroségrégation maximale de l'eutectique à travers la section correspond à la zone du dernier point de solidification. La macroségrégataion de l'eutectique produite pendant le moulage par centrifugation d'une pièce à paroi mince est une ségrégation normale. Elle varie en fonction de la vitesse de solidification et du rapport entre les vitesses des fronts de solidifictaion. D'autre part, il a été constaté que la position et la fraction volumique des particules sur la surface interne/externe et à travers la section du composite changent selon que la viscosité du métal liquide et le rayon de centrifugation utilisés sont constants ou variables. La modélisation de la ségrégation des particules en discrétisant la vitesse des particules dans le temps, conduit à des résultats plus proches de ceux obtenus expérimentalement.

Mots-clés: moulage par centrifugation, composite, macroségrégation, solidification.

CENTRIFUGAL CASTING OF ZA8 ZINC ALLOY AND COMPOSITE A356/SiC: STUDY AND MODELING OF PHASES' AND PARTICLES' SEGREGATION

Bahaa BALOUT

ABSTRACT

Centrifugation is a casting technology that allows the production of cylindrical and graduated parts with different mechanical properties through the section. The need for materials with good quality and specific mechanical properties has been driven this technology in order to produce different types of materials such as zinc alloys and graduated metal matrix composites reinforced by hard and wear resistant particles.

The goal of this research project is to study and model the eutectic macrosegregation, the solidification speed, and the speeds of solidification fronts during centrifugal casting of ZA8 zinc-aluminum alloy in order to improve the part quality and increase its strength and field reliability. Moreover, the segregation of the particles during centrifugal casting of an aluminum matrix composite reinforced by silicon carbide particles (A356/SiC) is also studied to improve and control the graduation of the parts. The cooling rate, the speed, acceleration/deceleration, displacement, and segregation of the particles across the section will be modeled by discretization of Stokes' law in time in order to take into consideration the change in the centrifugal radius and melt viscosity during cooling process. This study will allow the control of the graduation degree of particles across the section in order to improve the properties and wear resistance of the composite. This composite can be used in systems where friction is critical and load is high (reinforcements of parts for the cylinders of pneumatic systems).

The results show that the maximum macrosegregation zone of the eutectic across the casting section corresponds to the last point of solidification. The eutectic macrosegregation produced during centrifugal casting of thin walled part is a normal segregation which varies depending on the solidification speed and the ratio between the speeds of solidification fronts. On the other hand, it was found that the position and volume fraction of the particles on the outer/inner casting surface and across the section varies whether the viscosity of the liquid metal used and the centrifugal radius are considered constant or variable during the modeling. Modeling the particles' segregation while discretizing, in time, the particles' velocities gives more consistent results compared to those obtained experimentally.

Key-words: centrifugal casting, composite, macrosegregation, solidification.

TABLE OF CONTENTS

LISTE OF TABLES

Page

LISTE OF FIGURES

Page

LISTE OF ABBREVIATIONS AND ACRONYMS

m	Mass, kg
ω	Angular velocity, rad.s^{-1}
γ	Acceleration, mm.s^{-2}
γ_{SL}	Solid/liquid interfacial energy, N/m
γ_{LV}	Liquid/vapour interfacial energy, N/m
γ_{SV}	Solid/vapour interfacial energy, N/m
F_t	Force of surface tension, N
θ	Contact angle, deg
W	Thermodynamic work of adhesion, J/m^2
α	Coefficient
d_p	Particle diameter, mm
ρ_P	Particle density, kg/m^3
ρ_l	Liquid density, kg/m^3
ρ_c	Composite density, kg/m^3
ρ_{aire}	Air density, kg/m^3
η	Metal viscosity, Pa.s
η_c	Apparent viscosity, Pa.s
v_p	Particle velocity, mm.s^{-1}
e	Thickness, mm
L_i	Length of volume element, mm
S	Distance displaced by the particle, mm

V_i	Sub-volume, mm^3
V_s	Solidification speed, mm/s
V_p	Volume fraction of particles, %V
Q	Activation energy of viscous flow, $KJ.mol^{-1}$
R_g	Constant of perfect gases, $J.K^{-1}.mol^{-1}$
A	Constant
Δt	Time increment, s
p	Particle
c	Composite
g	Gravitationnel acceleration, mm/s^2
t_i	Centrifugation time, s
t_r	Cooling time, s
t_s	Solidification time, s
C	Specific heat, $J\cdot kg^{-1}\cdot K^{-1}$
H_f	Latent heat of fusion, J/kg
F_{net}	Net force on the particle, N
F_ω	Centrifugal force, N
F_η	Viscous force, N
F_R	Repulsive force, N
T_P	Temperature of superheated metal, K
T_s	Solidus Temperature, K
T_L	Liquidus Temperature, K
$R_{M,i}$	Inner composite radius, mm

$R_{M,e}$	Outer composite radius, mm
$R_{m,i}$	Inner mold radius, mm
$d_{m,e}$	Outer mold diameter, mm
$T_{m,ti}^{Rj}$	Temperature of liquid metal as a function of time and position, K
$fv_{V_i}^{t_0}$	Volume fraction of particles corresponding to the volume V_i at time $t = 0$, %V
$fv_{\rightarrow V_i}^{ts}$	Volume fraction of particles entering the sub volume V_i at time ts, before the solidification begins on this surface, %V
$fv_{V_i\rightarrow}^{ts}$	Volume fraction of particles leaving the volume V_i at time ts, before the solidification begins on this surface, %V
$fv_{V_i\left(Rj-\Delta R/2<R_{ini.}^{t=0}+S_{(ti)tot}^{Rj}<R_j\right)}^{ts}$	Volume fraction of particles moved to a sub volume V_i located between R_j and R_j-$\Delta R/2$ before the solidification begins, %V
$fv_{V_i\left(R_j<R_{ini.}^{t=0}+S_{(ti)tot}^{Rj}<R_j+\Delta R/2\right)}^{ts}$	Volume fraction of particles moved to a sub volume V_i located between R_j and R_j+$\Delta R/2$ before the solidification begins, %V
$\Delta fv_{V_{i+1}(fv_{(V_i+1)}>52\%)}^{ts}$	Excess of the particle volume fraction of the sub volume V_{i+1}, %V
ΔR	Radius increment, mm
$R_{(fv)_j^{t_s}\big\vert_{j=0}^{n}}$	Final position of particles volume fraction before the solidification starts, mm
$R_{(fv)_j^{t_0}\big\vert_{j=0}^{n}}$	Initial position of particles volume fraction, mm
$S_{(fv)_{R_j}}^{t_i}$	Displacement of the particle volume fraction located at an initial position (R_j) for a given time of centrifugation (t_i), before the solidification begins, mm
$v_{t_i}^{R_j}$	Velocity of particle located at an initial position (R_j) for a given time of centrifugation (t_i), mm/s

$a_{t_i}^{R_j}$	Particle acceleration as a function of time and position, mm/s^2
$C_p^{Ai}\Big\vert_{i=0}^{n}$	Mass concentration of the required phase in an area A_i, %wt
m_P^{Ai}	Mass of the required phase in an area A_i, kg
m_T^{Ai}	Total mass of all phases in an area A_i, kg
$S_{fs,i}\Big\vert_{i=1}^{2}$	Distance traversed by each solidification front (i = 1, i = 2 correspond to the solidification fronts advancing from the inner and outer casting surfaces, respectively), mm
d_{fs}	Initial distance separating the two solidification fronts, mm
$v_{fs,1,2}$	Average speed of solidification fronts advancing from the inner and outer casting surface, mm/s
V_c	Average cooling rate, K/s
Z_{fsp}	Zone of final solidification point
$C_{Eut,\ max}$	Maximum eutectic concentration, wt %
Al	Aluminum
Zn	Zinc
Cu	Copper
Mg	Magnesium
Mn	Manganese
Fe	Iron
Pb	Lead
Cd	Cadmium
Sn	Tin
Ti	Titanium

MMC_p	Metal matrix composite
ZA	Zinc-aluminium alloy
SiC	Silicon carbide
B_4C	Boron carbide
TiN	Titanium nitride
TiC	Titanium carbide
Al_2O_3	Alumine
Mg_2O	Oxyde de magnésium
BN	Boron nitride

LISTE OF SYMBOLS AND UNITS OF MESURE

BASE UNITS

m	meter (unit of length)
kg	kilogram (mass)
s	second (time unit)
K	Kelvin (temperature unit)
mol	mole (unit of amount of substance)
A	ampere (unit of electric current)
cd	candela (unit of luminous intensity)

Area

km^2	square kilometer (= 1 000 000 m^2)
hm^2	hectometer square (= 10 000 m^2)
m^2	square meter
dm^2	square decimetre
cm^2	square centimeter
mm^2	square millimeter

Volume

km^3	cubic kilometer
m^3	cubic meter
dm^3	cubic decimetre
cm^3	cubic centimeter
L	liter (= 1 dm^3)
dL	deciliter
cL	centiliter
mL	milliliter (= 1 cm^3)

GEOMETRIC UNITS

Length

m	meter
dm	decimeter
cm	centimeter
mm	millimeter
µm	micrometer

MASSE UNITS

Masse

t	tonne (= 1 000 kg)
kg	kilogram
g	gram
dg	decigramme
cg	centigram
mg	milligram
mg	microgram

Density

kg/m^3	kilogram per cubic meter

MECHANICAL UNITS

speed

m/s	meter par second
km/h	kilometer per hour

Angular velocity

rad/s	radian per second
r/s	revolution per second
r/min	revolution per minute

Acceleration

m/s^2	meter per squared second

TIME UNITS

h	hour
min	minute
s	second
ms	millisecond
µs	microsecond
a	year
d	day

CALORIFIC UNITS

K	kelvin
°C	degre Celsius

INTRODUCTION

Castings have a certain number of defects that are almost inevitable: voids, gas, and included oxides. For example, they all have very low ductility caused by the presence of pores which give the casting a brittle character. These pores are generated by the shrinkage and contraction. During solidification the liquid is unable to supply the interdendritic spaces and creates fine pores, often less than a tenth of a micron, which are responsible for the decrease of the alloys ductility. These fine pores are created due to the excessive viscosity of the liquid. When the temperature gets close to the melting point, the liquid is unable to flow between the fine details of the microstructure to feed the solidification shrinkage and thermal contraction. The cooling rate relatively low in gravity casting, resulting in a relatively coarse microstructure, which is obviously not favorable for the mechanical properties.

It is possible to produce graded parts not having the same mechanical properties on the exterior and interior surfaces. For this we use centrifugation, which allows for the segregation of phases and particles as a function of the acceleration. The centrifugal casting process allows us to use centrifugal force to produce a turned part. In the case of metal matrix composites (MMC_P), the centrifugal force acts on the distribution of reinforcing particles. By applying a centrifugal force, it is possible to produce turned parts of graduated composite with specific local properties. The effect of centrifugation is to change the composition of the alloy across the thickness and to modify the distribution of reinforcing particles.

Hearn (technique de l'ingénieur, AM 5210, 2002, p. 4) mentions that the main advantage of this method lies in its ability to implement large quantities of raw materials in a short time (1000 kg/h is not exceptional with rotation-projection-type installations) allowing it to compete on certain types of tubular parts in relation to concurrent technologies.

The need to train the mold, rotating at high speed, to generate a sufficient centrifugal force that will make a correct elaboration of the material imposes a physical limitation upon the combination of process parameters within the dimensions of the casting (rotation speed/part

diameter). It is common to distinguish two types of casting: those where the material is fabricated only under the influence of centrifugal force, and those named casting by (rotation-projection) where compaction and boiling are assisted by mechanics means.

According to Hearn (technique de l'ingénieur, AM 5210, 2002), during centrifugal casting, a permanent mold is rotated around its axis at high speeds (300 to 3000 rpm). The pouring is rejected under the influence of centrifugal force to the interior wall of the mold, where it solidifies after cooling. Only parts of cylindrical shape can be produced by this operation. The dimensions of the cylinder can vary up to 3 meters in diameter and 15 meters in length. The thickness of the section can vary from 2.5 to 125 mm. Materials that can be produced by centrifugal casting include cast iron, steel, stainless steel, aluminum alloys, copper, and nickel. The parts produced by this technique are numerous and include pipes, boilers, flywheels, etc.

During the casting of materials, two types of segregation may be found in the microstructure. The first is microsegregation, which is caused by the lack of diffusion of alloying elements with the high rate of cooling; the second is the macrosegregation of alloying elements and phases that occurs because of the density difference between alloying elements which, under the influence of solidification fronts, move in opposite directions simultaneously.

Microsegregation can be reduced or eliminated by a suitable heat treatment such as homogenization, for example, while macrosegregation is irreversible. A subsequent heat treatment has no effect on macrosegregation. In addition, macrosegregation can occur during centrifugal casting as well as during gravity and squeeze casting.

The macrosegregation phenomenon depends upon boundary conditions used during casting and upon solidification rate. A change in the initial mold and pouring temperatures can change the rate of macrosegregation and its variation across the casting section. Solidification fronts advancing from opposite sides reject during centrifugal casting the last

liquid to fill the area of shrinkage and thermal contraction located at the last point of solidification.

To increase the wear resistance without increasing the weight of materials, new alloys such as metal matrix composites (MMC_P) that contain soft and lubricant particles (graphite) and/or hard particles (SiC, Al_2O_3, B_4C, TiB_2, BN, and others) with improved machinability have been developed. MMC_P appeared on the market in the ’70s; they are known for their light weight and high wear resistance, but also for the difficulties encountered during their machining. Generally the reinforcement particles are abrasive and difficult to machine. Villar and Masounave (technique de l’ingénieur, M 2 448, 1996, p. 2) indicate that, in general, MMC_P are used primarily for their excellent wear resistance, as well as in abrasion, erosion, or friction, due to the presence of hard reinforcing particles. Compared with aluminum alloys, the Young’s modulus and yield strength of these materials are higher, around 10 to 15%.

Compared with carbon-carbon fiber composite, the yield strength of MMC_P reported to the density unit is higher, at about 40%, and they are cheaper and recyclable, which is not the case for polymer composite (polymer matrix). In addition, compared to steel, MMC_P offer much interest. Their density is lower, the yield strength and Young’s modulus are higher, and the wear resistance is better. Moreover, MMC_P have some interest because of their adjustable properties. According to the morphology of particles and their distribution, it is possible to vary the properties in interesting proportions.

The main objective of this research is to study and model the segregation of phases and particles during centrifugal casting of zinc-aluminum alloy ZA8 and functionally graded aluminum matrix composite A356/SiC, respectively. The research results will help in controlling the phenomenon of segregation of phases and particles, thus improving the quality and mechanical properties of the casting and increasing the wear resistance in the case of MMC_P.

For the centrifugal casting of zinc-aluminum alloy ZA8, we studied the phenomenon of macrosegregation by modeling the speed of solidification fronts and the macrosegregation of the interdendritic liquid produced through the matrix during the centrifugal casting. This analysis and modeling will permit to reduce the rate of macrosegregation variation across the section, to control the zone of maximum macrosegregation, to avoid the formation of brittle zones in the critical positions across the section, and thus to increase the toughness and part reliability in service.

On the other hand, in order to better control and specify the degree of graduation and variation of the volume fraction of the particles across the section during centrifugal casting of a graded composite, we intended to model the segregation of particles taking into account the variation in centrifugal radius and viscosity of the liquid metal during the cooling process and, therefore, the change in velocity of the particles during their displacement through the matrix. Modeling the segregation of particles using a variable particle velocity and a dynamic viscosity allows one to precisely determine their degree of graduation across the section and on the inner/outer casting surface, and to better control their mechanical properties at the critical points of the section. For example, this composite must resist friction and wear; on the other hand, it must be compatible with the casting alloys. The fabrication of such graded composite is difficult to achieve using traditional foundry processes; however, centrifugation allows us to overcome this difficulty. We produced a graded composite with specific mechanical properties by controlling the process parameters, the boundary conditions, and the cooling rate. We also studied the influence of the variation of the centrifugal radius during the displacement of the particles, as well as the change in viscosity during the cooling process, on the displacement and segregation of the particles.

We can summarize the specific objectives of the research as follows:

1. Study the macrosegregation of phases. Model the speed of solidification and the speeds of solidification fronts, the final solidification point, and the zone of maximum macrosegregation of the eutectic through the section.

2. Establish recommendations in order to increase the toughness at the critical points of the section while controlling the zone of maximum macrosegregation and the ratio between the speeds of solidification fronts.

3. Model and control the distribution and segregation of the particles across the section and on the inner/outer casting surface of MMC_P by discretization of Stokes' law in order to take into account the variations of viscosity, centrifugal radius, and particles' velocities during the cooling process, as well as their influence on the particles' segregation.

Structure of the thesis

The thesis consists of four chapters. It starts with an introduction, followed by chapter one on literature review, two other chapters on the various research tasks, and a chapter of general discussion, plus a general conclusion, recommendations, and a list of references. The experimental conditions and parameters used in our studies are presented at the beginning of each chapter. The chapters of the thesis are organized as follows:

Chapter 1: Literature review.

In this chapter, we analyze the works found in literature on the macrosegregation of phases, on the centrifugal casting of metal matrix composites (MMC_P), on MMC_P along with their properties and resistances, and on the wettability of particles. In addition, this chapter ends with a clear formulation of the problem and the methodology used.

Chapter 2: Modeling of Eutectic Macrosegregation in Centrifugal Casting of Thin-Walled ZA8 Zinc Alloy.

In this chapter, we present our research results on the macrosegregation of phases produced during centrifugal casting. The primary goal is to model the zone of maximum eutectic

macrosegregation through the section as well as the speeds of solidification and solidification fronts, taking into account the boundary conditions and process parameters used. In addition, an analysis of the microstructure with optical and electron microscopes is done. Finally, a conclusion is established to limit macrosegregation and control the zone of maximum macrosegregation of interdendritic liquid across the section. The use, in this study, of hypereutectic ZA8 zinc alloy with a high eutectic concentration makes it easier to identify and to model macrosegregation throughout the matrix. The results of this modeling can be used to study and characterize (by extension) the macrosegregation of phases in the metal matrix composites and other alloys produced by centrifugation.

Chapter 3: Modeling of Particle Segregation during Centrifugal Casting of Metal Matrix Composites.

In this chapter, we present the modeling of the displacement, segregation of particles, and variation in their volume fraction across the casting section using Stokes' law with a discretized particle velocity and deceleration/acceleration over time. The primary goal of this chapter is to identify and control the degree of particle graduation across the casting section while using variables centrifugal radius and pouring viscosity. This chapter shows the influence of the variation of particles' velocities on the change in their volume fraction on the outer/inner casting surface. Moreover, the developed models are validated experimentally and discussed.

Chapter 4: General Discussion.

In this chapter, a general discussion on the modeling and results presented is performed. The discussion allows us to link the found results and the previous studies, and helps clarifying certain aspects of the modeling and the different points identified in the problem and research objectives. This discussion allows, also, to show the importance of the found results on improving certain aspects of science related to the segregation of phases and particles during centrifugal casting.

CHAPTER 1

LITERATURE REVIEW

1.1 Principal of centrifugal casting

In centrifugal casting, a permanent mold is rotated around its axis at high speeds (300 to 3,000 rpm) while the molten metal is poured. The molten metal is thrown, under the influence of centrifugal force, to the inner wall of the mold, where it solidifies.

When a body is rotated around a fixed axis, it is subjected to a centrifugal acceleration. To keep the body in its trajectory, a centripetal force of the same magnitude is developed and, therefore, this body exerts an opposing centrifugal force on the device that constrains it.

The acceleration γ caused by the rotation is given by:

$$\gamma = v^2/R = \omega^2.R \tag{1.1}$$

The centrifugal force = the centripetal force, and is given by:

$$F_\omega = m\ .v^2/\ R = m\ .\omega^2.\ R \tag{1.2}$$

Where:

γ: acceleration, $m{\cdot}s^{-2}$;

F_ω: centrifugal force, N;

m: mass, kg;

R: radius, mm;

ω: angular velocity, $rad.s^{-1}$.

1.2 Macrosegregation

Macrosegregation is an irreversible phenomenon that affects the microstructure of the material. Macrosegregation can affect the uniformity of distribution of phases and alloying elements through the matrix and degrades the mechanical properties of the casting in creating, across the section, areas rich in certain brittle phases and poor in other ductile phases. This reduces the ductility and toughness of the material in some areas and limits its strength and use. Moreover, macrosegregation can not be eliminated by a subsequent heat treatment, as in the case of microsegregation, which is generated by the lack of diffusion of alloying elements. The only remedy for macrosegregation is control of process parameters and solidification rate, which can help reduce and control it without eliminating it.

According to Nadella *et al*. (2008, p. 451), the macrosegregation can be a normal or inverse segregation. The normal segregation is caused by the flow of the interdendritic liquid toward the hottest zone or the center of the part under the influence of the solidification fronts. The shrinkage is the driving force behind this transport of the liquid phase. In contrast, macrosegregation is called inverse segregation when the solute-enriched liquid is pushed toward the peripheries of the casting. In addition, it was mentioned by Nadella *et al.* (2008) that the formation of equiaxed structures promotes the normal segregation while the inverse segregation is promoted by the formation of columnar structures.

It has been shown by Gang *et al.* (1999, p. 306) that, during the centrifugal casting of zinc alloy ZA27, the lower the initial pouring temperature, the higher is the reduction in the macrosegregation of aluminum. Figure 1.1 represents the relative content of aluminum across the casting section. It can be seen, from this figure, that the relative content of aluminum increases from the outer to the inner surface. In addition, it has been found by these authors that the addition of manganese (Mn) to the alloy reduces the macrosegregation of alloying elements remarkably. An addition of 0.4–0.5 wt% of Mn gives the highest reduction rate of macrosegregation. Manganese in the ZA27 alloy can form a $MnAl_6$ phase at high temperature, which serves as a catalyst for the primary phase (α).

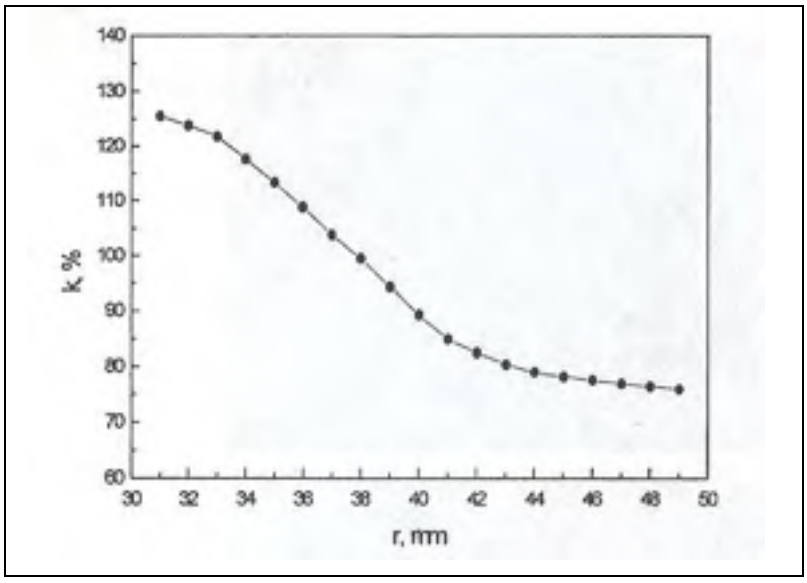

Figure 1.1 Curve of the relative content of aluminum versus the radial distance of the specimen (T_p = 833 K, t_p = 10 s).
From Gang Chen (1999, p. 307)

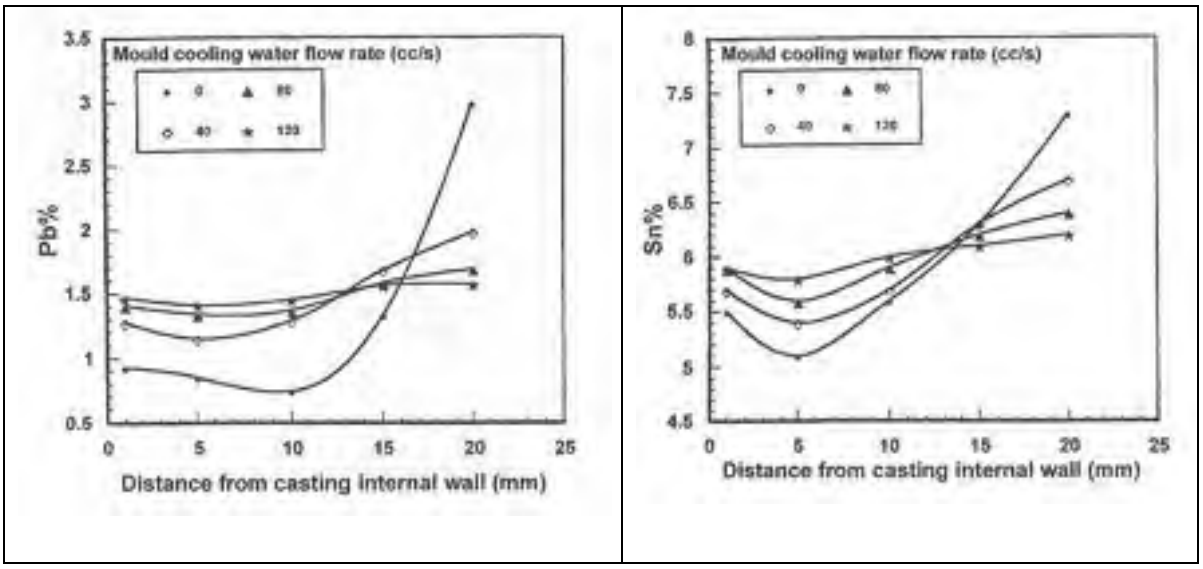

Figure 1.2 Lead and tin percents as a function of distance from the inner casting surface at different mold cooling water flow rates.
From Halvaee (2001, p. 126)

While studying the segregation generated during centrifugal casting of C92200 tin bronze alloy, Halvaee and Talebi (2001) mention that increasing pouring temperature intensifies the segregation of lead (Pb) and tin (Sn) across the matrix. On the other hand, increasing mold cooling rate reduces the segregation. The difference in lead and tin content between external and internal casting surfaces is diminished with increasing the mold cooling rate (Fig. 1.2). This increase in the solidification rate decreases the rejection of tin and lead.

Furthermore, it was found by Chakrabarti (1996) that during the centrifugal casting of zinc alloys, the density difference between the alloying elements produces a transverse and axial segregation, which affects the hardness and composition of the alloy through the section. On the other hand, it was shown by Zhang *et al.,* (1999) that the formation of silicon (Si) and Mg_2Si primary phases in zinc alloys improves wear resistance, but affects strength and ductility, which decrease. In contrast, the centrifugal casting of the in situ Zn-Al-Si alloy reduced the adverse effect of the brittle phases Si and Mg_2Si, on the ductility (Qudong *et al*., 2005; W. Chen *et al.,* 2001).

1.3 Zinc alloys

In addition to their excellent physical and mechanical properties, zinc alloys are characterized by a good corrosion resistance and excellent damping properties, which increases exponentially with temperature. In addition, zinc alloys have a very good wear resistance and excellent machinability.

According to the ASM handbook, vol.15, 2008, die casting is the process most often used for shaping zinc alloys. Sand casting, permanent mold casting, and continuous casting of zinc alloys are also practiced. However, for producing hollow and cylindrical parts, the centrifugal casting is used. The compositions of the different zinc alloys and their mechanical properties are given in Appendix I (Table I.1 and I.2).

The alloys ZA-8, ZA-12, and ZA-27 are higher-aluminum zinc-base casting alloys with small amounts of copper and magnesium. Aluminum is added to zinc to strengthen the alloy, reduce grain size, and minimize the attack of the molten metal on the iron and steel in the casting and handling equipment. Aluminum increases the fluidity of the molten alloy and improves its castability. The ZA8 alloy has high tensile, fatigue, and creep strength as well as low density, while the ZA12 alloy – for its part – has very good casting capabilities in a cold chamber under pressure. Its density is lower than that of all other zinc alloys except ZA27; furthermore, it has excellent wear resistance and acceptable ductility. The ZA8 and ZA12 alloys are used wherever high resistance is required, such as in auto parts, agricultural equipment, electronics, hardware, radios, etc. (ASM handbook, vol. 2, 1979). In addition, because of their high mechanical properties and low cost, zinc alloys can be used to replace the iron and copper alloys found in many structural applications.

The phase transformation of hypereutectic zinc-aluminum alloys depends on the aluminum concentration. The solidification of a hypereutectic ZA8 alloy begins with the formation of a primary phase (β) at the liquidus temperature. The phase (β) is stable just above 277˚ C, below which (β) is transformed eutectoidly into two phases, an aluminum-rich (α) phase and a zinc-rich (η) phase, which form the zinc-aluminum eutectic.

The microstructures of the squeeze-cast and gravity-cast ZA8 alloy are shown on figures 1.3 and 1.4, respectively. According to Fatih Çaya and Can Kurnaz (2005, p.480), the structures are consisted of numerous small and particulate primary β dendrites set in an eutectic matrix. The eutectic matrix is made up of α (aluminum-rich) and η (zinc-rich) phases. In the gravity cast of ZA-8, the primary β was both coarser and dendritic. The decomposition of β particles had coarse lamellar and granular in comparison with squeeze-cast technique. The eutectic is big and coarse, especially the space between α and η.

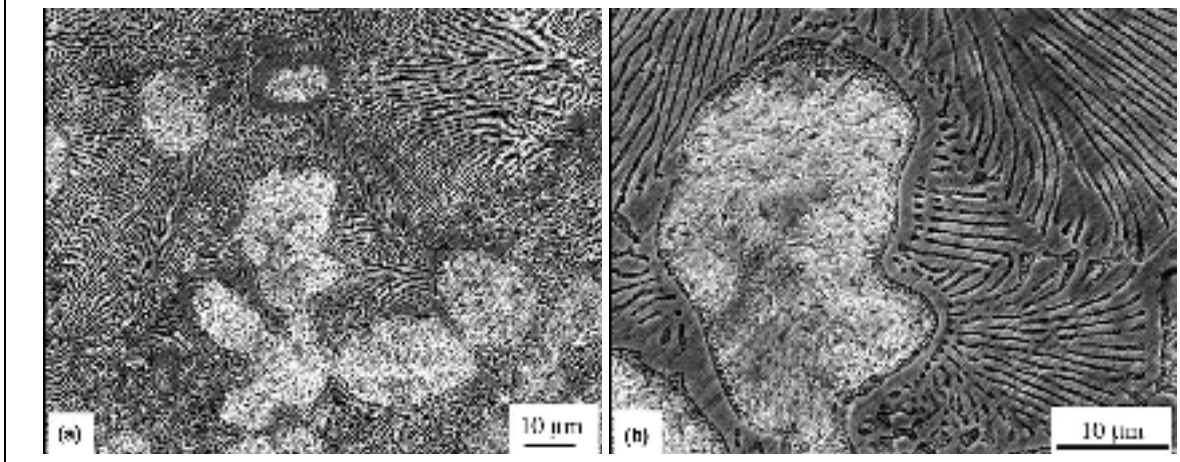

Figure 1.3 SEM microstructures of the squeeze-cast ZA-8 alloy at: (a) low and (b) higher magnification.
From Çaya and Kurnaz (2005, p.480)

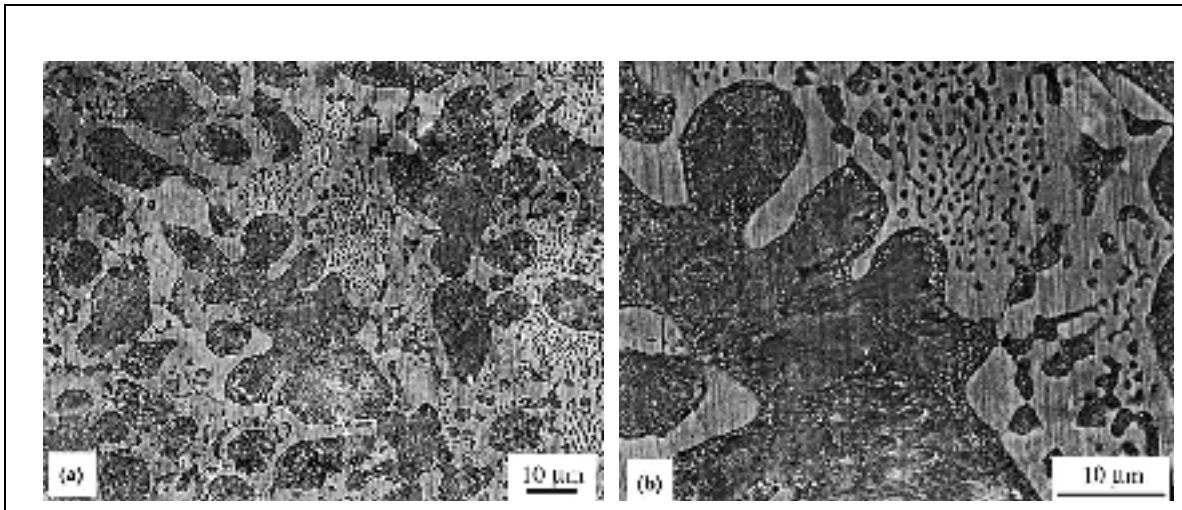

Figure 1.4 SEM microstructures of the gravity-cast ZA-8 alloy at: (a) low and (b) higher magnification.
From Çaya and Kurnaz (2005, p.481)

1.4 Metal matrix composites

The metal matrix composites (MMC_P) are well-known for their excellent mechanical properties, such as resistance to abrasion and wear. Their low cost and their relative ease of implementation explain the significant growth in the use of these materials.

Reinforcement particles play a key role in determining the mechanical properties of composites. A wide range of particles with different properties can be used to produce MMC_P, but the type, size and concentration of the particles must be accurately determined to obtain a material with desired properties and to avoid interface reactions between the particulate reinforcement and the matrix.

Hearn (technique de l'ingénieur, AM 5210, p. 4) mentions that the major feature of centrifugal casting is the fact that the reinforcements are not only embedded in a matrix under hydrostatic pressure, but also that the reinforcements themselves are individually subjected to direct pressure against the mold plate. The artificial gravity field created by centrifugal force acts on each element, depending upon its density. Often, it is the density difference in a mixture which is interesting. Since there is a fluid giving mobility to the particles, centrifugation allows for separation in order of increasing density.

Centrifugal casting is an effective method to produce graduated composites, but a full understanding of the mechanism of particle distribution has not yet been reached. Several parameters influence the characteristics of the graduated composite, such as metal and mold temperatures, variations in pouring viscosity during cooling, solidification speed, centrifugal force, and interaction between the particles and the liquid. The balance between these various parameters determines the distribution of reinforcing particles in the matrix. Furthermore, among the functionally graded materials (FGMs) with aluminum matrixes, most hard particulate reinforcements have densities larger than the density of the metal. Thus, the segregation of the particles occurs near the outer casting surface. However, Zhang *et al*. (1998, p. 1677-1679) show that it is possible to produce FGMs reinforced with magnesium

silicide particulate (Mg_2Si) on the casting's inner surface. The Mg_2Si, which is formed during solidification, has a lower density than the aluminum matrix (1.88 g/cm^3 against 2.4 g/cm^3), and it can be segregated toward the inner casting surface through centrifugal casting.

1.4.1 Particle velocity

The velocity of spherical particles during the centrifugation process depends on several parameters. According to Stokes' law, the velocity of a particle in a liquid is expressed by the following equation:

$$v_p = \frac{d_p^2(\rho_p - \rho_l)\cdot g}{18\eta} \tag{1.3}$$

Where:

d_p: particle diameter, mm;

ρ_P ,ρ_l: particle and liquid density, respectively, kg/m^3;

g: gravitational acceleration, m/s^2;

η: viscosity, Pa.s.

Kang *et al.* (1994, p. 249) specify that the segregation of the particles during centrifugal casting is caused by the difference between their density and that of the matrix. The particles suspended in the metal are subjected to different accelerations caused by the gravitational force (g) and centrifugal force ($\gamma = \omega^2 \cdot r$). The vertical motion of the particles can be ignored because of the acceleration caused by centrifugal force, which is much higher than gravitational acceleration. Thus, according to Szekely (1979), cited in Kang *et al.* (1994, p. 250), considering the various forces acting on the particle, the balance of forces can be expressed as follows:

$$\frac{4}{3}\pi R_p^3(\rho_p-\rho_l)\omega^2 r-6\pi\eta R_p\frac{dr}{dt}-F_R=\frac{4}{3}\pi R_p^3\rho_p\frac{d^2r}{dt^2} \quad (1.4)$$

According to Kang *et al.* (1994, p. 249), based on equation (1.4), the position of the particle during centrifugation may be expressed at any moment of time by the following equation:

$$r_i(t)=r_0\exp\left[\frac{4\omega^2(\rho_p-\rho_l)R_p^2t}{18\eta c}\right] \quad (1.5)$$

Where:

r_i (t): particle position at time t, s;

r_0 : particle position at time t = 0;

ω : angular velocity of the mold, rad/s;

R_p : particle radius, mm;

t : time, s;

η_c : viscosity of a metal containing particles, Pa.s.

Based on equation (1.4), the velocity of a spherical particle moving in a liquid with zero acceleration can be expressed by the following equation:

$$v_p=\frac{4\omega^2\cdot R\cdot(\rho_p-\rho_l)\cdot R_p^2}{18\eta} \quad (1.6)$$

Where:

R: centrifugal radius, mm;

ρ_P ,ρ_l: particle and liquid density, respectively, kg/m^3;

η: pouring viscosity, Pa.s.

Kang *et al.* (1994, p. 250) show that the thickness of the particles' zone versus time and rotation speed can be estimated. The variation of the volume fraction of particles moving in a liquid metal is calculated at time t = t + Δt, as a function of the distance separating them from the outer surface of the casting by the following relation:

$$V(t+\Delta t) = V(t)\frac{1-r_i(t+\Delta t)}{1-r_i(t)} + V(t) \tag{1.7}$$

where Δt is the time interval, s.

Equation (1.5) has been confirmed by Raju and Mehrotra (2000, p. 1628). These authors express the balance of forces acting on the particle during centrifugation as follows:

$$F_\omega - F_\eta - F_R = F_{net} \tag{1.8}$$

Where:

F_{net}: force acting on the particle, N;

F_ω: centrifugal force, N;

F_η: viscosity force, N;

F_R: repulsive force, N.

According to Raju and Mehrotra (2000, p. 1628), the effect of the repulsive force on the particle is significant only if the particle is close to the solid-liquid interface. If the particle is not influenced by the solid-liquid interface, then the balance of forces can be expressed as follows:

$$F_\omega - F_\eta = F_{net} \tag{1.9}$$

From equation (1.9) and for a particle that is not influenced by the solid-liquid interface and moves with constant velocity, the position of the particle at a time (t) is expressed by equation (1.5).

Velhinho *et al.* (2003, p. 260) mention that the increase of the viscosity of liquid alloy during cooling opposes the centrifugal force and prevents the particles from moving across the section. The viscosity that influences the segregation of particles is not simply the intrinsic viscosity of the liquid alloy, but that viscosity which changes depending on the alloy fraction already solidified.

The distribution of the particles in the matrix during centrifugation is influenced by several parameters (rotation speed, mold and pouring temperatures, size and volume fraction of particles, particles and matrix densities) and also by the change in the centrifugal radius and viscosity of the liquid metal during cooling. All these factors must be considered when predicting the motion of the particles and their distribution across the casting section.

1.4.2 Viscosity

Stefanescu *et al.* (1994, p. 250) express the viscosity of the metal-containing particles by the following equation:

$$\eta_c = \eta\,[1 + 2.5V(t) + 10.05V^2(t)] \tag{1.10}$$

Where:

η : viscosity of aluminum alloy, Pa.s;

V (t) : particle volume fraction as a function of time, %V.

Lucas (technique de l'ingénieur, M66, 1984, p. 3) specifies that the viscosity of the liquid metal as a function of temperature can be determined by the Arrhenius relationship:

$$\eta_{(T)} = A \exp\left(\frac{Q}{R_g \cdot T_k}\right) \quad (1.11)$$

Where:

A : constant;

T_k : absolute temperature, K;

Q : activation energy of viscous flow, $KJ.mol^{-1}$;

R_g : perfect gas constant, R = 8.31441, $J.K^{-1}.mol^{-1}$;

1.4.3 Effect of rotation speed and particles' size and concentration

While centrifugal casting a composite material (Al) reinforced by SiC particles (15%w, 10μm), Bonollo *et al.* (2004, p. 50) show, using different rotation speeds (500, 1000, 1500 rpm), that the speed of 500 rpm does not generate a high enough centrifugal force to ensure the segregation of particles on the external casting surface before solidification begins. The speed of 1500 rpm results in the formation of three different zones along the radial distance of the casting (Fig. 1.5):

1. A free particle zone near the inner casting surface;
2. A particle graduate zone between the inner and outer surfaces;
3. A particle concentrated zone at the outer casting surface.

The volume fraction of the particles has a significant effect on their distribution. The thickness of the section that does not contain particles decreases as the particle volume fraction increases, while the graded zone increases. Figure 1.6 shows the results of the effect of rotation speed and volume fraction of the particles on their positions across the section. It can be seen in this figure that the higher the rotation speed, the higher the particles' segregation on the outer casting surface and the larger the particles' free zone.

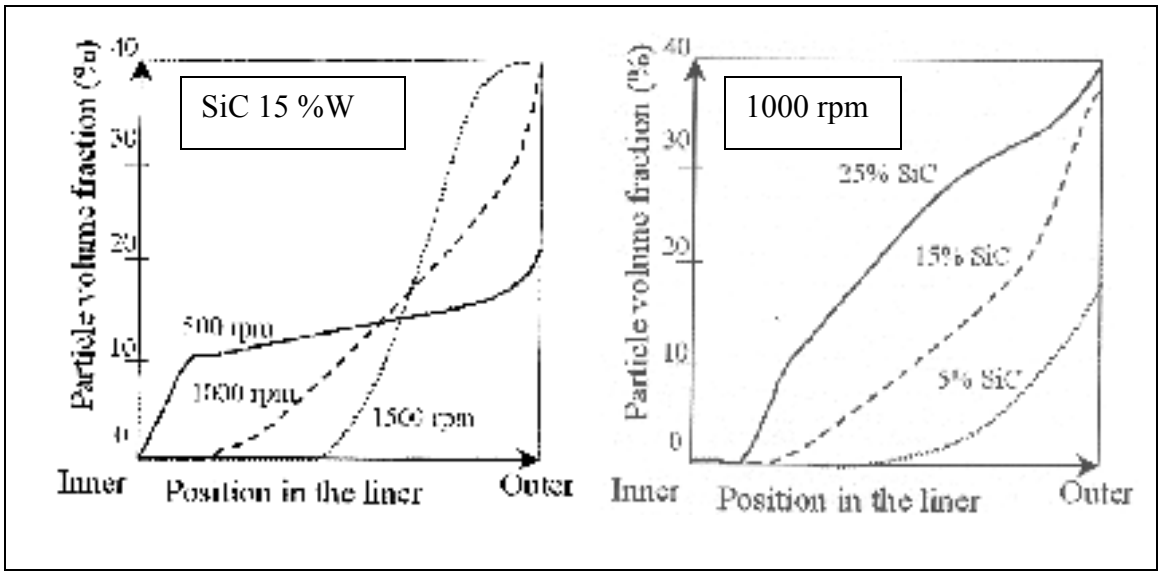

Figure 1.5 Influence of the rotation speed and volume fraction of the particles on their distribution.
From Bonollo (2004, p. 50)

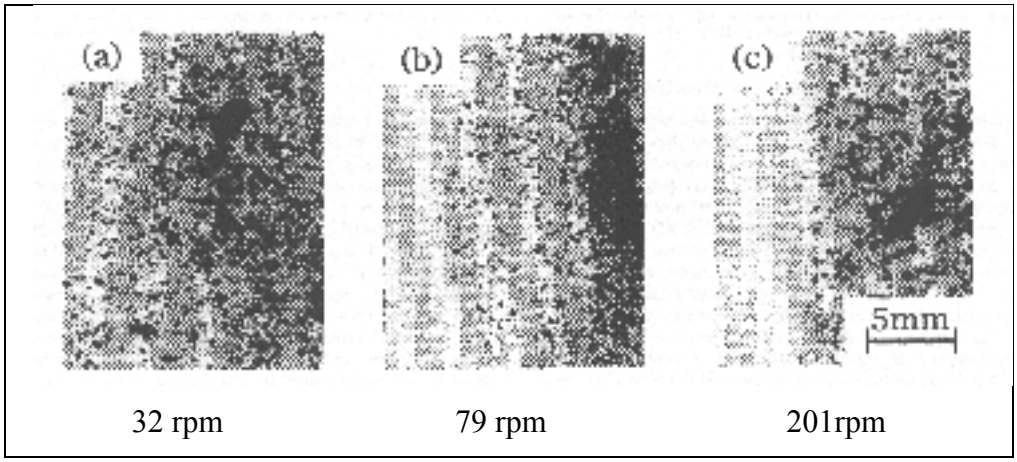

Figure 1.6 Micrograph of particle distribution across the section as a function of rotation speed.
From Watanabe (1998, p. 597)

While studying the influence of the rotation speed on the distribution of graphite particles in a A356 aluminum graded composite produced by centrifugal casting (noting that the density of graphite 2.2 g/cm^3 is smaller than that of liquid aluminum 2.4 g/cm^3), Kang *et al.* (1994, p. 251) show that the volume fraction of graphite particles on the inner casting surface increases

by increasing the rotation speed. On the other hand, Raju and Mehrotra (2000, p. 1631) found that the particle-rich zone on the outer or inner casting surface increases with increased particle size, depending on the density difference between the matrix and the particles (Fig. 1.7). In fact, during the movement of particles in a liquid, the centrifugal force and the force generated by the viscosity act in opposite directions. Both forces increase with increasing particle size, but the centrifugal force becomes much greater than that generated by the viscosity. Therefore, large particles move more quickly than small ones.

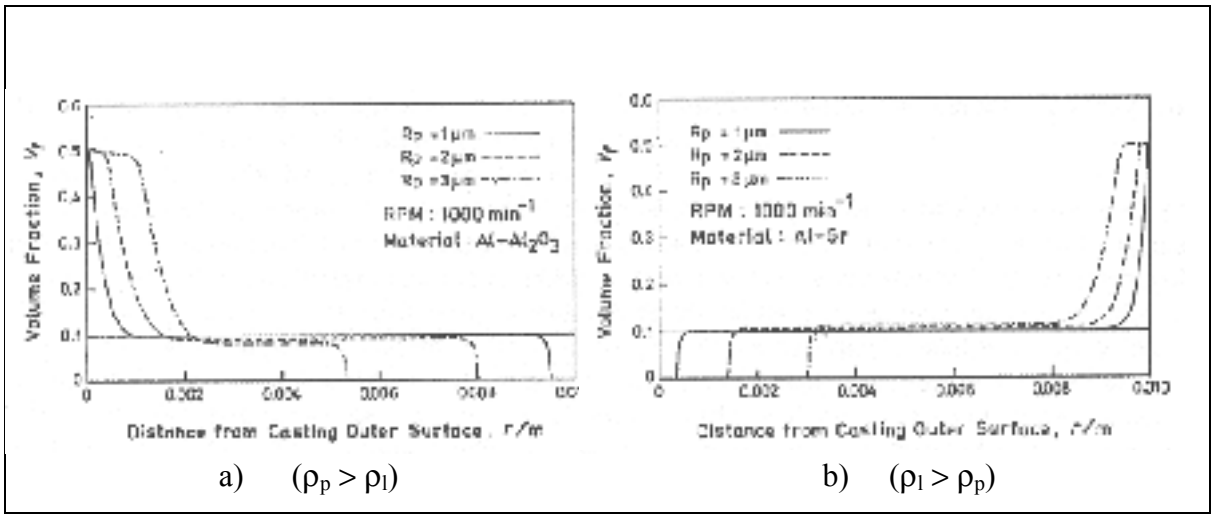

a) ($\rho_p > \rho_l$) b) ($\rho_l > \rho_p$)

Figure 1.7 Particles' volume fraction across the section as a function of their size.
From Raju (2000, p. 1631)

1.4.4 Effect of temperature and solidification time

Kang *et al.* (1994, p. 247) mention that the determination, during centrifugation, of the distribution of temperature and solidification time of the casting by experimental techniques is difficult to make with a mold rotating at very high speeds. These authors studied the temperature distribution inside a mold and a metal being solidified during the centrifugal casting of composite A356/Gr in order to show the influence of the initial pouring and mold temperatures on the temperature distribution in the mold and the composite during centrifugation (Fig. 1.8 a and b).

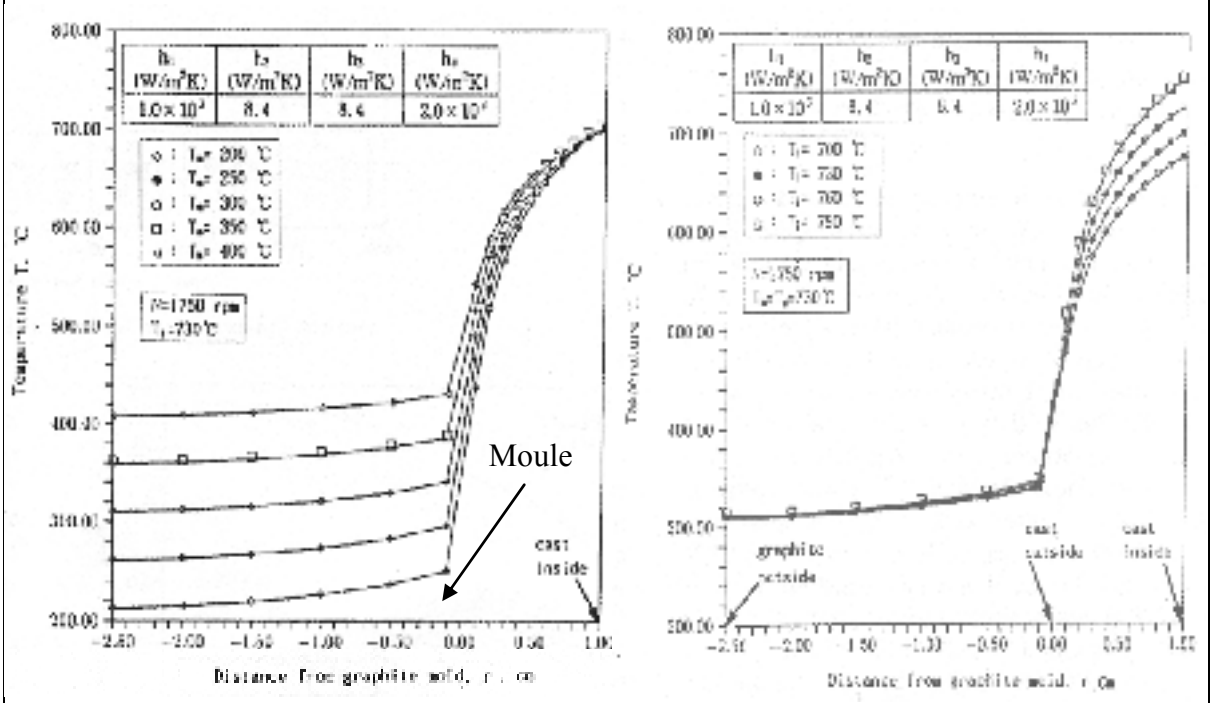

a) Effect of mold temperature on the temperature distribution in the metal and the mold during centrifugation.

b) Effect of pouring temperature on the temperature distribution in the metal and the mold during centrifugation.

Figure 1.8 Temperature distribution in the mold and the metal during the centrifugation process.
From Kang (1994, p. 251)

It can be seen (Fig 1.8 a) that, for a variation in the mold temperature of 200°C to 400°C, the temperature of the metal increases by increasing the initial mold temperature, except that the temperature on the inner casting surface remains constant as the solidification front advances from the outer to the inner surface. On the other hand, figure 1.8 b shows that, upon increasing the initial pouring temperature, the temperature reaches a higher value on the inner casting surface and drops gradually while advancing towards the outer surface.

The high pouring temperature means that there is more heat to be evacuated before solidification begins. Therefore, the cooling time increases and the particles move for a

longer time inside the matrix. On the other hand, increasing the mold temperature decreases heat transfer between the liquid metal and the mold, thereby increasing the cooling time and facilitating the segregation of the particles across the section.

1.4.5 Theoretical and experimental results of the particles' segregation

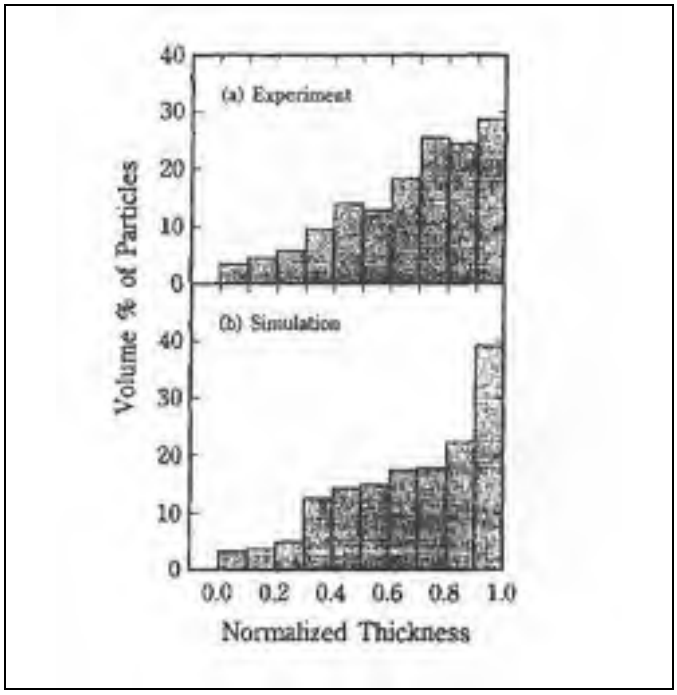

Figure 1.9 Volume fraction of corundum particles obtained theoretically and experimentally across the section.
From Watanabe (1998, p. 600)

According to the results of Watanabe *et al.* (1998, p. 597), during the centrifugal casting of a composite corundum/plaster, the volume fraction of the particles obtained experimentally across the casting section differs from that obtained theoretically (Fig. 1.9). It can be seen in this figure that the volume fraction of the particles obtained theoretically, on the outer casting surface, is quite higher than that obtained experimentally. This difference may be explained by the fact that the authors use, in modeling the particles' segregation, Stokes' law with constant centrifugal radius, temperature, and viscosity of liquid metal. This can increase the

distance displaced by the particles and their volume fraction on the outer surface for a given time of centrifugation. In fact, during cooling, the drop in temperature of the liquid metal increases its viscosity and the force opposing the centrifugal force, which slowed the particles' velocities and decreases the distance they travel before the solidification begins.

While studying the variation of the particles volume fraction in a SiC/A359 composite using Stokes' law with a constant particle velocity, Kelestemure and Castro (2002) also found a difference between the experimental and theoretical results (Fig. 1.10). It can be seen on this figure that the particles' volume fraction, obtained experimentally, is higher than that determined theoretically. Castro and Kelestemure (2002) explain these results by the fact that their model ignores superheating and the conditions of heat transfer on the mold wall. A cooling period of 10 seconds was used in the modeling. From these results we deduce the influence of superheat temperature, the time of superheat extraction, and the change in the particles' velocity on the particles' volume fraction. In fact, particle velocity is influenced by variations in the centrifugal radius and viscosity during particle displacement and the cooling process, respectively. The major movement of the particles occurs before the temperature falls below liquidus. When the temperature becomes lower than that of liquidus, solidification begins to block the movement of particles. The smaller particles continue to move at very short distances in the areas that remain liquid. The variation in the volume fraction of the particles, as a result of this displacement, is negligible.

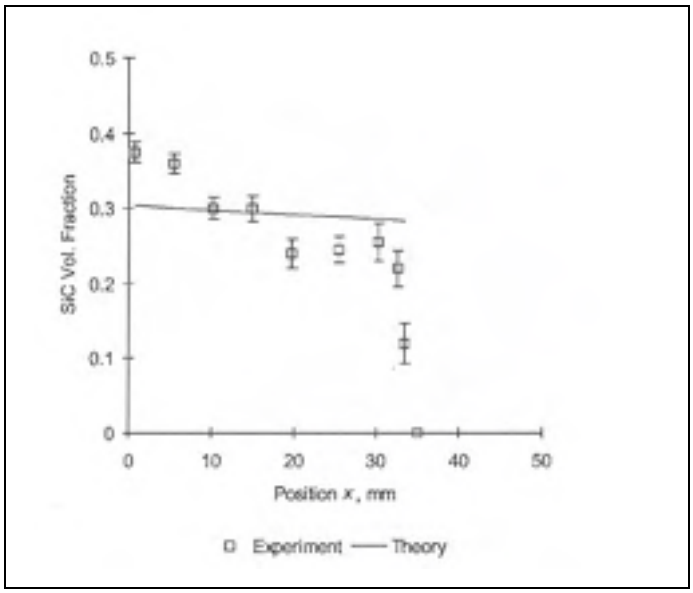

Figure 1.10 Volume fraction of SiC particles obtained theoretically and experimentally (d_p = 12.8 ± 4.2 µm, fv_{in} = 20 vol%).
From Castro and Kelestemure (2002, p. 1816)

The segregation of SiC particles and the influence of their initial volume fraction and size were studied by Lajoye and Suery (1988, p. 15–20), using Stokes' law with constant viscosity and centrifugal radius, and applying the finite difference method for calculating heat transfer. These authors found a good agreement between the theoretical and experimental results obtained (Fig. 1.11). In contrast, the viscosity used by these authors (0.0025 Pa.s) is too high and does not match the initial pouring temperature. In addition, the time of superheat extraction has not been mentioned. However, the viscosity of the liquid metal and its variation with temperature combined with the change in centrifugal radius have a significant influence on the particles' segregation, and they are strongly related to cooling time. A high liquid metal viscosity slows the movement of the particles and changes their volume fraction across the section. On the other hand, a short cooling time decreases the influence of the variation in viscosity and centrifugal radius on the particles' segregation before they are blocked by the liquidus front. Thus, the change in the particles' volume fraction on the outer casting surface as a result of the change in viscosity and centrifugal radius is negligible if the cooling time is very short.

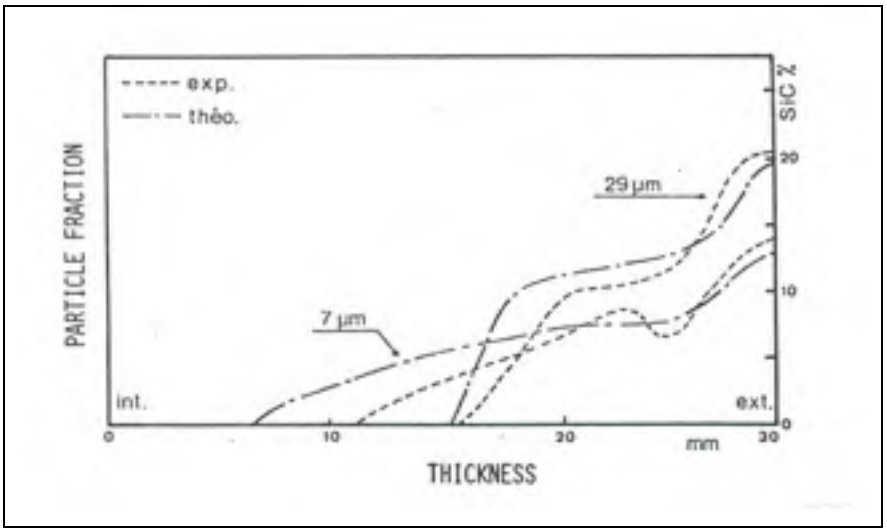

Figure 1.11 Volume fraction of particles across the section as a function of their size.
From Lajoye (1988, p. 19)

Using the same material (Al/SiC) and the same experimental conditions as Lajoye and Suery (1987), but taking into account the repulsive force, Panda et al. (2006) found a good agreement of their results with those of Lajoye (Fig. 1.12). However, comparing the two curves of the particles' volume fraction corresponding to the results of Lajoye and Panda, we can see that the free particle zone, in the case of Panda, is greater than that found by Lajoye; whereas, according to the modeling of Panda, this zone is supposed to be smaller if a repulsive force is taken into account. We explain this difference in the results by the fact that the viscosities used by these authors are different. In the work of Lajoye and Suery (1987), the viscosity used is 0.0025 Pa.s., while that one used by Panda et al. (2006) is 0.002 Pa.s. Thus, it can be deduced that the fact that Panda has used a viscosity smaller than the one used by Lajoye is the origin of this difference in results. In fact, the particle velocity becomes greater if the viscosity used is smaller. Therefore, the particles move to a larger distance and the particles' free zone becomes larger. This indicates the importance of viscosity on the segregation of particles. However, in comparing the results of Lajoye and Panda, it can be seen that the repulsive force does not have a great influence on the particles' volume fraction, especially on the outer casting surface.

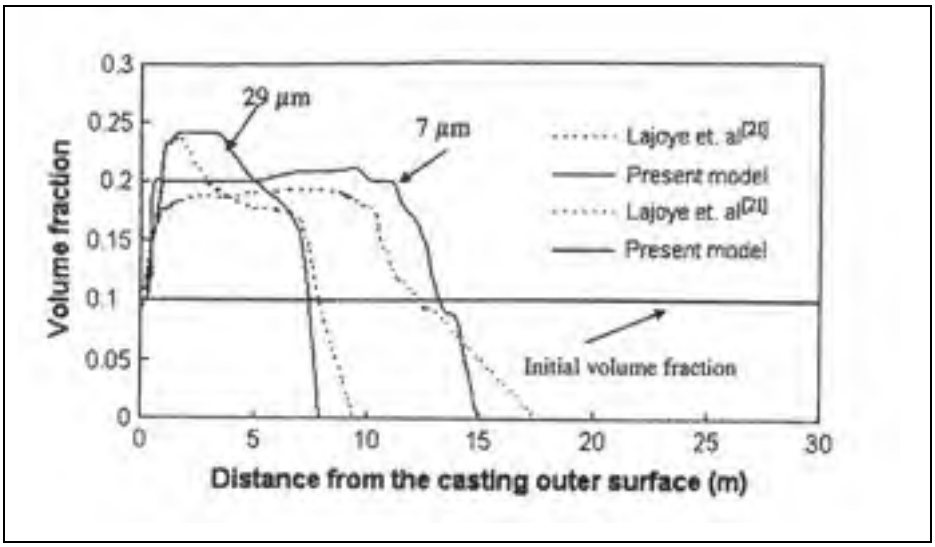

Figure 1.12 Volume fraction of particles as a function of their size.
From Panda (2006, p. 1686)

1.4.6 Properties of reinforcement particles and wear resistance

Table 1.1 shows the classification of reinforcement particles according to their size and hardness.

Table 1.1 Classification of reinforcement particles for MMC_P
(From Villar, 1996)

Particles	Fine	Large
Low hardness MoS_2, graphite, talc	I	II
High hardness SiC, SiO_2, Al_2O_3, B_4C	III	IV

Source: This table was taken from ' technique de l'ingénieur': Élaboration des composites à particules, vol. M2448, p. 1–17.

The fine particles with a diameter varying between 5 and 15 microns improve friction, while those with a diameter greater than 50 microns increase resistance to abrasion. Fine, hard

particles of class III (Table 1.1) that vary in diameter from 5 to 15 µm can be used to improve the resistance of parts subjected to friction.

Table I.1 (Appendix I) gives the general properties of the most-often used ceramics for the reinforcement of metals. However, these properties can vary depending on the manufacturing processes used. In general, the MMC_P with coarse particles are very difficult to machine, especially when the particles are hard.

According to Scheed *et al.* (1997, p. 164), the wear rate of MMC_P is related to the particle volume fraction and size. Whether the sliding speed is small or large, the minimum wear rate occurs with a volume fraction of particles of 10 %V. This result was obtained for a large particle size (120 µm).

Scheed *et al.* (1997, p. 164) indicate that when the volume fraction of particles is small (less than 10% V), wear occurs primarily by adhesion, whereas when the volume fraction of particles is higher than 10 %V, a solid lubrication mechanism occurs on the surface of contact between the two parts that are subject to friction, and the wear rate reaches its minimum value. On the other hand, the wear rate increases with decreasing particle size. When the particles are of large sizes, the mechanism of wear is slightly different; wear occurs by solid lubrication, and the wear resistance is higher.

1.4.7 Wettability of the particles

The process of metal matrix composites elaboration involves firstly the introduction of the particles in the matrix without the air being trapped. According to Cornie *et al*. (1990, p. 63), this insertion process is known as the wettability of particle-matrix and the surface energy controlling the wettability.

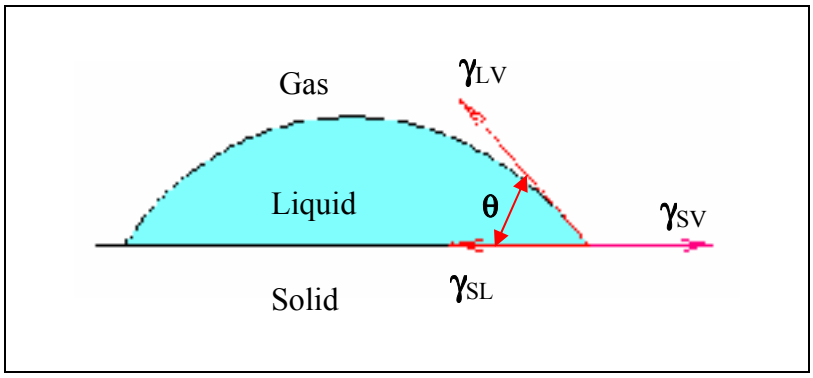

Figure 1.13 Liquid droplet on a solid substrate.

The wettability is expressed conventionally in terms of contact angle (θ) of a droplet of a liquid metal that is on a solid substrate (Fig. 1.13).

The particle wettability is good when the contact angle $\theta \leq \pi/2$, and it occurs spontaneously when $\theta = 0$. The contact angle is the result of the tension balance among three interfaces: solid/liquid (γ_{SL}), liquid/vapor (γ_{LV}), and solid/vapor (γ_{SV}). These quantities are related by the relationship of Young:

$$\gamma_{LV} \bullet \cos\theta = \gamma_{SV} - \gamma_{SL} \tag{1.12}$$

It can be deduced from equation 1.12 that, to have good wettability ($\theta \leq 90^{o}$), it is necessary that the solid surface energy be greater than or equal to the energy of the solid-liquid interface ($\gamma_{SL} \leq \gamma_{SV}$). On the other hand, to have a spontaneous wetting, it is necessary that the contact angle be equal to zero, which means that the surface energy of the solid minus the energy of the solid-liquid interface must be equal to the liquid surface energy ($\gamma_{LV} = \gamma_{SV} - \gamma_{SL}$).

The thermodynamic work of adhesion between a solid and a liquid drop is expressed by Dupre's equation as follows:

$$W = \gamma_{LV} + \gamma_{SV} - \gamma_{SL} \qquad (J/m^2) \tag{1.13}$$

Substituting equation (1.12) for equation (1.13), the work of adhesion can be obtained as follows:

$$W = \gamma_{LV} (1+\cos \theta) \tag{1.14}$$

This work can be expressed in terms of force by multiplying it by the perimeter of the liquid drop. Thus, we express the adhesion force between the liquid drop and the solid as follows:

$$F_t = \gamma_{lv} (1+\cos \theta) \cdot 2\pi r_p \tag{1.15}$$

Where:

F_t : force of surface tension, N; γ_{lv} : superficial tension of the liquid/vapor interface, N/mm; r_p : particle radius, mm; θ : contact angle, deg.

The immersion of a spherical particle in a liquid can be schematized in Figure 1.14:

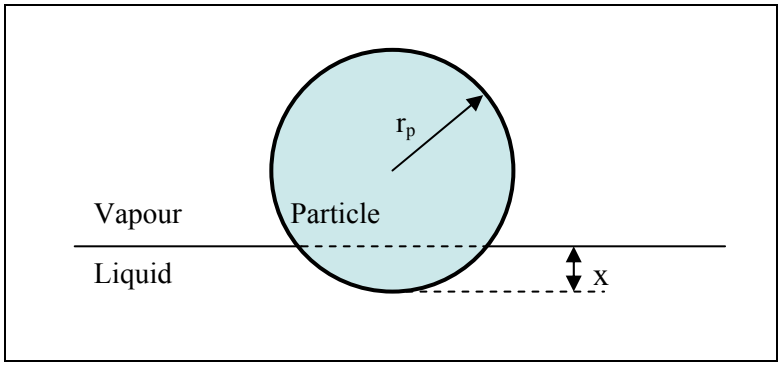

Figure 1.14 A spherical particle partially immersed in a liquid.
From Kaptay (1996, p. 461)

According to Kaptay (1996, p. 461), the interface energy of the system (Fig. 1.14) can be interpreted as follows:

$x < 0$: $$G_{\text{int}erface}^{x<0} = r_p^2 \pi \gamma_{LV} + 4 r_p^2 \pi \gamma_{PV} \quad (1.16)$$

$0 \le x \le 2\ r_p$ $$G_{\text{int}erface}^{0 \le x \le 2r_p} = \left(r_p - x\right)^2 \pi \gamma_{LV} + 2 r_p \pi x \gamma_{LP} + 2 r_p \pi \left(2 r_p - x\right) \gamma_{PV} \quad (1.17)$$

$x > 2\ r_p$ $$G_{\text{int}erface}^{x>2r_p} = r_p^2 \pi \gamma_{LV} + 4 r_p^2 \pi \gamma_{PL} \quad (1.18)$$

Where:

$G_{interface}$: interfacial energy, N·mm;

$_{P, L, V}$: particle, liquid, and vapor, respectively.

The interfacial force (F_{inter}) acting on the particle can be expressed as follows:

$$F_{\text{int}er} = \frac{d}{dx}\left(G_{\text{int}er}\right) \quad (1.19)$$

Thus, if we make the derivative of the interface energy versus the distance of immersion (x) of the particle we find:

$F_{inter} = 0$, for $x < 0$ (The particle is completely out of the liquid)

$F_{inter} = 0$, for $x > 2r_p$ (The particle is completely immersed in the liquid)

By definition, the interfacial force is the change of the interfacial energy while the particle moves into the liquid. Since the interfacial energy in Eq 1.18 (particle inside the liquid) is constant, the interfacial force is zero. Thus, we can conclude that when the particles are incorporated into the liquid metal through mechanical mixing, and they are completely immersed in the metal, there won't be any interfacial force opposing the centrifugal force. Therefore, when the particle is inside the liquid, the centrifugal force is not affected by the interface energy particle/liquid. In contrast, if the particles are not completely immersed in

the liquid and they are not perfectly wettable, in this case, it adds, to the forces opposed to the centrifugal force, a force of liquid surface tension. This force depends on the contact angle (θ). When the contact angle is zero, the wettability of the particle is spontaneous and the force of surface tension is zero.

In the case where the particle is not completely immersed in the liquid ($0 \leq x \leq 2r_P$), Kaptay (1996, p. 462) shows that the interfacial force acting on the particle is given by the following equation:

$$F_{interf} = -2\pi\gamma_{LV}[r_p(\cos\theta + 1) - x] \tag{1.20}$$

From this equation we can show that when the particle is completely immersed in the liquid ($x = 2r_P$, $\cos\theta = 1$), the interfacial force acting on the particle becomes zero:

$$F_{interf} = -2\pi\gamma_{LV}[r_p(1+1) - 2.r_p] = 0 \tag{1.21}$$

1.4.8 Influence of alloy type and characteristics

The matrix and heat treatment are both important for the mechanical properties of the composite and for the ease of the particles' incorporation. For example, according to Lloyd (1989, p. 162), the formation of carbides decreases the fluidity and thus makes it more difficult for the material to flow.

Villar and Masounave (technique de l'ingénieur, M 2448, 1996, p. 9) indicate that the wrought alloys (extrusion, forging, etc.) with low concentrations of silicon, like the 6061 alloy, are used primarily with alumina particles (Al_2O_3)—rather than silicon carbide particles (SiC)—in order to prevent the formation of aluminum carbide Al_4C_3. Casting aluminum alloys, on the other hand, are often used with SiC particles. The high concentration of silicon in the matrix slows the formation of Al_4C_3 even at high temperatures, and it provides good

flow ability. In addition, Villar and Masounave indicate that if the temperature is too high, a number of reactions between the particles and the metal can occur. These chemical reactions may be favorable or not, as explained in the following text.

$$4\ Al + 3\ SiC \Leftrightarrow Al_4C_3 + 3\ Si \tag{1.22}$$

The formation of aluminum carbide is not favorable. It forms on the particles and is soluble in water; therefore, it weakens the bond with the matrix. Furthermore, the formation of this carbide seriously degrades the fluidity, resistance to corrosion, and mechanical properties. To limit the carbide's formation, the Si content must be high enough. Generally, for a concentration of Si higher than 7% and for temperatures below 750 °C, the formation of this carbide is very limited. On the other hand, two types of interface reactions can occur with alumina particles:

$$3\ Mg + Al_2O_3 \Leftrightarrow 2\ Al + 3\ MgO \tag{1.23}$$

$$3\ Mg + 4\ Al_2O_3 \Leftrightarrow 2\ Al + 3\ MgAl_2O_4\ (spinel) \tag{1.24}$$

These reactions are possible with small amounts of Mg (less than 1% by mass, depending on temperature). The first reaction is particularly favored at high levels of magnesium. The presence of a layer of spinel is not always detrimental to mechanical properties. In the case of alumina particles, the formation of spinel ($MgAl_2O_4$) does not affect the characteristic of toughness.

1.5 Problem

During gravity casting, centrifugal casting, or squeeze casting of materials, a macrosegregation of phases may occur through the matrix under the influence of solidification fronts advancing from opposite sides. Solidification fronts advancing through the section push the last liquid to fill the area of shrinkage and thermal contraction near the

final solidification point where the two solidification fronts meet, causing an increase in the concentration of the eutectic in this area of the section. The macrosegregation of the last liquid (eutectic) and the change in its concentration across the section affect the mechanical and physical properties of the casting and produce areas of weakness where the toughness is low and the ductility is small. Moreover, the macrosegregation phenomenon depends on the initial pouring and mold temperatures, on the speed of solidification, and on the alloy composition and process parameters (rotation speed and thickness of the part section). The reduction of macrosegregation, using the process parameters, is limited. The lower initial pouring and mold temperatures decreases the solidification time and the rate of variation of macrosegregation, but may cause a defective and poorly formed surface, especially when the rotation speed is low. A subsequent heat treatment of the castings does not lead to the reduction of macrosegregation. Macrosegregation can affect the effectiveness of the heat treatment process on microstructure and properties of the castings. Moreover, the macrosegregation of phases can also occur during the casting of metal matrix composites, affecting the microstructure and the distribution of phases.

Very few are the studies that have examined the macrosegregation of phases and changes in the concentration of the eutectic that occurs across the casting section during solidification. Most studies have examined, during centrifugal casting, the macrosegregation of alloying elements such as aluminum and the influence of alloying additions on the microstructure.

In addition, in our research, we intended to produce a graded metal matrix composite reinforced by hard and wear-resistant ceramic particles. This composite must have varied and specific mechanical properties and high wear resistance, while having a lower weight compared to the parts used traditionally to resist friction. The difficulty on producing such parts and the need for particle-reinforced graded composites at the critical points of the section pushed us to use centrifugal casting technology. Centrifugal acceleration allows controlling the distribution and the degree of particle graduation at the desired locations of the section where the load and the stress are critical and high.

The casting of a graduated composite by centrifugation requires a good control of experimental parameters (rotation speed, mold and pouring temperatures, and cooling rate). Controlling the cooling rate, the change of viscosity with temperature, and the variation of centrifugal radius with the displacement of particles influences the graduation degree of the latter and may limit or increase their segregation to the outer/inner casting surface, simultaneously affecting the mechanical properties and wear resistance of the composite.

According to Stokes' law, which expresses the velocity of a solid particle in a liquid, the particle moves with a constant velocity and zero acceleration. The traditional models for particles' segregation, using Stokes' law, do not take into account the variation in the particle velocity due to the change in the liquid metal viscosity during the cooling process. In fact, the viscosity of the liquid metal changes during cooling according to the initial pouring and mold temperatures. On the other hand, the centrifugal radius is not constant over time. The combination and the competition between the variations of the centrifugal radius and viscosity of liquid metal through the matrix generates an acceleration/deceleration of the particles. This can affect the particles' displacement and segregation and change their concentration on the inner/outer casting surface and across the section.

Most studies found in literature on centrifugal casting of graduated composites were done using viscosity and centrifugal radius as constants. Some authors, such as Forster et al. (2003, p. 1217), have assumed that viscosity remains constant during the segregation of particles, which is not the case in practice. Others, as Lajoye and Suery (1988, p. 16), indicated that the increase in viscosity during cooling affects the segregation of the particles, although their studies were conducted with constant viscosity. Moreover, the viscosities used by different authors do not match the initial temperature of the molten metal. For example, Lajoye and Suery (1988) use a high viscosity of 0.0025 Pa.s; whereas, for the same parameters and experimental conditions, the viscosity used by Panda et al. (2006) is 0.002 Pa.s.

For reasons mentioned in the paragraph above, it comes that the phenomenon of phase macrosegregation will be of special interest in our research. The macrosegregation of the

interdendritic liquid and the microstructure will be studied and analyzed. In addition, modeling of the speeds of solidification fronts and of the zone of maximum eutectic macrosegregation through the matrix will be performed. This will permit us to analyze, taking into account the initial pouring and mold temperatures, the influence of solidification rate and speeds of solidification fronts on the microstructures, eutectic macrosegregation, and the last point of solidification across the section. In addition, a recommendation to reduce and drive away the zone of maximum macrosegregation from the critical surface of the part will be established to reduce the risk of failure produced by low toughness and ductility in the area of macrosegregation.

In our research, the macrosegregation of phases is studied and modeled during the centrifugal casting of hypereutectic ZA8 zinc-aluminum alloy. The microstructure of the alloy, which contains a high eutectic concentration, permits us to better identify and model the segregation of phases during solidification. On the other hand, to better control – during centrifugation – the volume fraction and the degree of the particles' graduation across the section, we model the segregation of particles while discretizing Stokes' law in time to reflect the influence of the change in pouring viscosity combined with the variation in centrifugal radius, on the segregation of particles. The variation of the particles' volume fraction on the inner/outer casting surface and across the section can lead to a change in the composites' properties.

1.6 Methodology

The methodology of the research is summarized as follows:

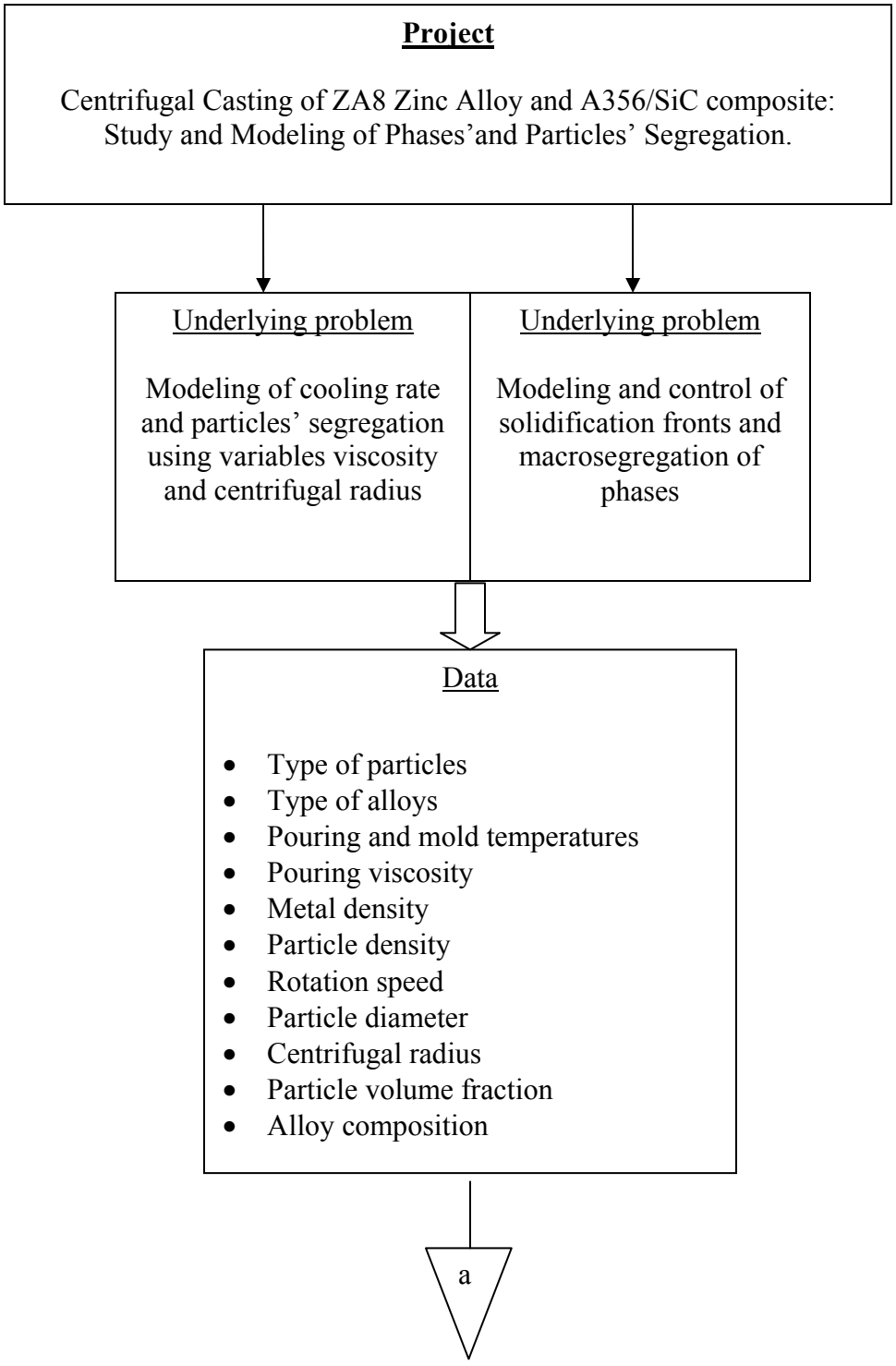
Project
Centrifugal Casting of ZA8 Zinc Alloy and A356/SiC composite: Study and Modeling of Phases'and Particles' Segregation.
Underlying problem
Modeling of cooling rate and particles' segregation using variables viscosity and centrifugal radius
Underlying problem
Modeling and control of solidification fronts and macrosegregation of phases
Data
Type of particles
Type of alloys
Pouring and mold temperatures
Pouring viscosity
Metal density
Particle density
Rotation speed
Particle diameter
Centrifugal radius
Particle volume fraction
Alloy composition
a

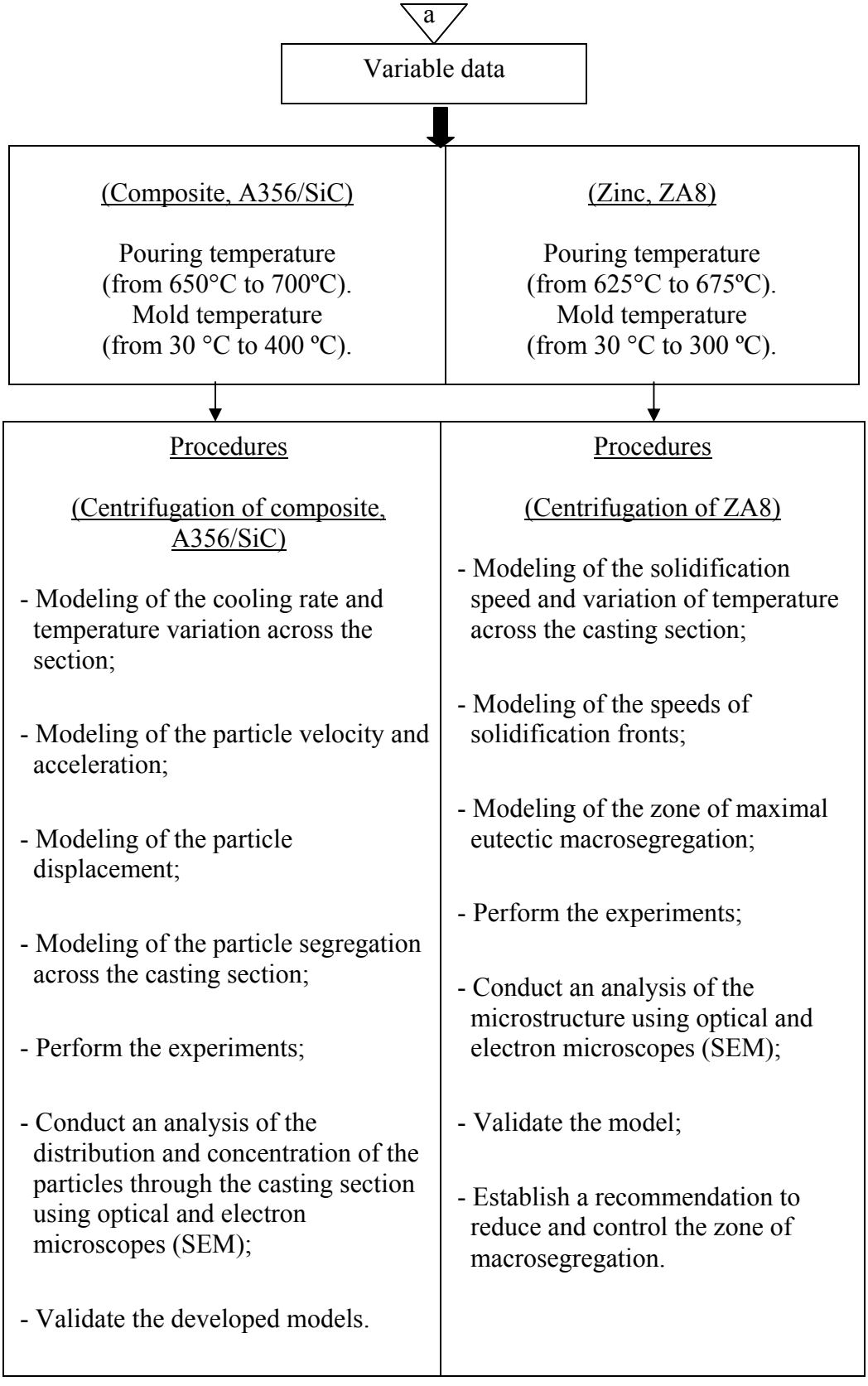
a
Variable data
(Composite, A356/SiC)
Pouring temperature
(from 650°C to 700ºC).
Mold temperature
(from 30 °C to 400 ºC).
(Zinc, ZA8)
Pouring temperature
(from 625°C to 675ºC).
Mold temperature
(from 30 °C to 300 ºC).
Procedures
(Centrifugation of composite, A356/SiC)
- Modeling of the cooling rate and temperature variation across the section;
- Modeling of the particle velocity and acceleration;
- Modeling of the particle displacement;
- Modeling of the particle segregation across the casting section;
- Perform the experiments;
- Conduct an analysis of the distribution and concentration of the particles through the casting section using optical and electron microscopes (SEM);
- Validate the developed models.
Procedures
(Centrifugation of ZA8)
- Modeling of the solidification speed and variation of temperature across the casting section;
- Modeling of the speeds of solidification fronts;
- Modeling of the zone of maximal eutectic macrosegregation;
- Perform the experiments;
- Conduct an analysis of the microstructure using optical and electron microscopes (SEM);
- Validate the model;
- Establish a recommendation to reduce and control the zone of macrosegregation.

1.7 Conclusions

The analysis of the research conducted by various authors allows us to conclude the following:

- During centrifugal casting, macrosegregation of alloying elements and phases can be generated through the matrix, which changes the morphology and uniformity of the microstructure and affects the properties of the casting. The macrosegregation of the eutectic has been studied very little. The eutectic forms a brittle phase that moves across the section, depending on experimental conditions, solidification rate, and solidification fronts, changing the concentration of phases and affecting their distribution. This pushes us to model the speeds of solidification fronts and eutectic macrosegregation through the matrix in order to limit and control the zone of maximum macrosegregation of the last liquid. This will permit to improve the quality of the part and increase its strength, toughness, and reliability in service.

- In order to model the segregation of the particles during centrifugal casting of MMC_P, Stokes' law has been used by different authors with a constant particle velocity. Modeling the segregation of particles by most authors does not take into account the increase of viscosity of the liquid metal with a drop in temperature, or the variation of the centrifugal radius with the displacement of the particles. This incentivizes us to discretize the velocity of the particles over time using Stokes' law. This discretization reflects the impact of the change in the particles' velocity and acceleration on their segregation and volume fraction across the casting section.

- The distribution of the particles along the radial direction of the part section varies depending on the variation of the rotation speed, particle size and concentration, and cooling time. The distribution of the particles is controlled by the cooling time combined with the experimental conditions and parameters, while the homogeneity of the casting surface is controlled mainly by the rotational and solidification speeds.

- The wear rate of MMC_P is related to the particle volume fraction and size. The wear rate increases with decreasing particle size. On the other hand, when the particles are of large sizes, the minimum wear rate occurs with a volume fraction of particles of 10 %V.

- The low wettability of the particles affects their incorporation in the liquid matrix and can cause their agglomeration, affecting – at the same time – their distribution. For particles completely immersed in the liquid metal, the interfacial energy is constant and the interfacial force, particle-to-liquid, is zero. In contrast, if the particles are not completely immersed in the liquid metal and have a low wettability, in this case it adds to the forces opposed to the centrifugal force a force of liquid surface tension. This force depends on the contact angle (θ). When the particles are incorporated into the matrix through mechanical mixing, the interfacial force between the particle and the liquid is assumed to be zero.

CHAPTER 2

MODELING OF EUTECTIC MACROSEGREGATION IN CENTRIFUGAL CASTING OF THIN WALLED ZA8 ZINC ALLOY

2.1 Introduction

In addition to their excellent physical and mechanical properties, zinc alloys such as ZA4, ZA8, ZA12, and ZA27 are characterized by good corrosion resistance and excellent damping properties, which increases exponentially with temperature. Moreover, due to their high mechanical properties and low cost, zinc alloys can be used to replace iron and copper alloys found in many structural applications.

Several authors have studied the solidification of Zn-Al alloys and other different alloys to predict the influence of the solidification variables on the microstructure and mechanical properties. Quaresma *et al*. (2000) used an analytical heat transfer model for determining expressions for the temperature gradient and solidification rate during a unidirectional unsteady-state solidification of binary alloys. The model was an extension of the one developed earlier by Garcia and Prates (1978). Quaresma *et al*. (2000) reported that during the solidification of Al-Cu alloys, the interdendritic liquid more effectively feeds the solidification contraction for alloys having a longer mushy zone, thus leading to an increase in the tip growth rate (V_L). V_L and the cooling rate decreases with the increase in the position from the metal/mold interface while the primary-and-secondary dendrite arm spacing increase. Osorio and Garcia (2001) used this model for determining an expression for the local solidification time (t_{SL}). By using t_{SL} in the formulae derived by Kirkwood (1985), which determines the secondary dendrite arm spacing (SDAS) as a function of t_{SL}, Osorio and Garcia (2001) found that the SDAS in Zn-Al alloy increases with the increase of t_{SL}.
Furthermore, Ares et al. (2007) reported that during the directional solidification of Zn-Al alloys, a transition zone where equiaxed grains co-exist with columnar grains might form in the casting section. The position of the transition zone depends of several parameters such as

cooling rate, solidification time, temperature gradients, velocity of liquidus and solidus fronts, and recalescence. In addition, it was reported by Ares and Schvezov (2007) that the size of equiaxed grains increases with the increase in solidification time.

During casting, a macrosegregation of alloying elements, solid fragments, and growing crystals may occur in the produced part under the influence of their differences in density relative to the liquid density. Furthermore, macrosegregation may be manifested as the segregation of phases within the mushy zone. The physical displacement of phases leads to macrosegregation. This displacement is produced by the movement of liquid in the liquid–solid zone due to thermal contraction, solidification shrinkage, and density difference in the interdendritic liquid (Flemings, 1974).

According to Nadella *et al*. (2008), the relative movement between the solid and liquid phases and the solute rejection by the solid phase are the two essential conditions for macrosegregation. Macrosegregation may either be normal or inverse segregation. Macrosegregation is called normal segregation when the liquid enriched in the solute is pushed towards the hotter part or to the center of the casting under the influence of the solidification front. Convection or shrinkage-driven flow is the driving force behind this transport of the liquid phase. In contrast, macrosegregation is called inverse segregation when the peripheries of the casting are enriched in the solute. In this case, macrosegregation occurs by the displacement of the enriched solute liquid towards the casting peripheries. Nadella *et al*. (2008) mentioned in accordance with the analysis of Gulliver (1920) and Bauer and Arndt (1921), that inverse segregation is driven by interdendritic feeding when the liquid, which is driven by capillary forces, moves in a direction opposite that of the solidification front. Therefore, it is assumed that normal segregation occurs in equiaxed structures while inverse segregation occurs in a columnar structure because the latter provides interdendritic channels. Nadella *et al*. (2008) also report that according to Voronov (1929), the increase in the cooling rate increases the degree of inverse segregation. Furthermore, it was found by Chakrabarti (1996) that the density difference between the alloying elements may produce a transverse and axial segregation.

During the centrifugal casting of zinc-aluminum alloys, phases may undergo macrosegregation through the casting section. The properties of this macrosegregation depends on the initial pouring and mold temperatures, the cooling rate, the composition of the alloy, the solidification fronts, and the experimental conditions. The macrosegregation of the phases during centrifugation can cause a change in the eutectic and primary phase concentration throughout the section of the casting. Only limited success can be achieved in reducing macrosegregation using process parameters. The reduction in the initial pouring and mold temperatures reduces the solidification time and the rate of macrosegregation, but can cause a defective and poorly shaped surface. On the other hand, subsequently heating the produced part does not reduce macrosegregation.

G. Chen *et al*. (1999) studied the macrosegregation of aluminum in the zinc alloy ZA27, produced by centrifugation and showed that longer pouring times and lower the initial pouring temperatures reduces macrosegregation in aluminum. They also found that adding manganese (Mn) to the alloy dramatically reduces macrosegregation.

Very few studies have examined the macrosegregation of phases and the variation of the concentration that occurs in the eutectic through the casting section during solidification. This work aims to study the phase macrosegregation that can occur during the centrifugal casting of the ZA8 zinc alloy. It will allow one to analyze, based on the initial mold and pouring temperature, the influence of the cooling rate and solidification fronts on the microstructures and the macrosegregation of the eutectic through the section; the influence of the final solidification point on the maximum eutectic concentration zone and its variation across the section. From the experiments and theoretical analysis of this study, the zone through the section with the maximum concentration of eutectic was modeled.

2.2 Experimental procedures

Figure 2.1 presents the centrifugation system.

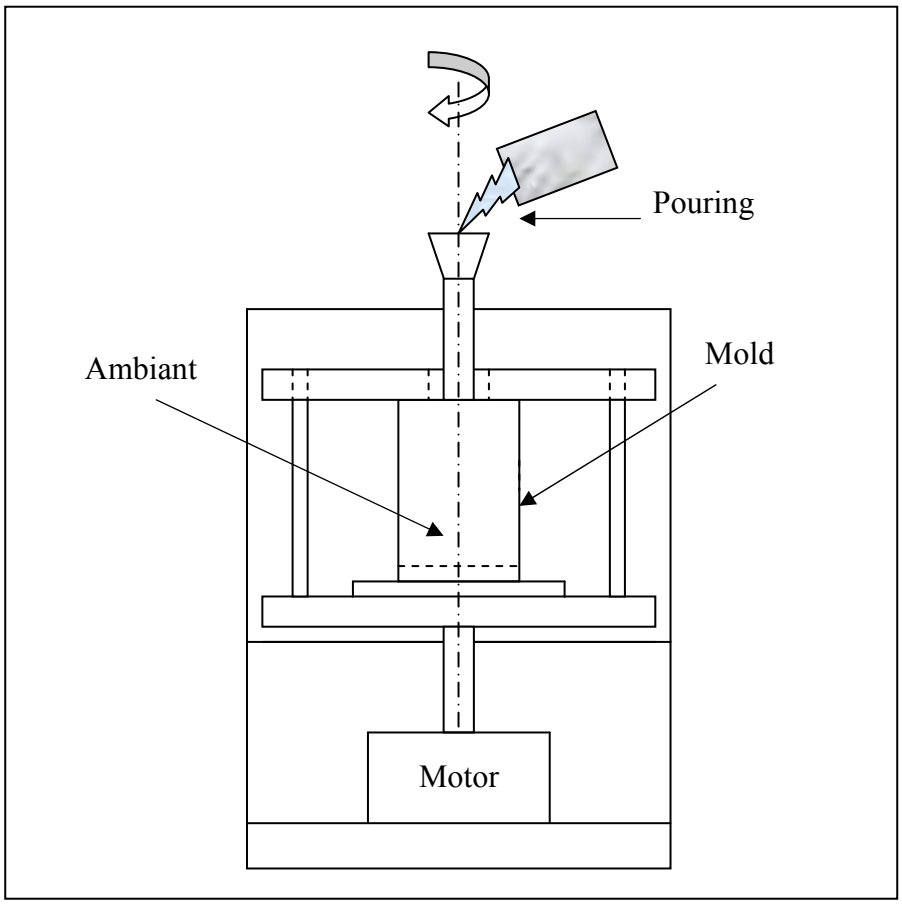

Figure 2. 1 Schematic representation of the centrifugal casting system.

A vertical centrifugation machine was used in these experiments. The alloy used was ZA8, containing 8.2% wt to 8.8% wt of aluminum as a main alloy component. An ordinary steel mold, 5 mm thick and 32 mm in diameter, was used together with a 100-micron thick hematite coating (Fe_2O_3). The dimensions of the mold and the casting, as well as the parameters used and the composition of the alloy are presented in Table 2.1.

Table 2.1 Parameters used, composition of ZA8 and dimensions of mold and casting

Rotation speed, rpm	**Initial mold temperature, K**	***Initial pouring temperature, K***
650	303, 373, 473, 573	*698, 723, 748*

Composition % ZA8							
Additions				***Impurities***			
Al	Cu	Mg	Zn	Fe max	Pb max	Cd max	*Sn max*
8.2-8.8	0.8-1.3	0.02-0.030	bal	0.065	0.005	0.005	*0.002*

Dimensions of the casting				
Length, mm	Thickness, Mm	Mass, kg	External radius, mm	*Internal radius, mm*
62	3	0.232	32	*29*

Dimensions of the mold				
Length, mm	Thickness, mm	External radius, mm	Internal radius, mm	*Length, mm*
62	*5*	*37*	*32*	*62*

Different mold and pouring temperatures were chosen in order to analyse the variation of the temperature and cooling rate on the obtained results. The temperature of pouring didn't exceed 748 K in order to avoid the oxidation of the liquid metal at high temperature.

The samples used for microscopic analysis were etched with a reagent composed of a mixture of 5 mL of HNO_3 and 100 mL of H_2O. The microstructure of ZA8 was analyzed using optical and electron microscopes.

To measure the concentration of the eutectic and the primary phase, photos of the microstructure were obtained with an optical microscope along the radial direction of the section. Each photo represented a distance of 315 microns from the inner surface of the casting. The photos were printed, and the regions of the eutectic cut and separated from the

primary phase. The phases of the eutectic and the primary β were weighed together, and then separately. Then the concentration of the phases was calculated as the ratio between each phase and the whole microstructure, as follows:

$$C_p^{Ai}\Big|_{i=0}^{n} = \frac{m_P^{Ai}}{m_T^{Ai}} \times 100\ \% \tag{2.1}$$

where $C_p^{Ai}\Big|_{i=0}^{n}$ is the mass concentration of the required phase in an area A_i, m_P^{Ai} is the mass of the required phase in an area $A_{i,,}$ and m_T^{Ai} is the total mass of all phases in an area A_i.

2.3 Analysis

2.3.1 Solidification

The heat transfer mechanism produced between the metal and the mold is transient in nature. It occurs by conduction between the mold and the metal and by forced convection by air and thermal radiation. The cooling rate and the temperature variation across the casting and mold sections were modeled through the implicit finite-difference formulation using FLUENT for a transient unsteady state of solidification. The modeling was conducted using Cartesian coordinates due to the small thickness of the part compared to its diameter (3mm/64mm).

An enthalpy-porosity technique was used in FLUENT for modeling the solidification/melting process. In this technique, the liquid fraction was computed at each iteration based on an enthalpy balance. The model accounted for the variation of the mold/metal heat transfer coefficient and the contact resistance, and the air gap formed between the mold and the metal due to the contraction of the latter during the solidification process. This calculation was done using an additional heat transfer resistance mold/metal, with a liquid fraction of less than 1.

The physical and thermophysical properties and the coefficients of heat transfer (mold/air and metal/air) are represented in Tables 2.2 and 2.3. The heat transfer coefficients were calculated based on Poirier D. & Poirier E., 1991 (Appendix III).

Table 2.2 Physical and thermophysical properties of ZA8 and steel mold used in the modeling

Thermophysical and physical properties	**Mold (steel)**	***Casting (ZA8)***
Density, ρ (kg/m^3)	7800	*6300*
Viscosity (Kg/m.s)	-------	*0.003*
Thermal conductivity, k ($W \cdot m^{-1} \cdot K^{-1}$)	42.2	*115*
Specific heat capacity, C ($J \cdot kg^{-1} \cdot K^{-1}$)	473	*435*
Heat of fusion, H_f, (J/kg)	-------	*$112 \cdot 10^3$*
Liquidus temperature, T_L, (K)	-------	*677*
Solidus temperature, T_s, (K)	-------	*648*

Table 2.3 Metal/air and mold/air heat transfer coefficients used in the modeling

Total heat transfer coefficients metal/air (convection + radiation)		
T_{metal}, K	$h_{total,\ metal/air}$ $W \cdot m^{-2} \cdot K^{-1}$	
698	104.06	*Rot. speed : 650 rpm*
723	104.21	
748	104.40	
Total heat transfer coefficients mold/air (convection + radiation)		
T_{mold}, K	$h_{total,\ mold/air}$ $W \cdot m^{-2} \cdot K^{-1}$	
303	82.84	*Rot. speed : 650 rpm*
373	84.00	
473	84.37	
573	*86.12*	

2.4 Modeling and results

2.4.1 Temperature, cooling rate, and speed of solidification front

We express the variation in the cooling rate with time and position through the casting section by the following equation:

$$V_{c,t_i}^{R_j}\Big|_{i,j=0}^{n} = \frac{T_p - T_{m,t_i}^{R_j}}{t_{s,i}} \tag{2.2}$$

where $V_{c,t_i}^{R_j}$ is the cooling rate for a given time and position (K/s), $T_{m,ti}^{Rj}$ is the metal temperature for a given time and position (K), T_p is the temperature of a superheated metal (K), and $t_{s,i}$ is the solidification time (s), with i=1,2 from the inner and outer casting surfaces, respectively.

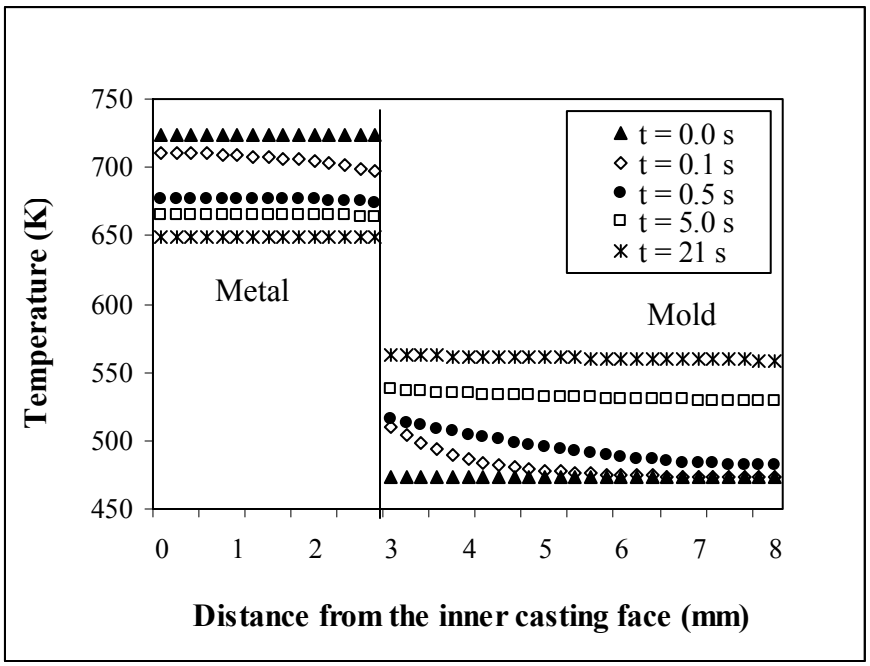

Figure 2. 2 Variation of the temperature as a function of time and position through the mold and metal sections ($T_{metal, in}$ = 723 K, $T_{mold, in}$ = 473 K).

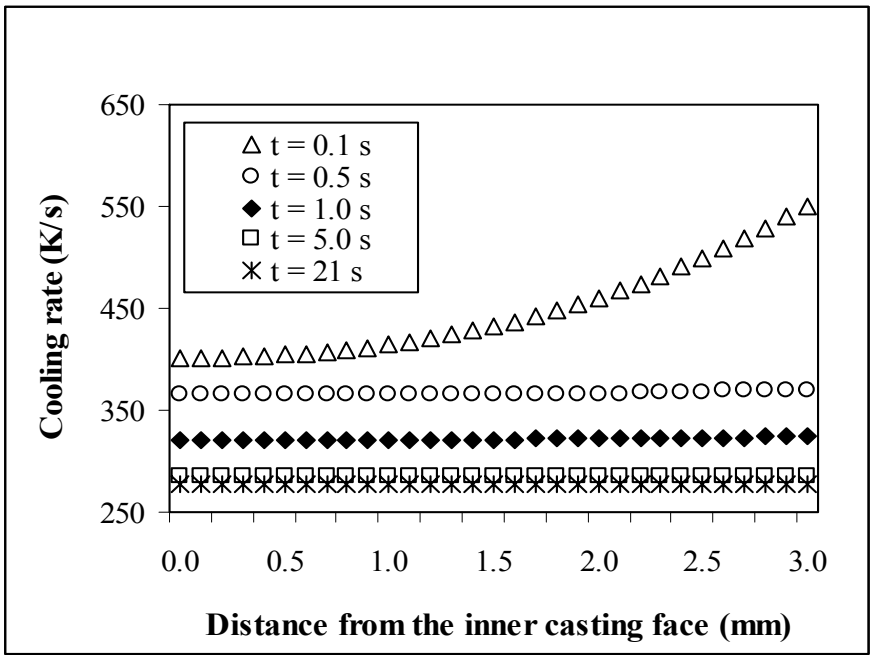

Figure 2. 3 Variation of the cooling rate as a function of time and position through the casting section ($T_{metal, in}$ = 723 K, $T_{mold, in}$ = 473 K).

The variation in the temperature and cooling rate as a function of time and position through the section is presented in Figs. 2.2 and 2.3 for a given initial pouring and mold temperatures. It can be seen (Fig. 2.2) that at the beginning of the cooling, the temperature of the metal decreases quickly with time, and the temperature variation becomes smaller during the solidification. This behavior is attributable to the heat that escapes rapidly at the beginning of cooling. Moreover, during solidification, and with the formation of primary solidification crystals, the heat transferred by internal conduction decreases, which in turn also decreases the variation in temperature and cooling rate as a function of time (Figs. 2.2 and 2.3).

The changes in the cooling rate, as a function of experimental conditions and initial pouring and mold temperatures, influences the macrosegregation caused advancing solidification fronts from the inner and outer casting surfaces, and the zones of thermal contraction generated across the section. During the solidification, two solidification fronts move through the section in opposite directions; the first, produced by conduction, advances from the mold side toward the inner surface of the casting, while the second, produced by forced convection

and radiation, advances from the inner casting surface toward the outer surface. The two solidification fronts meet at a point in the section determined by the speed of each front. This point will be the final point of solidification, which contributes due to thermal contraction and solidification shrinkage to the macrosegregation of the interdendritic liquid, and changes its concentration through the section.

We express the average speed of the solidification fronts from the inner and outer casting surfaces as follows:

$$v_{fs,i}\Big|_{i=1}^{2} = \frac{d_{fs} \cdot V_{c,i}}{T_p - T_s} \tag{2.3}$$

where $v_{sf,i}$ is the average speed of the solidification front (mm/s), with $i=1,2$ from the inner and outer casting surfaces, respectively; d_{fs} is the distance displaced by the solidification front (mm), V_c is the average cooling rate (K/s), and T_s is the solidus temperature (K).

Figs. 2.4 and 2.5 show the average speed of the solidification fronts and the average cooling rate from the inner and outer casting surfaces with different initial pouring and mold temperatures. It can be seen (Figs. 2.4 and 2.5) that in general, and according to the initial pouring and mold temperatures, the cooling rate and the speed of solidification front are higher when heat transfer is dominated by conduction between the mold and the casting than when it is dominated by forced convection and radiation between the casting and the ambient. Thus, the cooling rate and the speed of solidification front are higher while moving from the outer casting surface toward the inner one than when moving in opposite directions. As the mold/metal heat transfer occurs by conduction, the heat exchange and the rate of cooling increases and the solidification time decreases.

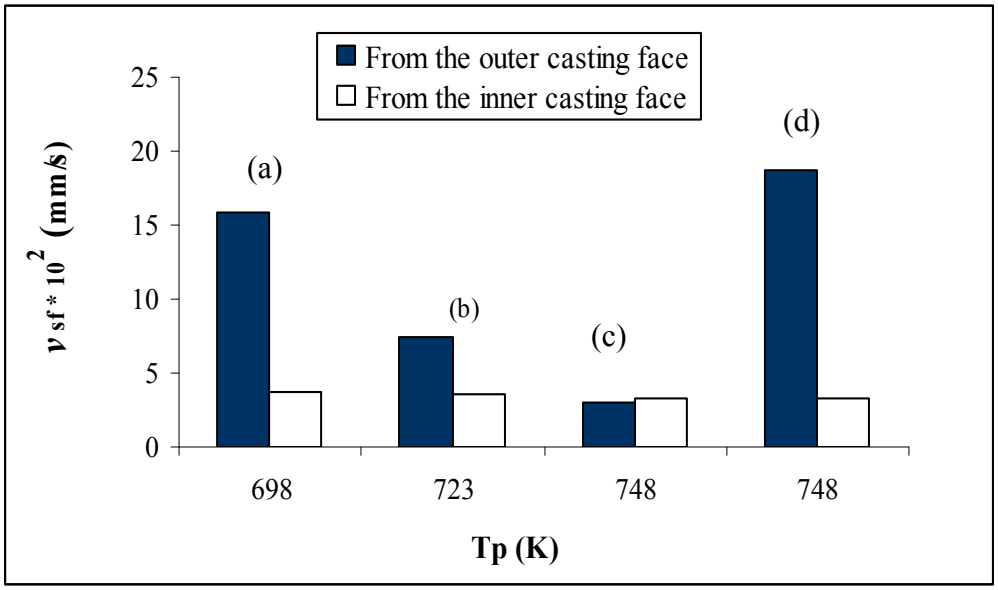

Figure 2. 4 Average speeds of solidification fronts advancing from the inner and outer casting surfaces for different initial pouring and mold temperatures: (a) T_{mold} = 373 K, $t_{s,1}$ = 81 s, $t_{s,2}$ = 19 s, (b) T_{mold} = 473 K, $t_{s,1}$ = 85 s, $t_{s,2}$ = 40 s, (c) T_{mold} = 573 K, $t_{s,1}$ = 90 s, $t_{s,2}$ = 100 s, (d) T_{mold} = 303 K, $t_{s,1}$ = 90 s, $t_{s,2}$ = 16 s.

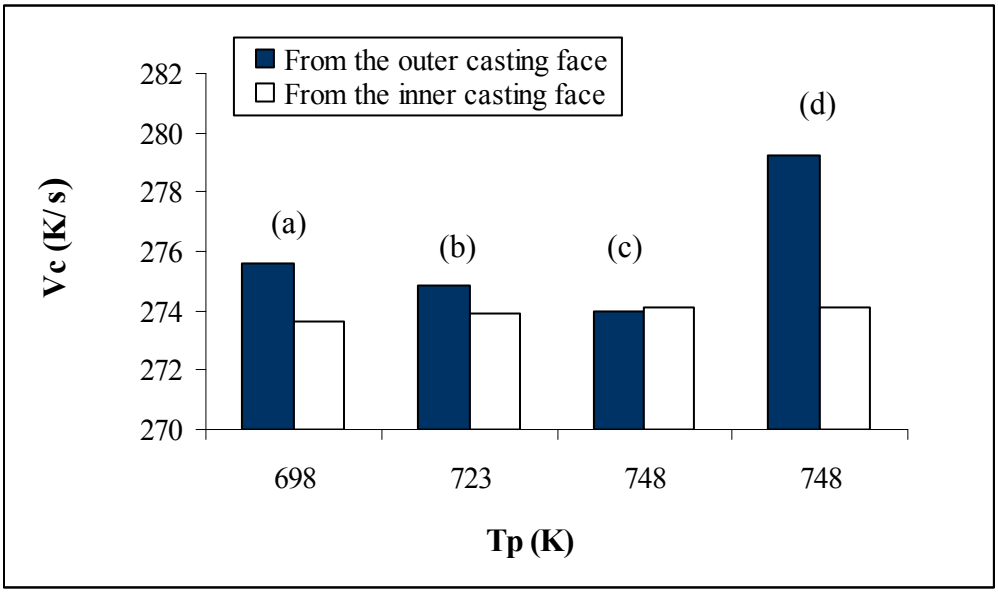

Figure 2. 5 Average cooling rate for different initial pouring and mold temperatures from the inner and outer casting surfaces: (a) T_{mold} = 373 K, (b) T_{mold} = 473 K, (c) T_{mold} = 573 K, (d) T_{mold} = 303 K.

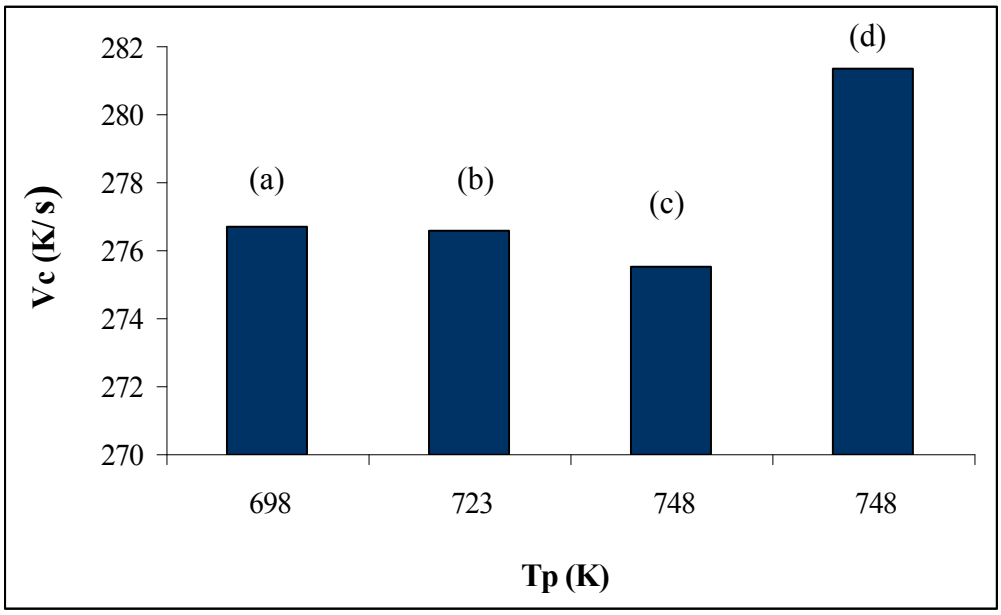

Figure 2. 6 Average cooling rate for the different initial pouring and mold temperatures, simultaneously considering the cooling from the inner and outer casting surfaces: (a) T_{mold} = 373 K, (b) T_{mold} = 473 K, (c) T_{mold} = 573 K, (d) T_{mold} = 303 K.

The cooling rate of the casting is influenced by the initial mold and pouring temperatures, and low and high temperatures can influence the cooling rate in different ways (Fig. 2.6). It can be seen in Fig. 2.6 that higher initial pouring and mold temperature lowers the cooling rate, while simultaneously considering the cooling from the inner and outer casting surfaces. The changes in the cooling rate will influence the macrosegregation. This is analyzed by examining the experimental results and the change in the eutectic concentration across the casting section.

2.4.2 Zone of the final solidification point

The zone of the final solidification point is the zone across the casting section where the two solidification fronts advancing from opposite sides intersect. During the solidification process, the flowing interdendritic liquid tends to fill shrinkage zones close to the final point of solidification. From Fig. 2.7, we express the zone of the final solidification point by

determining the distance traversed by each solidification front from the inner and outer casting surfaces when they intersect at a given position, as follows:

$$t \cdot v_{fs,1} + t \cdot v_{fs,2} = d_{fs} \tag{2.4}$$

$$t = \frac{d_{fs}}{v_{fs,1} + v_{fs,2}} \tag{2.5}$$

$$dt = \frac{dx}{v_{fs,i}} \Rightarrow t = \frac{1}{v_{fs,i}} \int_0^{S_{fs,i}} dx \tag{2.6}$$

$$t = \frac{S_{fs,i}}{v_{fs,i}} \tag{2.7}$$

By replacing Eq. (2.7) in Eq. (2.5) and deducing S, an equation that expresses the zone of the final solidification point through the casting section can be deduced:

$$S_{fs,i}\Big|_{i=1}^{2} = \frac{d_{fs} \cdot v_{fs,i}}{v_{fs,1} + v_{fs,2}} \equiv Z_{fsp} \tag{2.8}$$

where $S_{fs,i}\Big|_{i=1}^{2}$ is the distance traversed by each solidification front (i = 1, i = 2 correspond to the solidification fronts advancing from the inner and outer casting surfaces, respectively), Z_{fsp} is the zone of the final solidification point, d_{fs} is the initial distance separating the two solidification fronts, v_{fs} is the speed of solidification front.

Fig. 2.7 shows the part and the mold sections and the parameters used in Eq. (2.8).

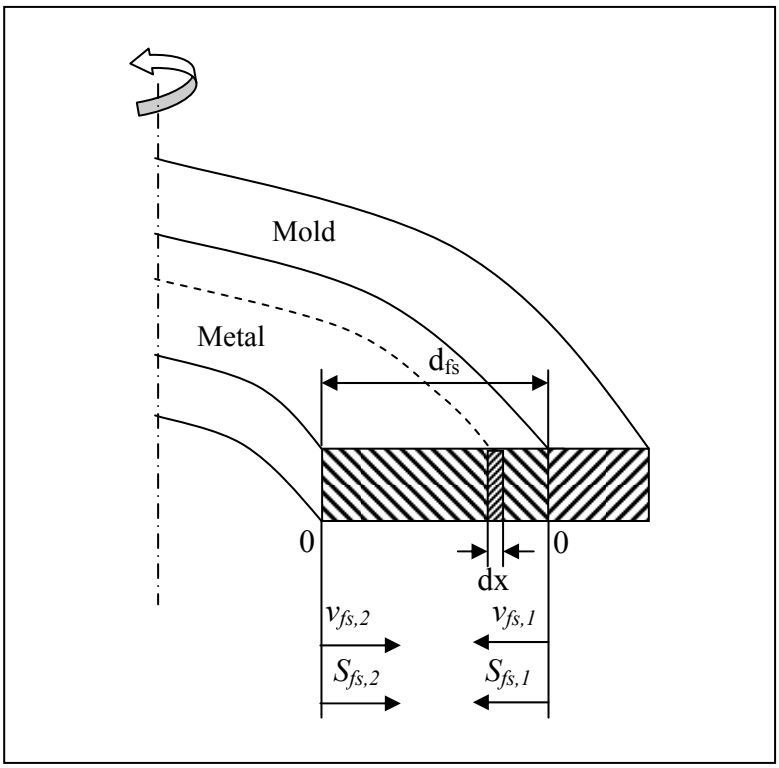

Figure 2. 7 Schematic representation of mold and casting sections and parameters used in Eq. (2.8).

Equation 2.8 allows the determination of the zone in which both solidification fronts intersect through the section. This zone will be the site of a segregation that influences the concentration of the eutectic and the primary phase as compared to the whole section. Furthermore, this zone will be the weakest throughout the section, because of the decreased toughness and ductility as the interdendritic liquid concentration in this area increases.

2.4.3 Concentration of phases through the section

Figures 2.8, 2.9, 2.10, and 2.11 show the mass percentage of the eutectic ($\alpha + \eta$) and the primary phase (β) surrounded by zinc-rich haloes as a function of the distance across the casting section. These figures are generated using different initial pouring and mold

temperatures. It is evident from these figures that the concentration of eutectic undergoes a variation through the section as a function of cooling rate and initial pouring and mold temperatures. The interdendritic liquid tends to fill the zones of thermal contraction and solidification shrinkage produced across the casting section during solidification process. Furthermore, the concentration of the eutectic reaches a maximum value at a given position across the section. The macrosegregation and the variation in the eutectic concentration are generated by the movement of the interdendritic liquid within the liquid-solid zone due to thermal contraction and solidification shrinkage, and under the influence of solidification fronts. Therefore, the macrosegregation generated during this casting appears to be a normal segregation. In this kind of segregation, the fronts of solidification advance from the inner and outer casting surfaces simultaneously, and the primary phase solidifies first, rejecting the last liquid to fill the zone of shrinkage at the final point of solidification where the two solidification fronts intersect. Thus, the concentration of the eutectic in this zone becomes higher compared to the rest of the section, simultaneously generating a reduction in the primary phase concentration in this zone.

Comparing Figs. 2.8–2.11 with Fig. 2.6, which represents the average cooling rates across the casting section for different initial pouring and mold temperatures, the variation in the eutectic concentration through the part section becomes smaller and more stable with increase in the cooling rate. With the increase in cooling rate, the primary and secondary phases solidify very quickly without allowing the primary phase and the solidification fronts to reject the interdendritic liquid or the eutectic. Furthermore, by comparing Figs. 2.8, 2.9, 2.10, and 2.11, the zone of maximal macrosegregation changes across the section relative to the distance from the inner/outer casting surface. This change is due to the ratio between the speeds of the solidification fronts advancing from opposite sides across the casting section.

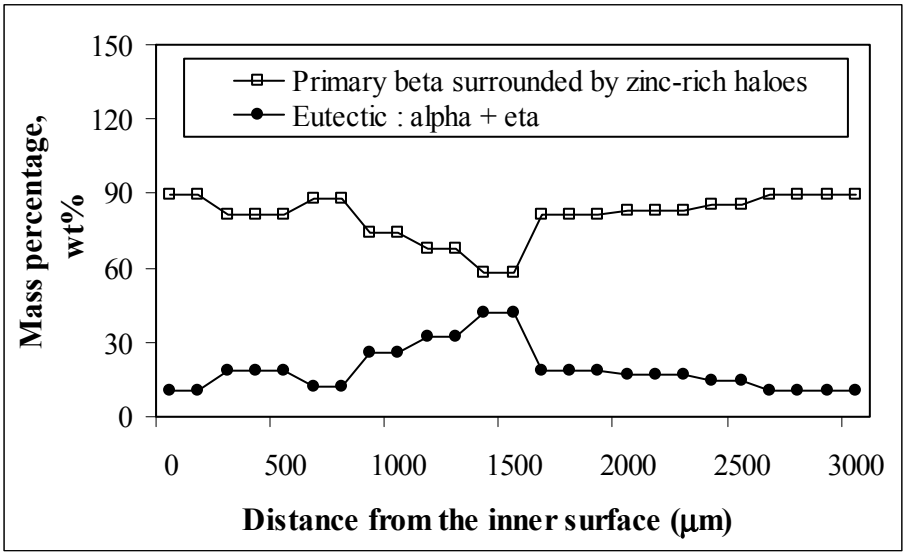

Figure 2. 8 Mass percentage across the section of the eutectic (α+η) and the primary phase (β) surrounded by zinc-rich haloes, during centrifugal casting of ZA8 ($T_{metal, in}$ = 748 K, $T_{mold, in}$ = 573 K, V_c = 275.5 K/s).

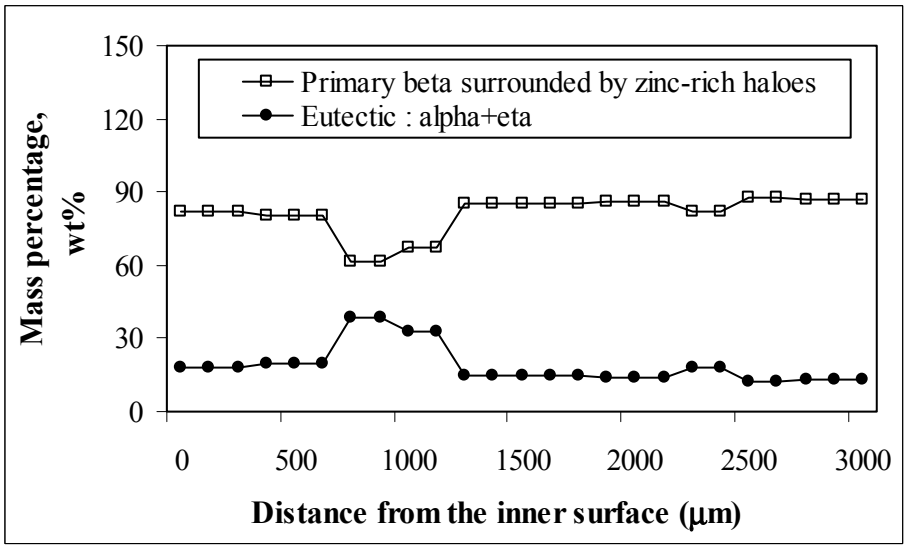

Figure 2. 9 Mass percentage across the section of the eutectic (α+η) and the primary phase (β) surrounded by zinc-rich haloes, during centrifugal casting of ZA8 ($T_{metal, in}$ = 723 K, $T_{mold, in}$ = 473 K, V_c = 276.6 K/s).

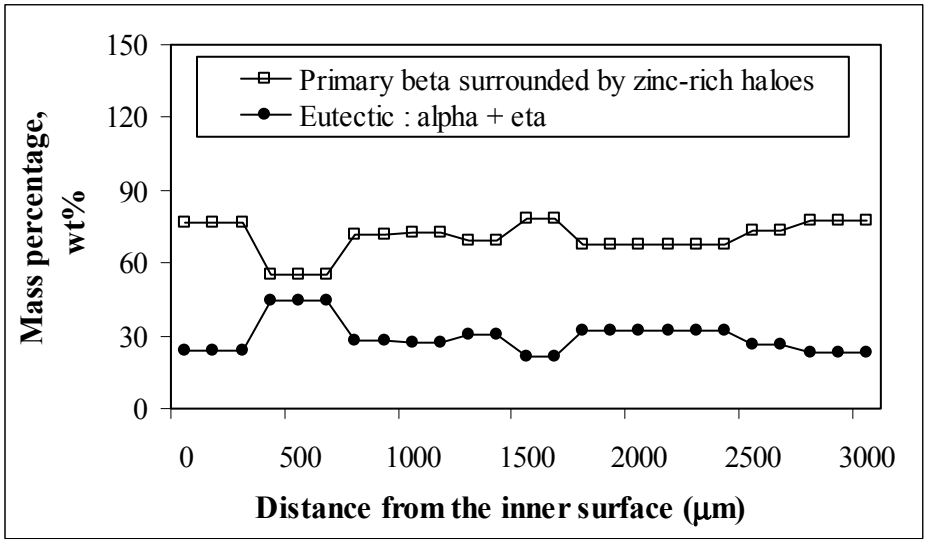

Figure 2. 10 Mass percentage across the section of the eutectic (α+η) and the primary phase (β) surrounded by zinc-rich haloes, during centrifugal casting of ZA8 ($T_{metal, in}$ = 698 K, $T_{mold, in}$ = 373 K, V_c = 276.7 K/s).

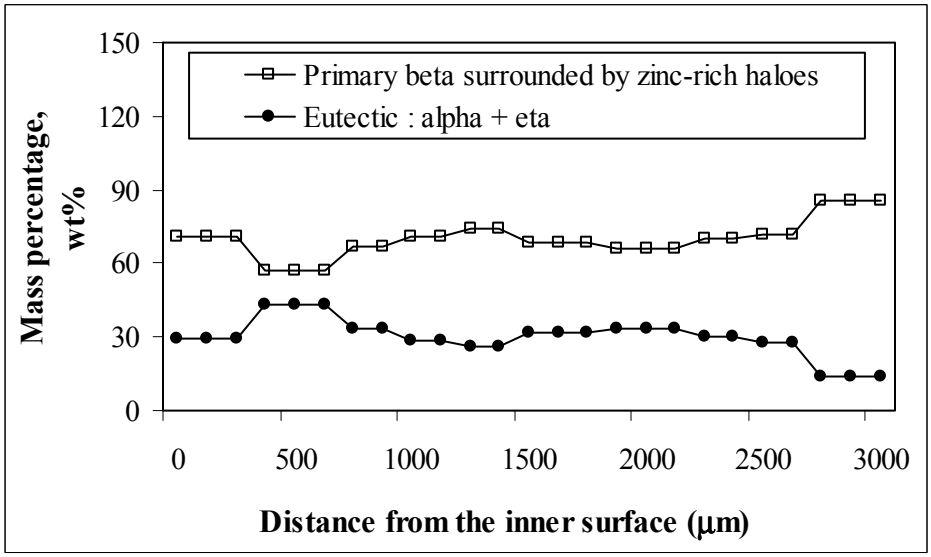

Figure 2. 11 Mass percentage across the section of the eutectic (α+η) and the primary phase (β) surrounded by zinc-rich haloes, during centrifugal casting of ZA8 ($T_{metal, in}$ = 748 K, $T_{mold, in}$ = 303 K, V_c = 281.3 K/s).

The radial distance of the part section and the zone of final solidification point as a function of the speeds of the solidification fronts produced during centrifugal casting with different initial pouring and mold temperatures are shown in Fig. 2.12. This figure was generated with the same initial mold and pouring temperature as Figs. 2.8, 2.9, 2.10, and 2.11 and shows the average speeds of solidification fronts advancing from both inner and outer casting surfaces ($v_{fs,1}$, $v_{fs,2}$), the distance they traverse before they intersect at some point through the section ($S_{fs,1}$, $S_{fs,2}$), and the zone of final solidification point (Z_{fsp}).

The values of the parameters represented on Fig. 2.12 for different initial mold and pouring temperatures are represented in Table 2.4.

Table 2.4 Values of the average speeds of solidification fronts and the distances they displace for different initial mold and pouring temperatures represented in Fig. 2.12

Variables	**(a)**	**(b)**	**(c)**	***(d)***
T_{metal} (K)	748	723	698	*748*
T_{mold} (K)	573	473	373	*303*
$v_{fs,1}$ (mm/s)	0.03	0.035	0.037	*0.033*
$v_{fs,2}$ (mm/s)	0.033	0.075	0.158	*0.187*
$S_{fs,1}$ (mm)	1.579	0.961	0.571	*0.453*
$S_{fs,2}$ (mm)	*1.421*	*2.039*	*2.429*	*2.547*

Figure 2.12 shows that the zone of intersection of solidification fronts across the part section depends on the ratio of their speeds and on the initial pouring and mold temperatures. This zone is the zone of final solidification point and the site of macrosegregation produced by the flow and segregation of the interdendritic liquid under the influence of the solidification fronts. Thus, the ratio between the solidification fronts and the zone where they intersect through the section greatly influences the segregation of the interdendritic liquid and the zone of maximal macrosegregation.

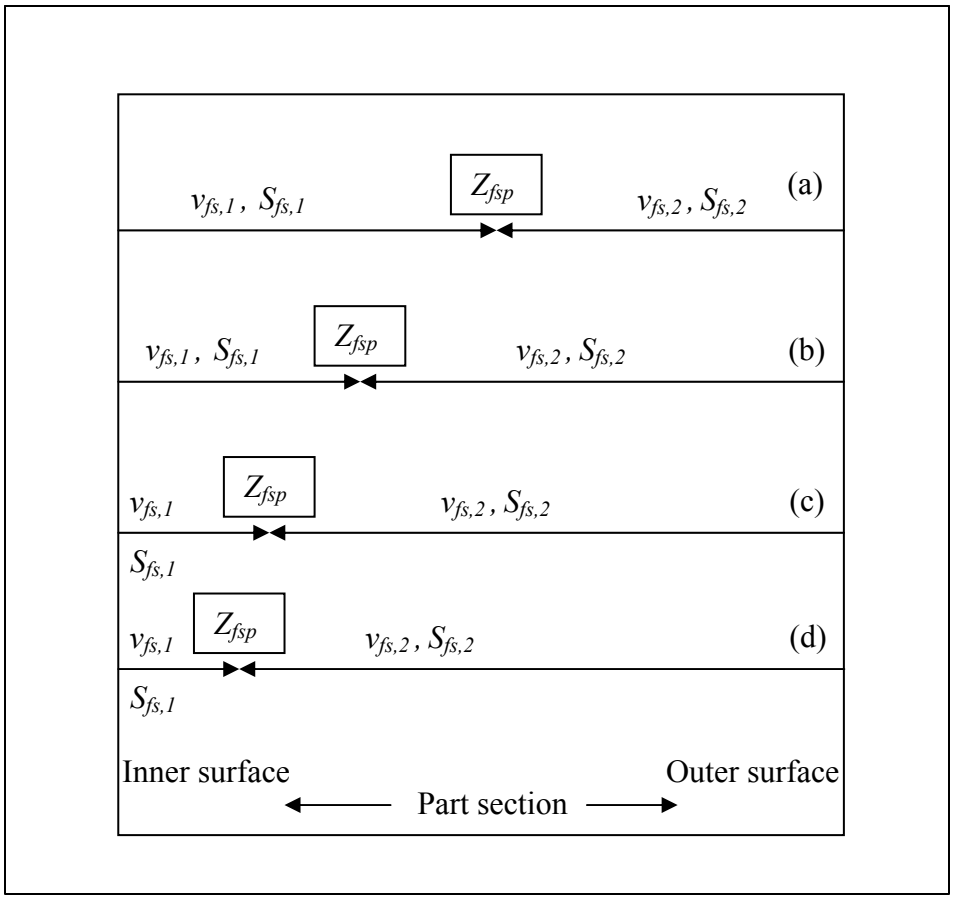

Figure 2. 12 Schematic representation of the distances displaced by the solidification fronts and of the zone of final solidification point for different initial mold and pouring temperatures: (a) T_{metal} = 748 K, T_{mold} = 573 K, (b) T_{metal} = 723 K, T_{mold} = 473 K, (c) T_{metal} = 698 K, T_{mold} = 373 K, (d) T_{metal} = 748 K, T_{mold} = 303 K.

In comparing Fig. 2.12 a, b, c and d with Figs. 2.8, 2.9, 2.10, and 2.11, respectively, the zone of macrosegregation formed at the area where the two solidification fronts intersect corresponds to the zone of maximum macrosegregation and highest eutectic concentration. Thus, the maximum macrosegregation of eutectic produced during centrifugation is generated in the zone of the final point of solidification; hence, this zone can be expressed by Eq. (2.8), which determines the zone of final solidification point generated during solidification process. Therefore, we can express Eq. (2.8) as follows:

$$S_{fs,i}\Big|_{i=1}^{2} = \frac{d_{fs} \cdot v_{fs,i}}{v_{fs,1} + v_{fs,2}} \equiv Z_{fsp} \equiv C_{Eut,\max} \tag{2.9}$$

where $C_{Eut,max}$ is the maximal concentration of eutectic in wt %, and $v_{fs,1}$, $v_{fs,2}$ are the speeds of the solidification fronts advancing from different sides.

2.5 Microstructures

The microstructure of hypereutectic ZA8 and ZA12 alloys is predominantly composed of the primary dendrite phase (β) and eutectic structure composed of aluminum-rich (α) and zinc-rich (η) phases. Furthermore, it was reported by Çay and Kurnaz (2005) that during gravity and squeeze casting of Zn-Al alloys (ZA8- ZA12, and ZA27) zinc-rich haloes may be found around the primary phase (β). On the other hand, a ε phase rich in copper (Cu) can be distributed in interdendrite (Ma et al. 2004).

Figures 2.13 a, b, c and d show the microstructure and the eutectic segregation at different locations through the section and for different initial pouring and mold temperatures corresponding to the temperatures shown in Figs. 2.8, 2.9, 2.10, and 2.11, respectively. In these figures, the segregation and the increase in the concentration of the eutectic at different distances from the inner and outer casting surfaces, depending on the cooling rate and speeds of the solidification fronts, are clearly seen. In addition, it can be seen in these figures that the equiaxed grains dominate, which promotes (according to Nadella *et al*. 2008) the normal segregation through the casting section. However, it can be found inside of the matrix, areas where equiaxed grains co-exist with columnar grains, especially when the cooling rate was high (Fig. 2.13 d).

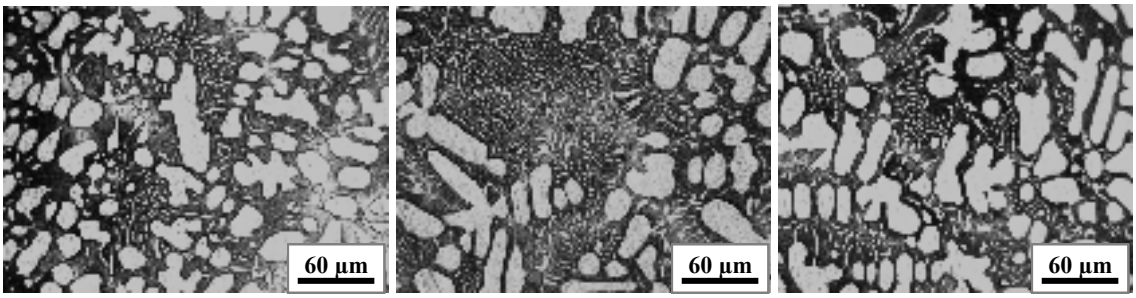

0-315 µm 1575-1890 µm 2530-2845 µm

a) (T_{metal} = 748 K, T_{mold} = 573 K, $v_{fs,1}$ = 0.03 mm/s, $v_{fs,2}$ = 0.033 mm/s, V_c =275.5 K/s)

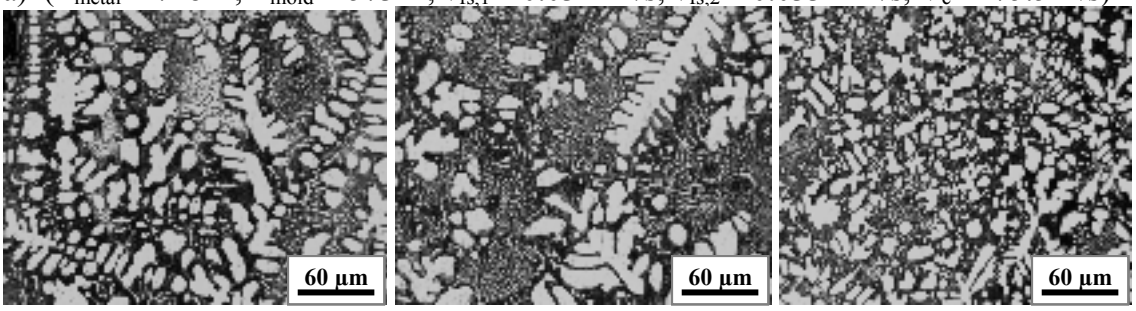

0-315 µm 630-945 µm 2685-3000 µm

b) (T_{metal} = 723 K, T_{mold} = 473 K, $v_{fs,1}$ = 0.035 mm/s, $v_{fs,2}$ = 0.075 mm/s, V_c =276.6 K/s)

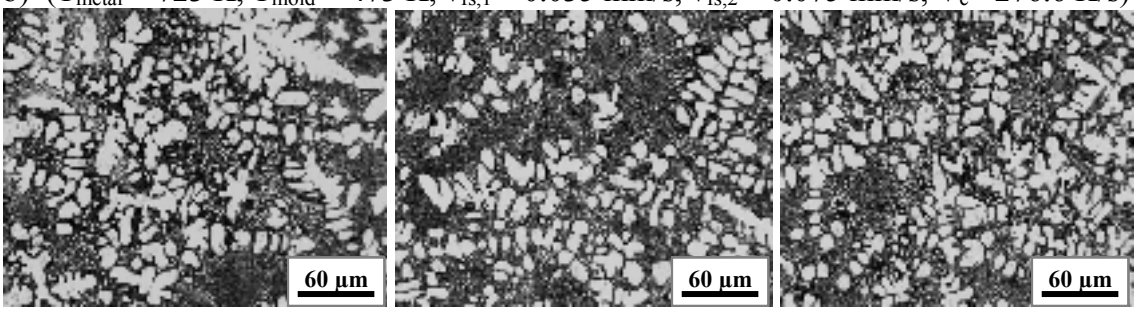

0-315 µm 315-630 µm 1575-1890 µm

c) (T_{metal} = 698 K, T_{mold} = 373 K, $v_{fs,1}$ = 0.037 mm/s, $v_{fs,2}$ = 0.158 mm/s, V_c =276.7 K/s)

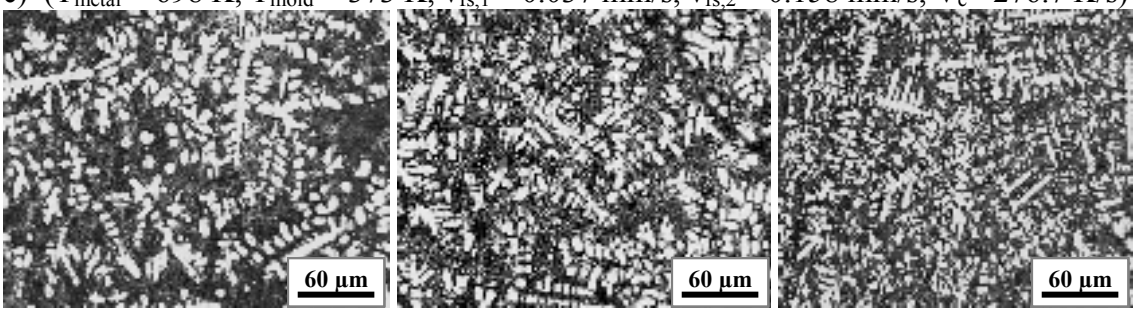

315-630 µm 1575-1890 µm 2685-3000 µm

d) (T_{metal} = 748 K, T_{mold} = 303 K, $v_{fs,1}$ = 0.033 mm/s, $v_{fs,2}$ = 0.187 mm/s, V_c =281.3 K/s)

Figure 2. 13 Microstructures representing the variation in the concentration of the eutectic and primary phase across the section (distance from the inner casting surface).

Note, from Figs. 2.13 a, b, c, and d, that the dendrite size and the microstructure become finer as the cooling rate (V_c) increases. Furthermore, aluminum and the high rate of solidification generated during centrifugal casting act as a grain refiner. On the other hand, the formation of equiaxed structures is an important factor in increasing the strength, ductility, and toughness of the alloy.

The eutectic ($\alpha + \eta$) may be lamellar or granular in structure. The increased cooling rate and the presence of impurities change the structure and forms granular eutectic (Fig. 2.14 a), while for a smaller cooling rate (Fig. 2.14 b), the eutectic becomes lamellar. This change in the morphology of the formation of the eutectic is related to the temperature gradient in the liquid-solid interface and to the growth velocity. For a small growth rate and a small temperature gradient, the eutectic forms with a lamellar structure.

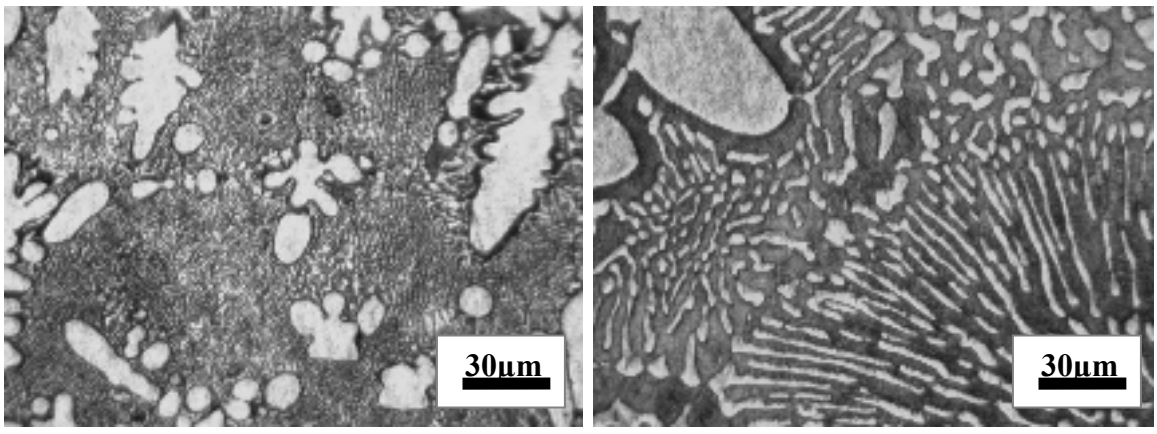

a) Cooling rate: 281.3 K/s ($T_{metal,in}$ = 748 K, $T_{mold,in}$ = 303 K)

b) Cooling rate: 275.5 K/s ($T_{metal,in}$ = 748 K, $T_{mold,in}$ = 573 K)

Figure 2. 14 Structure of eutectic for different cooling rates.

Figures 2.15 a, b are scanning electron microscope (SEM) images showing the microstructure and phase distribution in centrifugal casting of ZA8 alloy. The microstructure is formed of primary dendrites (β) and a eutectic matrix ($\alpha+\eta$). In addition, zinc-rich haloes

consisting of zinc as a main component and very small concentrations of aluminum and copper can be found around the primary phase (β). On the other hand, the space between the eutectic components (α and η) is small due to the relatively high speed of solidification. These results agree with those of Fatih Çay and S. Can Kurnaz (2005).

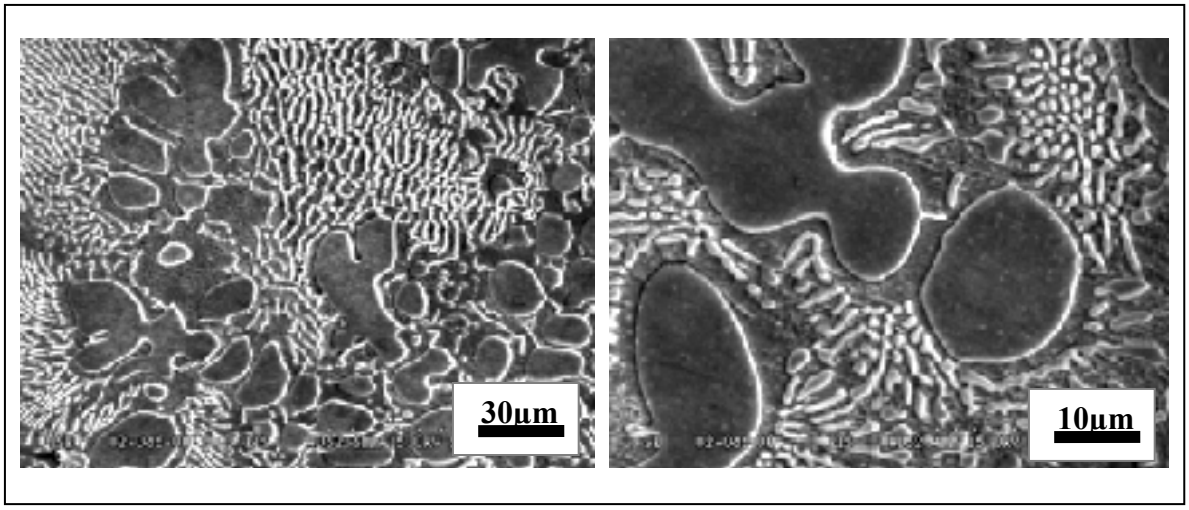

Figure 2. 15 SEM microstructure of centrifugal-cast ZA8 alloy: ($T_{metal,in}$ = 748 K, $T_{mold,in}$ = 573 K, V_c = 275.5 K/s).

2.6 Discussions

Centrifugal casting leads to the refinement of grain size, but can also lead to a heterogeneous distribution of phases, a macrosegregation, and a change in the eutectic concentration through the section. These unwanted effects can be reduced by controlling the initial casting and mold temperatures, and the cooling rate. In addition, the zone, through the section, of the final solidification point to which the maximum segregation of the eutectic corresponds, can be controlled by varying the ratio between the two solidification fronts advancing from the internal and external surfaces. Figure 2.16 shows the influence of the speed ratios of solidification fronts on the zone of maximum eutectic concentration and segregation across the section for different initial pouring and mold temperatures used in this work.

If the speed of a solidification front advancing from the external casting surface is too high compared to a low speed when advancing from the inner surface, a macrosegregation zone and a maximum eutectic concentration form close to the inner surface, and vice versa. In contrast, two solidification fronts advancing with similar speeds from the outer and inner surfaces produce a zone of maximum eutectic concentration at the center of the section.

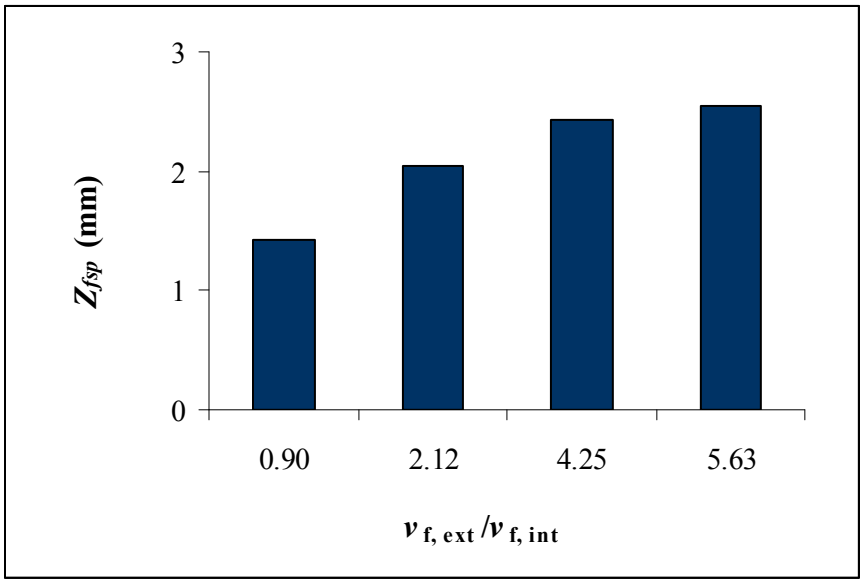

Figure 2. 16 Zone of final solidification point and maximum eutectic concentration from the outer surface of the casting as a function of the ratio between the speeds of solidification fronts for a 3mm thick section.

As a result of the normal segregation, the interdendritic liquid (α + η) is pushed during solidification process to fill the zones of solidification shrinkage and thermal contraction through the section and at the final point of solidification, which promotes the increase in the eutectic concentration away from the inner and outer casting surfaces, while the concentration of the primary phase (β) decreases. Thus, the macrosegregation of phases during centrifugal casting and solidification process can produce, through the casting section, higher or lower concentrations of eutectic and primary phase depending on cooling rate, solidification speed, and position through the section. The change in the concentration of the eutectic and primary phase through the section is influenced by several parameters.

Phenomena such as cooling rate, ratio between the speed of solidification fronts, solidification shrinkage, grain structure, and final solidification point affect the maximum segregation of the eutectic. An increase or decrease in β and α + η through the casting section are the result of a combination of these parameters.

According to our study, the ratio between the speeds of the solidification fronts influence the zone of maximal eutectic macrosegregation. The centrifugal force may contribute to the macrosegregation of alloying elements, growing crystals, and solid fragments depending on the initial pouring temperature, cooling rate, and diameter of grains before the grains are captured by the solidification front or attached to other grains. On the other hand, according to Stokes law, for a particle suspended in a liquid, a small particle diameter and a high liquid metal viscosity result in a low particle velocity. Therefore, the displacement of small diameter grains in the mushy zone varies and may be small before they are blocked by the solidification front depending on the initial pouring temperature, cooling rate, pouring time, growth velocity, and viscosity increase during the solidification process. The influence of the centrifugal force on grains displacement decreases with the decrease in their diameter and the increase in solidification speed, growth velocity, and liquid metal viscosity during the solidification process.

Furthermore, the eutectic and primary phase concentrations on the inner and outer casting surfaces may change under the influence of the centrifugal force due to the difference in densities between the primary phase and the remaining melt (G. Chen *et al*. 1999). On the other hand, in other types of casting, such as sand casting, the denser phase tends to segregate or to settle to the bottom of the casting due to gravity.

The type of segregation produced during casting is influenced by the dimension of the casting and microstructure formation. According to Nadella *et al*. (2008), the transition from normal to inverse segregation occurs with increasing thickness of the solidified shell of an ingot. The inverse segregation is more noticeable in columnar or coarse dendritic structures than in equiaxed structure.

From our results, the maximum segregation and concentration of the eutectic across the casting section are found in the zone of the final solidification point. Moreover, according to Flemings (1974), the interdendritic liquid flow due to thermal contraction and solidification shrinkage appears to be the most important cause of phase macrosegregation. A concentration gradient of the interdendritic liquid occurs across the section and tends to compensate for the zones of contraction and shrinkage under the influence of the solidification fronts. Therefore, the macrosegregation generated is a normal segregation and the zone of maximal eutectic macrosegregation across the casting section can be characterized by the flow of the interdendritic liquid towards the final point of solidification. While this type of macrosegregation compensates for the porosity and improves the properties, it forms a brittle phase that reduces the ductility of the material and affects its resilience.

The change in the concentration of the eutectic and primary phase during centrifugal casting varies with the variation in initial pouring and mold temperatures. The boundary conditions used during casting and the change in the speeds of solidification fronts and cooling rate have an important impact on the rate of macrosegregation through the section and the zone of maximum macrosegregation of the eutectic. This zone is the weakest point in the section, and can lead to low mechanical properties, low ductility and decreased toughness. Controlling the maximum macrosegregation zone is very important and may prevent possible premature failure, reduces distortion, and increases the life of the part in service.

2.7 Conclusions

In this work, the zone of final solidification point, the zone of maximum macrosegregation of eutectic, and the microstructure were studied. The authors conclude the following:

- During centrifugal casting and with the conditions used in this study, the interdendritic liquid macrosegregation is a normal segregation, and the rate of the change in the eutectic concentration across the section depend on the boundary conditions used, the initial

pouring and mold temperatures, the cooling rate, and the ratio between the speeds of the solidification fronts.

- The zone of the maximum concentration of the eutectic generated during centrifugal casting corresponds to the zone of the final solidification point. This zone is created under the influence of the solidification fronts that push the interdendritic liquid to the zone of the final solidification point. The shrinkage-driven flow is the driving force behind the interdendritic flow.

- A high cooling rate reduces the rate of change in the eutectic concentration through the section. The zone of the maximum macrosegregation of the eutectic can be controlled by the ratio between the speeds of the solidification fronts.

- Centrifugal casting leads to a refinement of grain size due to the increase in the solidification speed. In centrifugal casting and with the dimensions of the casting used in this study, the grains are equiaxed and the eutectic could be granular or lamellar depending on the speed of solidification.

CHAPTER 3

MODELING OF PARTICLE SEGREGATION DURING CENTRIFUGAL CASTING OF METAL MATRIX COMPOSITES

3.1 Introduction

Centrifugal casting is a technology that relies on a centrifugal force to produce hollow and axisymmetric parts (cylinders, pipes etc). The technique is an effective method for the casting of particles' reinforced metal matrix composites (CMMp). The distribution of particles at the critical points of the section can be carried out by centrifugation. The centrifugal casting of CMMp allows the production of high-strength and light parts with very acceptable microstructures, and that are almost free of porosities, while being fairly compatible with the other parts in service.

The movement of the particles in a liquid matrix was studied Watanabe *et al*., (1998) in order to establish a method for controlling their concentration and distribution in a graded composite. However, to simplify analysis, and because determining the solidification time and temperature distribution during the centrifugation process is a complicated problem, the authors considered the metal to be a liquid, thus obeying the Stokes law (constant temperature and viscosity). The authors thus found that the displacement of the particles toward the outer casting surface ($\rho_P > \rho_l$) increases with an increase in the rotation speed and particle size. Moreover, it was noted that when the temperature of the mold and the metal are elevated, the metal becomes less viscous, and the desired distribution of the reinforcing particles along the part section cannot be reached (Bonollo *et al*., 2004). In addition, the particles' size also influences their distribution inside the matrix. The zone rich in particles on the outer/inner surfaces increases with particle size, depending on the particle/matrix density ratio (Raju and Mehrotra, 2000). On the other hand, under certain conditions, the particles close to the outer surface are small in diameter, a phenomenon which is attributable

to the solidification front, which tends to prevent large-size particles from moving freely toward the outer casting surface (Velhinho *et al*., 2003).

According to Stokes law, for a laminar flow, the velocity of a particle in a liquid is constant and its acceleration is zero. However, during the centrifugation process, the centrifugal radius changes with the displacement of the particle and the melt viscosity increases during the cooling process. Thus, the particle velocity is not constant with time. Therefore, for optimal production using a graded metal matrix composite, the centrifugation laws and the variation of the particle velocity through the matrix must be specified.

Several authors have studied the impact of centrifugation parameters, such as particle size and rotation speed, on the particles' segregation. However, the change in the particles' velocity, along with its impact on their segregation, was not taken into account. Some authors have assumed that viscosity remains constant during particle segregation (Forester *et al*., 2003). In addition, by studying the segregation of the particles during centrifugation in an Al/Si alloy, some authors have assumed constant – but different – initial viscosities: Lajoye and Suéry (1988) assumed a constant melt viscosity of 0.0025 Pa.s, while Panda *et al*. (2006) took one of 0.002 Pa.s. However, as mentioned by Lajoye and Suéry (1988), change in viscosity as a function of temperature affects particle velocity and segregation, and, therefore, must be taken into account.

The primary goal of this study is to model, during centrifugation process, the particle segregation and volume fraction through the matrix and on the outer/inner casting surface while taking into account the change in the centrifugal radius combined with variations in viscosity as a function of time and position through the matrix. This will be done by discretizing Stokes's law in time and modeling each physical parameter that affects the particle movement as the speed, deceleration/acceleration, and displacement of the particles. This modeling enables an accurate measure of the particles' speed and the prediction of their volume fraction across the section, knowing that an increase or decrease in the particle

velocity affects the particles' degree of graduation and volume fraction through the matrix and on the outer/inner casting surface.

3.2 Experimental conditions

The material used in this analysis is the aluminum alloy A356 reinforced by 10V% of silicon carbide particles (SiC), 12 ± 2.5 μm in diameter. The mold is made of ordinary steel with a layer of 100-micron thick hematite coating (Fe_2O_3).

The dimensions of the mold and the casting, as well as the parameters used and the composition of the alloy are presented in Tables 3.1 and 3.2.

The themophysical properties of the matrix, particle and mold, are presented in Table 3.3, where ρ is the density, K is the thermal conductivity, C is the specific heat, H is the latent heat of fusion, T_L and T_s are the liquidus and solidus temperatures, respectively.

Table 3.1 Dimensions of the mold and the casting

Dimensions of the casting				
Length, mm	Thickness, mm	Mass, Kg	External radius, mm	Internal radius, mm
62	3	0.1	32	29
Dimensions of the mold				
Length, mm	Thickness, mm		External radius, mm	Internal radius, mm
62	5		37	32

Table 3.2 Parameters used and composition of A356 aluminum alloy

Rotation speed, rpm	**Initial mold temperature, K**	**Initial pouring temperature, K**	**Time increment (Δt), s**
650	303-373-623-673	923-953-973	0.005

Composition of A356								
Si %	Mg %	Cu %	Ti %	Fe %	Zn %	Mn %	Others	Al%
6.5-7.5	0.3-0.45	≤ 0.2	≤ 0.2	≤ 0.15	≤ 0.1	≤ 0.1	≤ 0.15	balance

Table 3.3 Thermophysical properties of aluminum A356, particles and steel mold

Thermophysical properties	**Steel**	**A356**	**SiC**	**Composite A356/SiC**
ρ (kg/m^3)	7800	2400	3200	2480
K ($W \cdot m^{-1} \cdot K^{-1}$)	42.2	151	24	130
C ($J \cdot kg^{-1} \cdot K^{-1}$)	473	938	690	913
$H_{f,}$ (J/kg)	-------	389000	-------	-------
$T_{L,}$ (K)	-------	885.8	-------	-------
$T_{s,}$ (K)	-------	830	-------	-------

The density and the specific heat of the composite are determined using the law of mixture, which takes into account the volume fraction of the ceramic particles.

The thermal conductivity of the composite was calculated based on the theory of effective middle EMT expressed by Grabowski *et al.* (2005, p. 241)**:**

$$K = K_m (1-V_p) / (1+0.5V_p) \quad (3.1)$$

where K_m is the matrix thermal conductivity (W/m K) and V_p is the particle volume fraction.

The heat transfer coefficients by radiation and forced convection on the inner surface metal/air and the outer surface mold/air (Table 3.4) are calculated, based on Poirier D. & Poirier E. (1991), taking into account the air properties, the boundary conditions, and the rotation speed.

Table 3. 4 Heat transfer coefficients by forced convection and radiation

Total heat transfer coefficient, metal/air (convection + radiation)	
Metal Temperature, K	$h_{total,\ metal/air}$, $W \cdot m^{-2} \cdot K^{-1}$
923	107.27
953	107.72
973	108.01
Total heat transfer coefficient, mold/air (convection + radiation)	
Mold Temperature, K	$h_{total,\ mold/air}$, $W \cdot m^{-2} \cdot K^{-1}$
303	82.84
373	84.00
623	87.04
673	88.02

To measure the concentration of the particles across the casting section and to analyse their distribution, photos of the microstructure were obtained with optical and scanning electron microscopes along the radial direction of the section. Each photo represents a distance of 125 microns from the outer surface of the casting. The photos were printed, and the particles cut and separated from the matrix. The particles and the rest of the matrix were weighed together, and then separately, and the concentration of the particles calculated as the ratio between the particles mass and the total mass of the whole microstructure using equation 3.2. The photos of the section, which were used to measure the particles' concentration, were obtained with a magnification of 500 times, which facilitated the easy cutting of the particles.

$$C_p^{Ai}\Big|_{i=0}^{n} = \frac{m_P^{Ai}}{m_T^{Ai}} \times 100\ \% \tag{3.2}$$

where $C_p^{Ai}\Big|_{i=0}^{n}$ is the concentration of the particles in an area A_i, m_P^{Ai} is the mass of the particles in an area $A_{i,,}$ and m_T^{Ai} is the total mass of the whole microstructure in an area A_i.

Figure 3.1 shows the centrifugal casting system used to conduct the experiments.

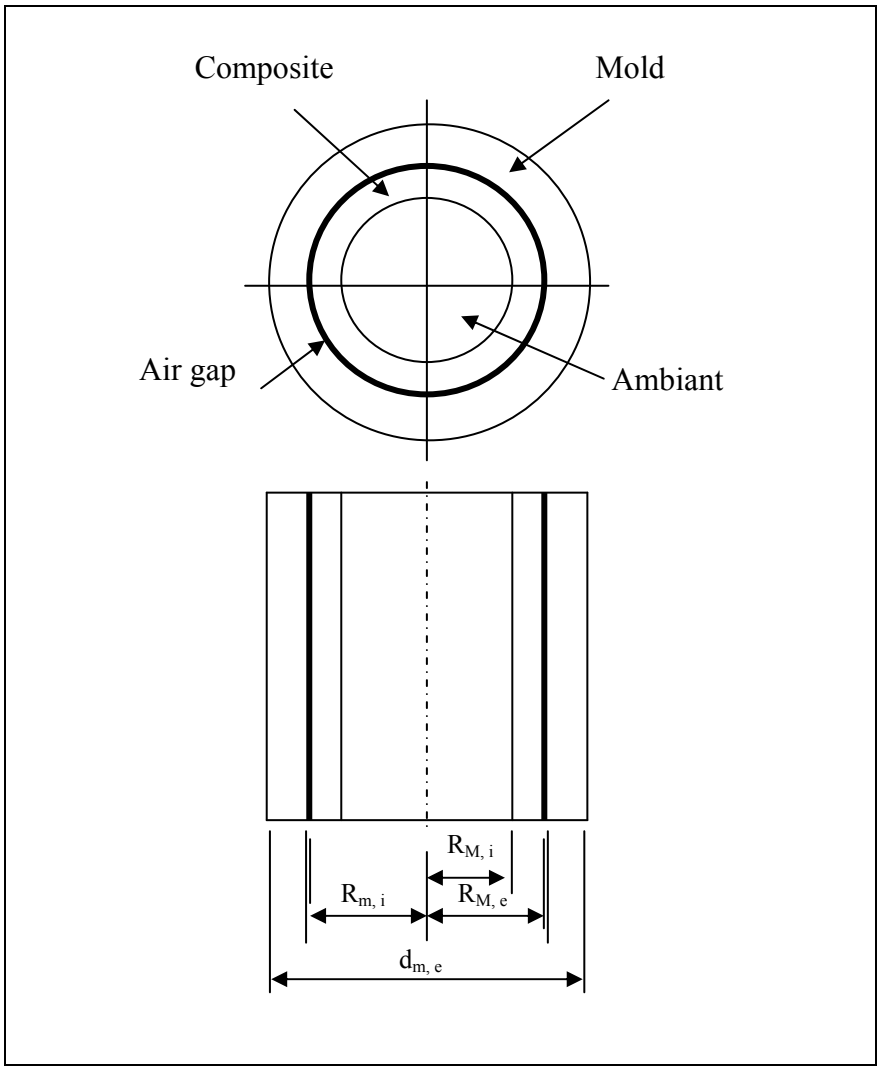

Figure 3. 1 Schematic representation of centrifugal casting system.

The following dimensions are presented in Fig. 3.1:

$R_{M,\,i,}$ $R_{M,e:}$ the inner and outer composite radiuses, respectively (mm);

$R_{m,\,i,}$ $d_{m,e}$: the inner mold radius and the outer mold diameter, respectively (mm).

3.3 Analysis and modeling of particle velocity, deceleration, displacement, and segregation during cooling process

The graduation degree of the particles and the variation of their distribution during centrifugation depend on several parameters, such as the density difference between the reinforcements and the matrix, the particle diameter, the melt viscosity and the rotation speed.

Under a laminar flow, the particle velocity in a liquid is deduced from Stokes' law for a constant liquid temperature and viscosity, and under zero acceleration.

According to Raju and Mehrotra (2000), during centrifugal casting, a particle which is suspended in the liquid is subjected to different forces, such as the centrifugal force, the viscous force, the repulsive force, and the gravitational force (Fig. 3.2). The centrifugal acceleration (γ) is much greater than the gravitational acceleration (g), and so the gravitational force and the vertical displacement of the particle can be ignored. Thus, the force balance equation on the particle can be expressed as:

$$F_{\omega} - F_{\eta} - F_{R} = F_{net} \tag{3.3}$$

where F_{net} is the net force on the particle, F_{ω} is the centrifugal force, F_{η} is the viscous force, and F_R is the repulsive force.

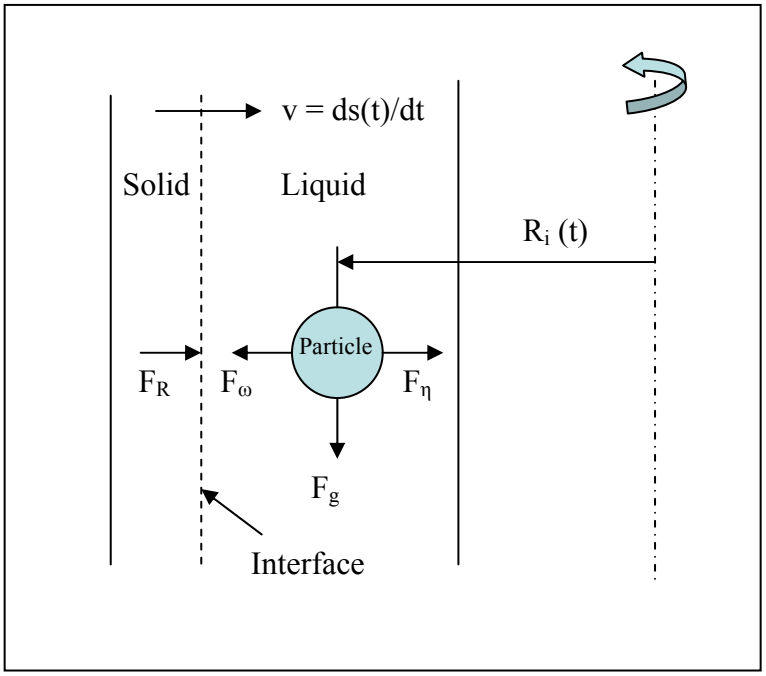

Figure 3. 2 Schematic representation of the forces acting on a moving particle in the melt.
From Raju (2000, p. 1628)

The effect of the repulsive force on the particle is only significant if the particle is close to the solid-liquid interface. If the particle is not influenced by the solid-liquid interface, then the force balance can be expressed as (Raju and Mehrotra, 2000):

$$F_{\omega} - F_{\eta} = F_{net} \tag{3.4}$$

Eq. 3.3 can be written as (Raju and Mehrotra, 2000):

$$\frac{4}{3}\pi R_p^3 \left(\rho_p - \rho_l\right) \omega^2 R - 6\pi\eta R_p \frac{d_r}{d_t} = \frac{4}{3}\pi R_p^3 \rho_p \frac{d^2R}{dt^2} \tag{3.5}$$

Where R_p is the radius of the particle (mm), ω is the angular velocity (rad/s), R is the centrifugation radius (mm), ρ_p, ρ_l are the particle and liquid densities, respectively (kg/m^3), and η is the melt viscosity (Pa.s).

Based on Eq. 3.4, the velocity of a spherical particle which is moving in a liquid with zero acceleration is expressed as:

$$v_p = \frac{4\omega^2 \cdot R \cdot \left(\rho_p - \rho_l\right) \cdot R_p^2}{18\eta} \tag{3.6}$$

Again based on Eq. 3.4, for a particle moving with a constant velocity, the position of the particle at time t can be written as (Raju and Mehrotra, 2000):

$$R(t) = R_0 \exp\left[\frac{4\omega^2 \cdot (\rho_p - \rho_l) \cdot R_p^2 \cdot t}{18\eta}\right] \tag{3.7}$$

where R_0 is the position of the particle at time t = 0

When the liquid metal is overheated, the extraction of the superheat could last for a short or long time before the onset of solidification, depending on the initial pouring temperature, the molding conditions, and the cooling rate. On the other hand, the melt viscosity changes during cooling process as a function of time and position through the matrix. This variation of the viscosity as a function of temperature can be determined by the Arrhenius relation:

$$\eta = A \exp\left(\frac{Q}{R_g \cdot T_m}\right) \tag{3.8}$$

where A is a constant, Q is the activation energy of viscous flow (kJ.mol^{-1}), R_g is the constant of perfect gases (R_g = 8.31441, J.k^{-1}.mol^{-1}), and T_m is the absolute metal temperature (K).

The apparent melt viscosity also changes depending on the particle volume fraction, through the following equation (Stefanescu *et al.* 1990):

$$\eta_c = \eta \cdot \alpha \tag{3.9}$$

$$\alpha = 1 + 2.5 \cdot V_p(t) + 10.05 \cdot V_p^2(t) \tag{3.10}$$

where η_c is the apparent melt viscosity (Pa.s), α is a coefficient, and V_p (t) is the volume fraction of particles as a function of time.

According to Stokes' law (Eq. 3.6), the particle moves in the liquid with zero acceleration. Moreover, according to Eq. (3.7), the particle position at any time (t) is calculated using a centrifugal radius corresponding to its position at time (t_0). However, the position of the particle at time (t) is influenced by the variation of the centrifugal radius during its displacement and the increase in the melt viscosity during the cooling process. The centrifugal radius between the rotation axis and the particle increases during the movement of the particle toward the outer surface of the casting and decreases during its movement toward the inner surface. This increase/decrease in the centrifugal radius generates an acceleration/deceleration of the particles during their displacements. Moreover, the temperature variation of the molten metal during the cooling process affects its viscosity. An increase or decrease in viscosity during the casting process may affect the velocity of the particles, and thereafter, their degree of graduation. Therefore, the final behavior of the particle is the result of the competition between the deceleration caused by the increase in the melt viscosity and the acceleration/deceleration caused by the change in the centrifugation radius. Thus, for the given experimental conditions, the centrifugal radius, the viscosity, and the velocity of the particle are not constant with time and position and must be taken into account when modeling the segregation of particles, as will be shown later in this study.

3.3.1 Modeling of particle velocity

Figure 3.3 schematizes the variation of the centrifugal radius with time for a particle which advances toward the outer surface.

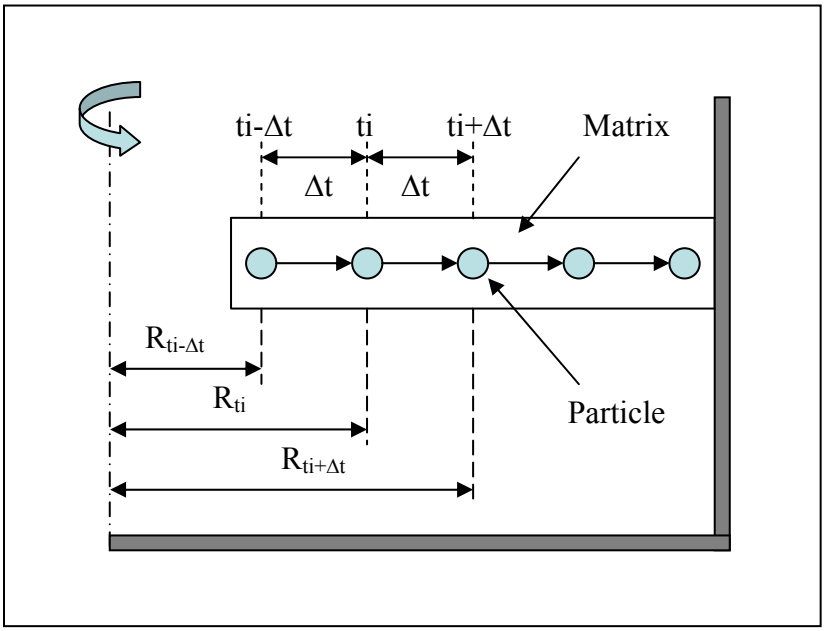

Figure 3. 3 Schematization of the centrifugal radius variation with time during the centrifugation process ($\rho_p > \rho_l$).

By combining Eqs. (3.6, 3.8, 3.9, and 3.10), the particle velocity at each interval of time can be determined while taking into account the variation of the centrifugal radius and melt viscosity as a function of time interval and position through the matrix, through the following equation:

$$v_{p(ti \to ti+\Delta t)} = \frac{\left(\rho_p - \rho_L\right) \cdot d_p^2 \cdot \omega^2 \cdot R_{(ti)}}{18 \cdot A \cdot \exp\left(\frac{Q}{R_g \cdot T_{m,(ti)}^{Rj}}\right) \cdot \alpha} \tag{3.11}$$

We express the variation of the melt temperature and of the centrifugal radius at each time interval, taking into account the position across the casting section, through the following equations:

$$T_{m,(ti+\Delta t)}^{R_j} = T_{m,(ti)}^{R_j} - v_{c,(ti)}^{R_j} \cdot \Delta t \tag{3.12}$$

- Particle density smaller than that of liquid metal ($\rho_p < \rho_l$):

$$R_{ti+\Delta t} = R_{ti} - v_{p(ti)} \cdot \Delta t \tag{3.13}$$

- Particle density bigger than that of liquid metal ($\rho_p > \rho_l$):

$$R_{ti+\Delta t} = R_{ti} + v_{p(ti)} \cdot \Delta t \tag{3.14}$$

where $T_{m,ti}^{Rj}$ is the melt temperature as a function of time and position through the matrix (K), $R_{ti+\Delta t}$ is the centrifugal radius at time $t_i+\Delta t$ (mm), R_{ti} is the centrifugal radius at time ti (mm), $v_{p\ (ti)}$ is the particle velocity at time t_i (mm/s), v_c is the cooling rate (K/s), and Δt is the time increment (s).

The combination of Eqs. (3.11, 3.12, and 3.14) allows us to discretize the particle velocity and to deduce its real variation across the casting section due to the increase in the centrifugal radius and melt viscosity. Furthermore, according to Stokes' law, the particle velocity is constant, and its acceleration is zero. In our study, these conditions are met because according to our modeling, the centrifugal radius and viscosity stay constant during the movement of the particle over a given small time interval (for example, from t_i-Δt to t_i), which means that the velocity at which the particle moves in this time interval is constant and its acceleration is zero. The centrifugal radius and viscosity change and increase when switching to another time interval (for example, from t_i to $t_i+\Delta t$). In this new time interval,

the velocity of the particle is influenced by another centrifugal radius and another viscosity value. Thus, the velocity of the particle changes, but remains constant with zero acceleration in this new time interval.

3.3.2 Modeling of particle acceleration/deceleration

We express the average particle acceleration/deceleration as a function of time and position taking into account the constant velocities of the particle at every two successive time intervals, through the following equations:

$$a = \frac{\partial v}{\partial t} \tag{3.15}$$

$$\int_{v1}^{v2} dv = \int_{t1}^{t2} a \cdot dt \tag{3.16}$$

$$a_{t_i}^{R_j} = \frac{v_{(ti \rightarrow\ t_i+\Delta t)}^{R_j} - v_{(t_i-\Delta t \rightarrow t_i)}^{R_j}}{\Delta t} \tag{3.17}$$

where R_j is the initial position of the particle from the rotation axis.

The average deceleration/acceleration of the particle is modeled based on the change of particle velocity between two successive intervals of time. Thus, the deceleration/acceleration of the particle between two successive time intervals is constant, and Stokes' law, which expresses the particle velocity with zero acceleration, is respected for each time interval during which the particle moves. The deceleration changes when switching to two other successive time intervals. This is repeated for many time intervals until the temperature reaches the liquidus temperature of the metal, where the particle velocity is considered zero.

3.3.3 Modeling of particle displacement

We express the distance travelled by the particle for a given position and time interval considering its velocity and acceleration/deceleration, as follows:

$$S = \int_{v1}^{v2} \frac{v}{a} \partial v \tag{3.18}$$

$$S = \frac{v_2^2 - v_1^2}{2a} \tag{3.19}$$

$$S_{t_i}^{R_j} = \frac{\left(v_{t_i \to t_i + \Delta t}^{R_j}\right)^2 - \left(v_{t_i - \Delta t \to t_i}^{R_j}\right)^2}{2a_{t_i}^{R_j}} \tag{3.20}$$

We express the total distance travelled by the particle as a function of time and position through the matrix as follows:

$$S_{tot.}^{R_j} = \sum_{i,j=0}^{n} S_{t_i}^{R_j} = \sum_{i,j=0}^{n} \frac{\left(v_{t_i \to t_i + \Delta t}^{R_j}\right)^2 - \left(v_{t_i - \Delta t \to t_i}^{R_j}\right)^2}{2a_{t_i}^{R_j}} \tag{3.21}$$

where S is the travelled distance (mm), R is the position from the rotation axis (mm), v is the particle velocity (mm/s), and a is the acceleration (mm/s^2).

In the modeling of the particle velocity, acceleration/deceleration, and displacement, the part section was divided into several sub-surfaces. The distance from the rotation axis to the middle of each sub-surface (R_j) represents the initial position of the particle. Moreover, based on the work of Lajoye and Suéry (1988), Raju and Mehrotra (2000), and Panda *et al*., (2006), it was assumed that the particles are stopped by the liquid front, and that they move during the extraction of superheat before the temperature drops below liquidus. The influence of the movement of the particles on their segregation during solidification is assumed to be

negligible. Thus, the maximum segregation of the particles on the outer/inner surfaces is produced during the cooling process before the solidification begins.

3.3.4 Modeling of particle segregation

In order to determine the maximum particle volume fraction on the outer casting surface and their degree of graduation across the section during centrifugation, the casting thickness was divided into several sub-volumes (V_i) of length (L_i), height (h), and thickness (e), each containing an initial particle volume fraction of 10%V (Fig. 3.4). We calculate the final volume fraction of the particles in each sub-volume through Eq. 3.22, taking into consideration the variation of the particle velocity due to the increase in viscosity and centrifugal radius as a function of time and position. On the other hand, according to Watanabe *et al*. (1998), the maximum volume fraction for the close packing of spherical particles in a composite is 74% V, and 52 % V for a simple cubic packing of SiC.

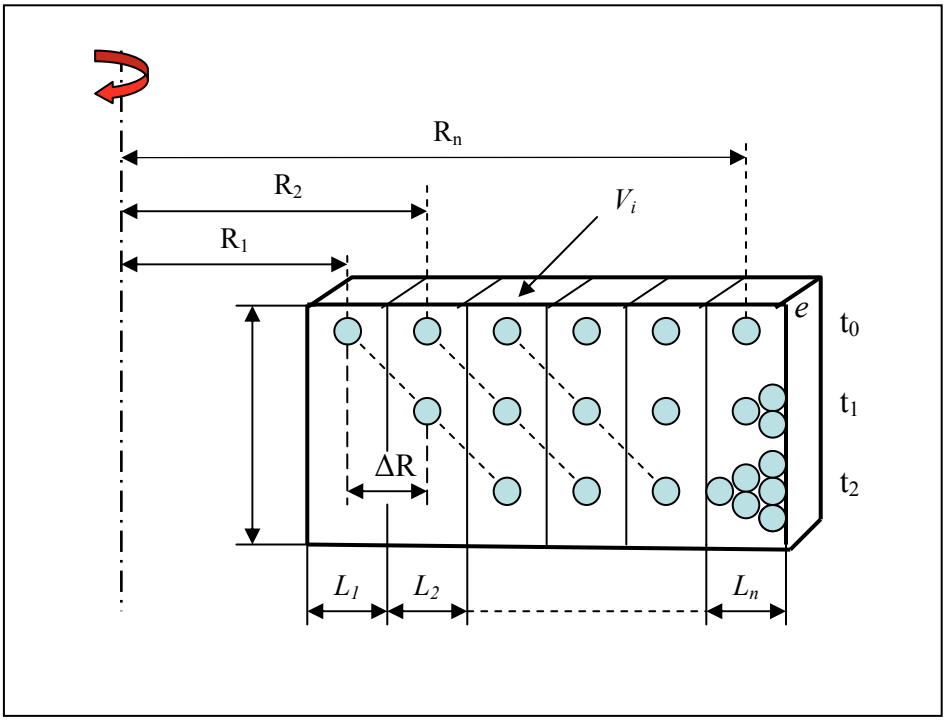

Figure 3. 4 Representation of particle displacement and segregation during centrifugation.

$$fv_{V_i}^{ti} = fv_{V_i}^{t_0} + fv_{\to V_i}^{ts} - fv_{V_i\to}^{ts} + \sum_{i=0}^{n} \Delta fv_{V_{i+1}\,(fv_{(V_i+1)}>52\%)}^{ts} \tag{3.22}$$

where:

$$\begin{aligned} fv_{\to V_i}^{ts} = &\left[\sum_{i,j=0}^{n} fv_{V_i,ini}^{ts}{}_{\left(R_j-\Delta R/2<R_{j(ini.)}^{t=0}+S_{(ti)tot}^{Rj}<R_j\right)}\right] - \sum_{i,j=0}^{n}\frac{fv_{V_i,ini}^{ts}}{\Delta R}\cdot\left[R_j-\left(R_{j(ini.)}^{t=0}+S_{(ti)tot}^{Rj}\right)\right]+ \\ &+\left[\sum_{i,j=0}^{n} fv_{V_i,ini}^{ts}{}_{\left(R_j<R_{j(ini.)}^{t=0}+S_{(ti)tot}^{Rj}<R_j+\Delta R/2\right)}\right] - \sum_{i,j=0}^{n}\frac{fv_{V_i,ini}^{ts}}{\Delta R}\cdot\left[\left(R_{j(ini.)}^{t=0}+S_{(ti)tot}^{R_j}\right)-R_j\right] \end{aligned} \tag{3.23}$$

$$fv_{V_i\to}^{ts} = \left(fv_{V_i(ini.)}^{t_0} + \sum_{i=0}^{n} fv_{\to V_i}^{ti}\right)_{(fv_{V_{i+1}<52\%}^{ti+\Delta t},\, T_{V_{i+1}}^{ti+\Delta t}\geq T_L)} \tag{3.24}$$

$$R_{(fv)_j^{t_s}}\Big|_{j=0}^{n} = R_{(fv)_j^{t_0}}\Big|_{j=0}^{n} + \sum_{i,j=0}^{n} S_{(fv)_{R_j}}^{t_i} \tag{3.25}$$

where $fv_{Vi\to}^{t_0}$ is the volume fraction of particles corresponding to the volume V_i at time t = 0,

$fv_{\to Vi}^{ts}$ is the volume fraction of particles entering the sub volume V_i at time ts, before the solidification begins on this volume,

$fv_{Vi\to}^{ts}$ is the volume fraction of particles leaving the sub volume V_i at time ts, before the solidification begins on this volume,

$fv_{V_i,ini}^{ts}{}_{\left(R_j-\Delta R/2<R_{ini.}^{t=0}+S_{(ti)tot}^{Rj}<R_j\right)}$ is the initial volume fraction of particles moved to a sub volume V_i located between R_j and R_j-$\Delta R/2$ before the solidification begins on this volume,

$fv^{ts}_{V_i,ini}\ \left(R_j < R^{t=0}_{ini.} + S^{Rj}_{(ti)tot} < R_j + \Delta R/2\right)$ is the initial volume fraction of particles moved to a sub volume V_i located between R_j and $R_j+\Delta R/2$ before the solidification begins on this volume,

$\Delta fv^{ts}_{V_i+1(fv_{(V_i+1)}>52\%)}$ is the excess of the particle volume fraction of the sub volume V_{i+1},

ΔR is the radius increment,

$R_{(fv)^{t_s}_j}\big|^{n}_{j=0}$ is the final position of the particle volume fraction before the solidification begins,

$R_{(fv)^{t0}_j}\big|^{n}_{j=0}$ is the initial position of the particle volume fraction at time t = 0,

T_L is the liquidus temperature,

$S^{t_i}_{(fv)_{R_j}}$ is the distance travelled by the particle volume fraction located at an initial position (R_j) for a given time of centrifugation (t_i), before the solidification begins,

$v^{R_j}_{t_i}$ is the velocity of particle located at an initial position (R_j) for a given time of centrifugation (t_i),

$a^{R_j}_{t_i}$ is the acceleration of particle located at an initial position (R_j) for a given time of centrifugation (t_i).

3.4 Modeling of cooling rate

In our analysis, Cartesian co-ordinates were considered during the modeling of the cooling rate because of the small thickness of the part compared to its diameter (3mm/64mm). The heat transfer mechanism produced between the metal and the mold is a transient mechanism. The variation of the cooling rate and temperature as a function of time and position across the mold and metal sections were modeled through the implicit finite difference formulation using FLUENT for a transient one-dimensional unsteady state of solidification.

We express the variation of the cooling rate with time and position through the matrix by the following equation:

$$v_{c,t_i}^{R_j}\Big|_{i,j=0}^{n} = \frac{T_p - T_{m,t_i}^{R_j}}{t_{c,i}} \tag{3.26}$$

where $T_{m,ti}^{Rj}$ is the metal temperature for given time and position (K), T_p is the temperature of superheated metal (K), and t_c is the cooling time (s).

The modeling of the solidification/cooling on FLUENT takes into account the variation of the heat transfer coefficient mold/metal, as well as the contact resistance and the air gap formed between the mold and the metal as a result of the shrinkage of the latter during the solidification process. This is done by using an additional heat transfer resistance mold/metal, with a liquid fraction less than 1 (Fluent 6.2 documentation, L:/fluent.inc/help/index.htm).

3.5 Results

The main purpose of this paper is to show the influence of the increase in viscosity on the particle movement and segregation while taking into account the change in the centrifugal radius during the particle displacement. As a first step, the influence of the change in the initial particle volume fraction on the apparent melt viscosity during centrifugation was not considered. Doing so allowed us to determine the influence of the increase in viscosity on the particle velocity, acceleration/deceleration, and displacement due to the decrease in the temperature alone without it being influenced by other phenomena, such as changes in the particle volume fraction. Thereafter, the calculation of the particle volume fraction and segregation across the casting section is done with and without taking into account the influence of the variation in the particle volume fraction on the apparent melt viscosity and particle velocity and segregation across the casting section. This calculation allows us to clarify the influence of the increase in viscosity on the particle segregation across the casting section due to the decrease in temperature, on the one hand, and increase in the particle volume fraction, on the other.

In this modeling, the following assumptions were considered:

- The particles are spherical in shape;
- There is no clustering of the particles during their displacements;
- The particles are not rejected by the solidification front;
- The particles do not move in the mushy zone of the cast;
- There is no thermal resistance between particles and liquid metal;
- The vertical particle movement is neglected because of the high centrifugal force.

3.5.1 Variation of cooling rate, temperature, and viscosity

For a composite produced by centrifugal casting, the change in the rotation speed and in the initial pouring and mold temperatures also change the cooling rate. Figure 3.5 shows, for a given rotation speed and initial pouring and mold temperatures, the change in the cooling rate of the composite as a function of time and position through the matrix.

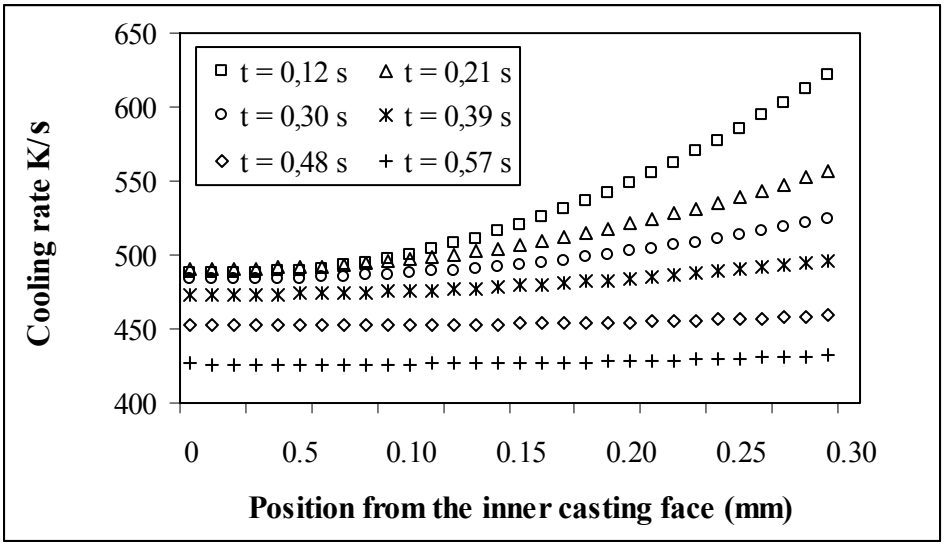

Figure 3. 5 Cooling rate as a function of time and position across the section ($T_{metal,in}$ = 973 K, $T_{mold,in}$ = 673 K).

It can be seen (Fig. 3.5) that the cooling rate increases when moving from the inner to the outer casting surface, which is in contact with the mold, as a result of the high mold/metal heat exchange. The variation in the cooling rate through the matrix decreases and stabilizes with time. As the metal temperature falls during the cooling process, it leads to a reduction in thermal exchange by internal conduction. Consequently, the cooling rate decreases, and becomes more stable.

The variation in temperature across the metal and mold sections during the extraction of superheat is influenced by the initial mold and pouring temperatures and their thicknesses. It can be seen (Fig. 3.6) that during the extraction of the superheat, the temperature of the metal decreases as a function of time and position as it advances to the outer casting surface. On the other hand, the mold temperature increases with time, but decreases when moving along the mold section toward the outer surface. These results can be explained by the liquid front which, in this case, advances from the outer to the inner casting surface, while in the mold, the temperature increases when advancing toward its inner surface.

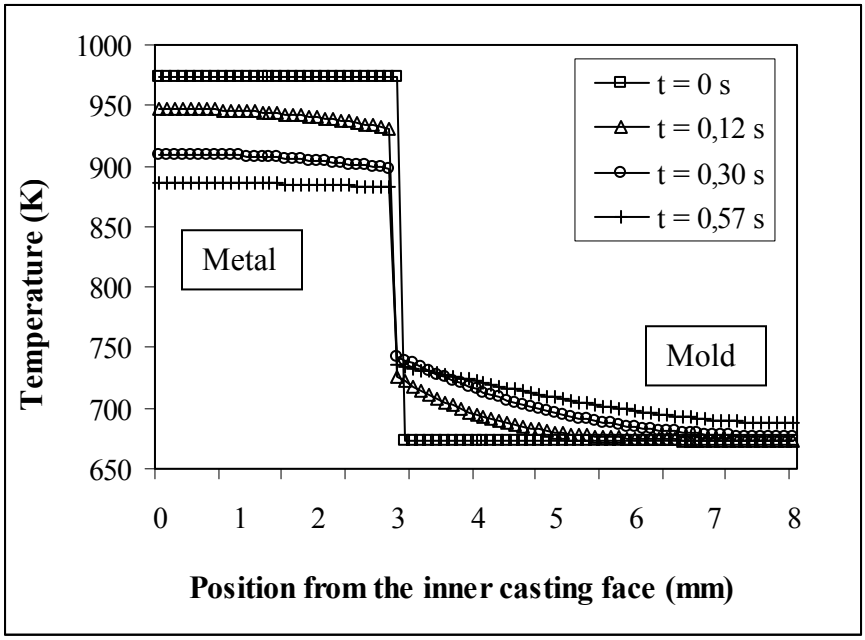

Figure 3. 6 Metal and mold temperatures as a function of time and position across the section ($T_{metal,in}$ = 973 K, $T_{mold,in}$ = 673 K).

The variation in the melt viscosity during the cooling process is a function of time, position, cooling rate and initial pouring and mold temperatures (Fig. 3.7). Fig. 3.7 was generated based on the viscosity value at each time interval. Based on the discretization done, the viscosity stays constant for a given time interval, and changes when switching to another time interval.

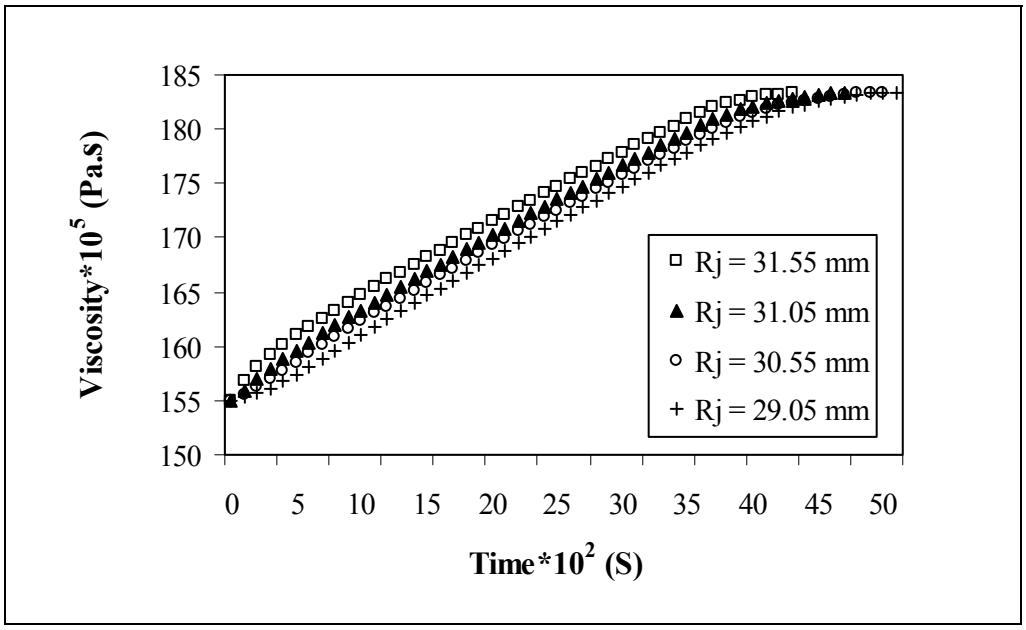

Figure 3. 7 Variation in viscosity as a function of time and position through the matrix ($T_{metal,in}$ = 973 K, $T_{mold,in}$ = 673 K).

It can be seen from Figs. 3.7 that the viscosity increases with time as well as with position when moving from the inner to the outer casting surface. The variation of the viscosity with the cooling time was calculated as the temperature was dropping to liquidus, as a minimum threshold. Thus, the metal was still in the liquid state. When the temperature of the metal drops below liquidus, the first solidification nucleus starts to form, making the movement of the particles difficult, and greatly increasing the viscosity of the metal.

3.5.2 Variation of particle position

Eq. 3.7 gives the position for a particle moving at a constant velocity, as a function of time. Since the centrifugal radius changes with time during the movement of the particle and the viscosity changes as a function of time and position during the cooling process, the particle velocity varies with time and its position across the part section changes. Fig. 3.8 shows the particle position, as a function of time, for a particle moving at a constant velocity (Eq. 3.7) and at a variable velocity due to the change in the centrifugal radius and melt viscosity during the centrifugation process (Eq. 3.14). It can be seen (Fig. 3.8) that the particle position varies with time and becomes different whether the centrifugal radius, viscosity, and therefore, the velocity of the particle, are constant or variable. This variation becomes more pronounced when advancing towards the outer surface of the casting, where the position from the rotation axis of a particle moving at a variable velocity is decreased in comparison with a particle moving at a constant velocity. The particle therefore undergoes a high deceleration caused by the great increase in the melt viscosity as it approaches the inner mold surface, due to the high rate of cooling and heat exchange at the mold-metal interface.

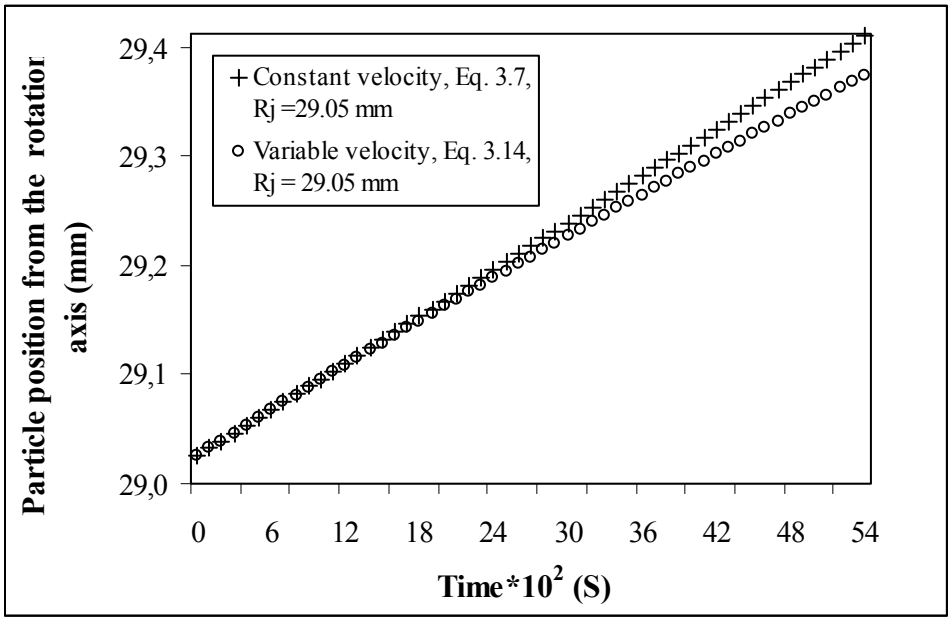

Figure 3. 8 Position of a particle as a function of time with constant and variable velocities ($T_{metal,in}$ = 973 K, $T_{mold,in}$ = 673 K).

3.5.3 Distance travelled by the particle

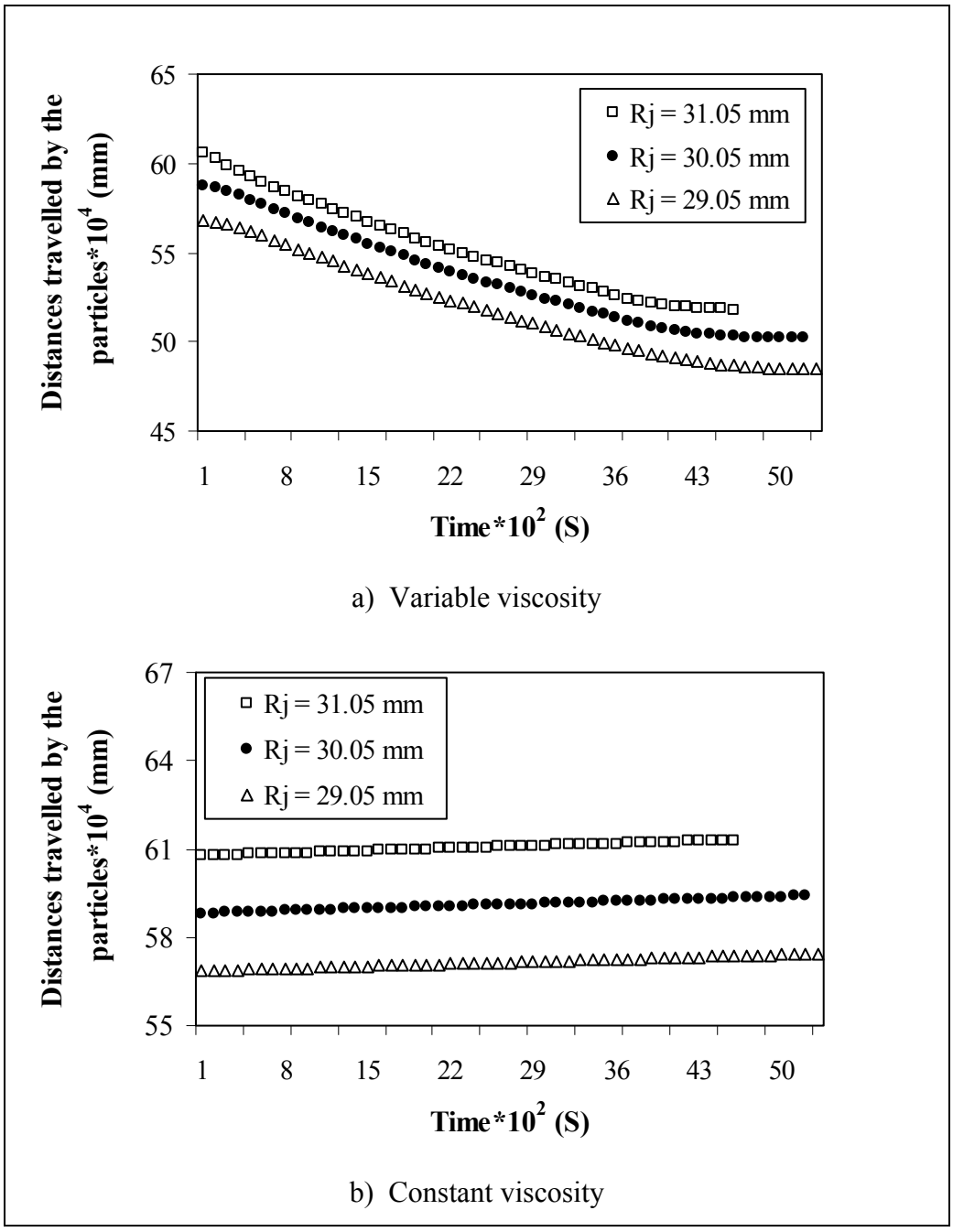

Figure 3. 9 Distances travelled by the particles as a function of time and position through the matrix ($T_{metal,in}$ = 973 K, $T_{mold,in}$ = 673 K): a) variable viscosity, b) constant viscosity.

When the variation of the viscosity with time and position is taken into account (Fig. 3.9 a), the distances travelled by the particles decrease with time to reach a minimum value at a given time and position when the metal temperature approaches liquidus and the viscosity sharply increases. On the other hand, when the viscosity is constant (Fig. 3.9 b), the distances travelled by the particles increase linearly with time before the particle is trapped by the liquid front. Moreover, the particles move at variable distances, depending on their original positions across the casting section. The decrease or the increase in the distances travelled by the particles influences their degrees of graduation through the section and affects their volume fraction on the inner/outer casting surface.

3.5.4 Theoretical and experimental results: Segregation of particles

The following figures (3.10, 3.11, 3.12, and 3.13) show the change in the particle volume fraction through the matrix and on the outer surface of the composite for different initial mold and pouring temperatures, and with variable and constant viscosities while taking into consideration the change in the centrifugal radius during particle displacement.

The results show the impact of the variation in viscosity on the particle volume fraction. Modeling the particle volume fraction with a variable viscosity gives results that are closer to those obtained by experiments on the outer casting surface (Fig. 3.10 a). In contrast, modeling using a constant viscosity of 0.00155 Pa.s, which corresponds to the initial pouring temperature taking into account the initial particle volume fraction, gives higher particle volume fraction on the outer casting surface compared to that obtained experimentally (Fig. 3.10 b). The difference in the results is less pronounced far from the outer casting surface because of the small increase in the particles' volume fraction across the casting section.

It may be noted (Fig. 3.10 a), for the initial temperatures and rotation speed used, that the particle volume fraction on the outer casting surface does not reach a high value (≈ 15 %V). The volume fraction of the particles increases as they advance toward the outer surface of the casting.

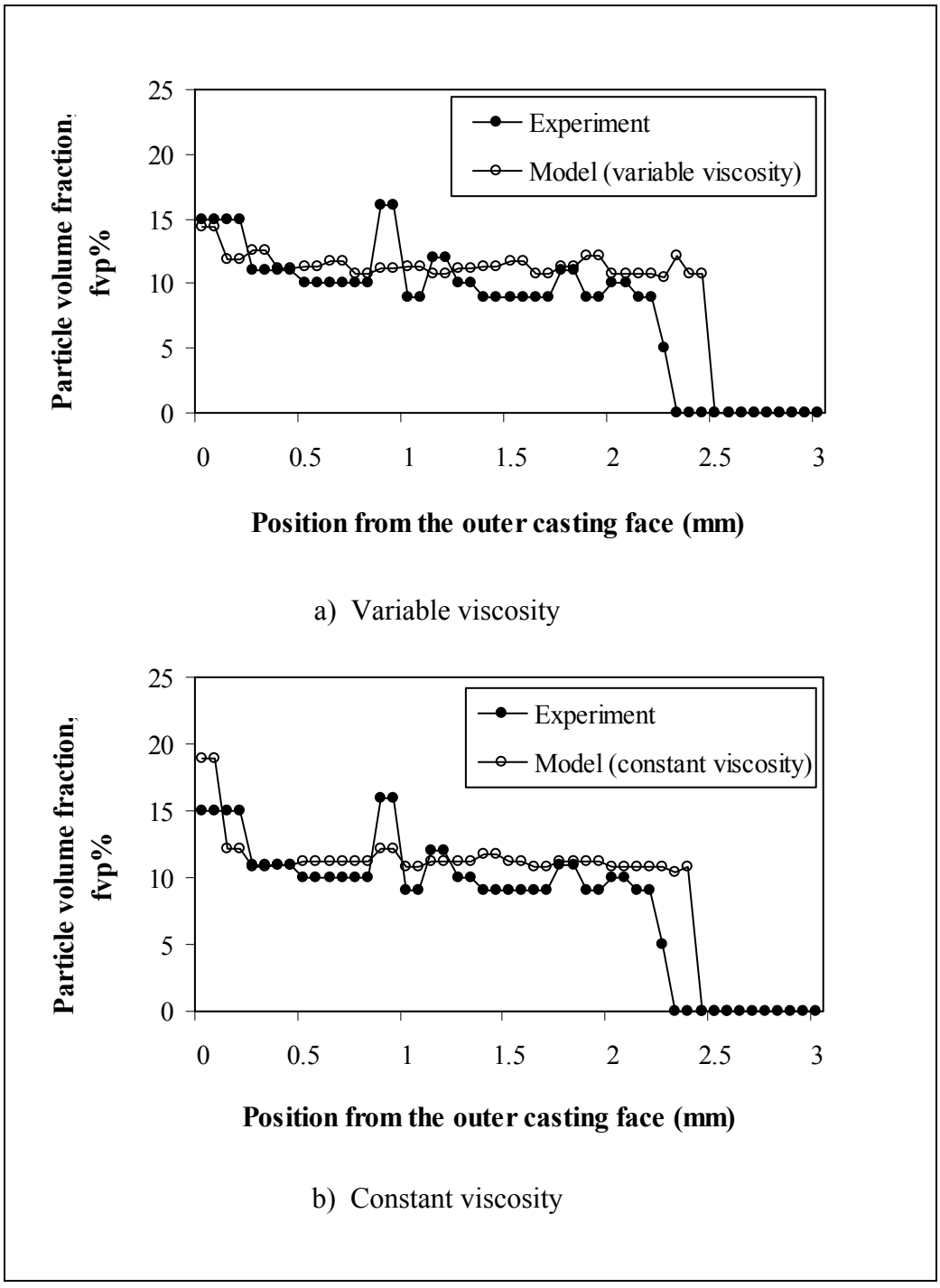

Figure 3. 10 Volume fraction of the particles across the section ($T_{metal,in}$ = 973 K, $T_{mold,in}$ = 373 K): a) variable viscosity, b) constant viscosity.

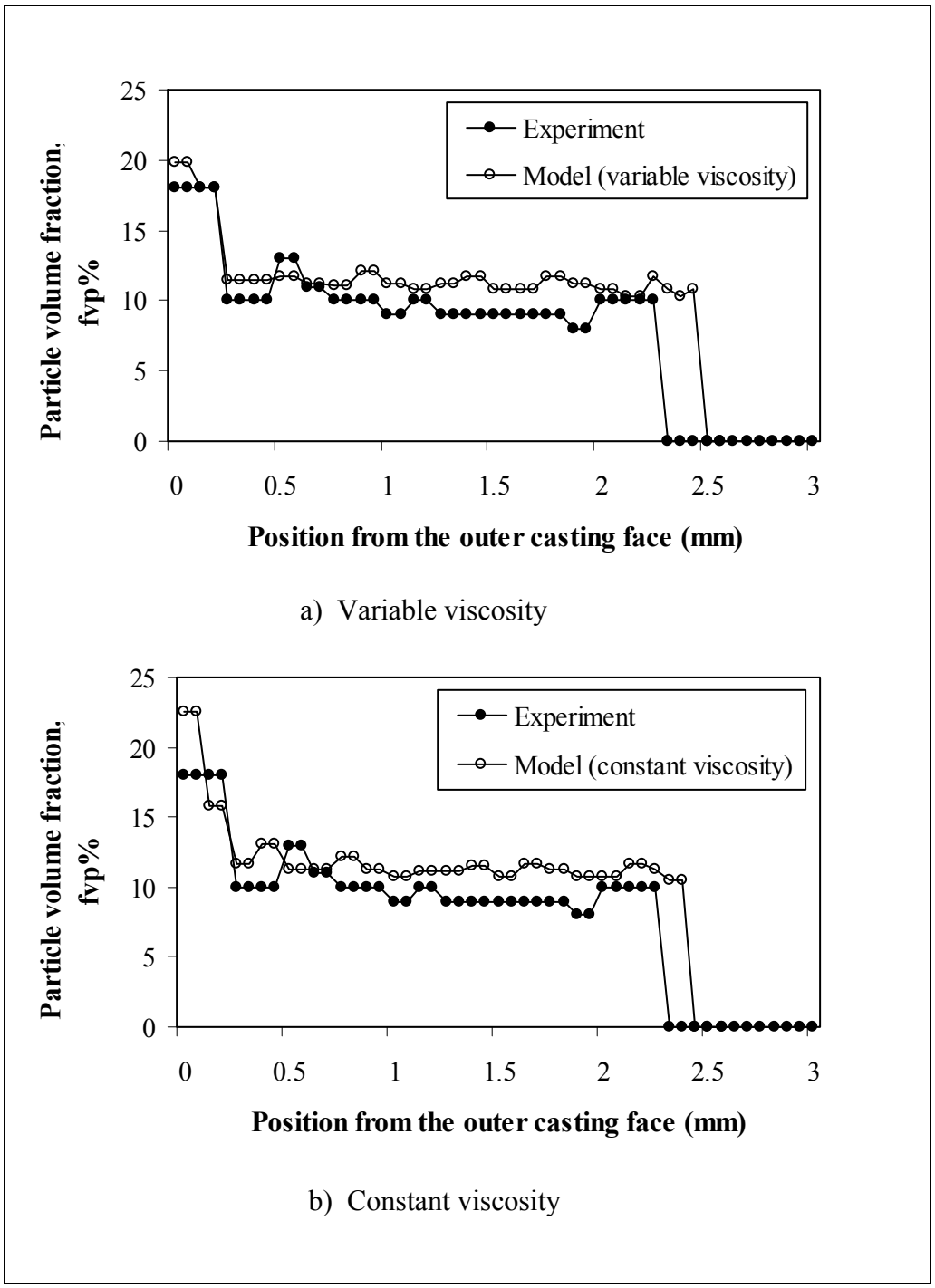

Figure 3. 11 Volume fraction of the particles across the section ($T_{metal,in}$ = 973 K, $T_{mold,in}$ = 673 K): a) variable viscosity, b) constant viscosity.

The effect of the change of the viscosity on the particles concentration can be also noted by comparing Figs. 3.11 a and 3.11 b. Modeling with a constant viscosity (0.00155 Pa.s), corresponding to the initial pouring temperature, leads to a higher volume fraction of the particles on the outer casting surface (Fig. 3.11 b). This is due to the higher distances travelled by the particles and to the accelerations that they undergo when only the change in the centrifugal radius is considered. Furthermore, the increase in the initial mold temperature leads to an increase in the volume fraction of particles on the outer casting surface whether the modeling is done with a variable or constant viscosity (Fig. 3.11 a, b).

The same analysis can apply to Figs. 3.12 a, b. The volume fraction of the particles through the matrix and on the outer casting surface changes whether the used viscosity is constant or variable. Furthermore, with a low initial pouring and mold temperatures, the change in the particle volume fraction on the outer casting surface for variable and constant viscosities becomes smaller (Figs. 3.13 a, b). When the difference between the initial pouring temperatures and liquidus is small, and the initial temperature of the mold is low, the required time for superheat extraction, during which the viscosity undergoes a change, is decreased. Consequently, the change in the initial viscosity does not generate a big impact on the displacement of particles before the solidification begins. Moreover, with low initial mold and pouring temperatures (Figs. 3.13 a, b), the volume fraction of the particles on the outer casting surface is low and close to that near the inner surface. The cooling time at these temperatures is small, which does not allow the particles to move across a large distance before the solidification begins. Furthermore, the concentration of the particles changes across the section due to the interaction between the particles and the liquid front in addition to the variation of cooling rate through the matrix. This interaction generates a variation in the particles travelled distances and leads to a change in their concentration, depending on their initial positions and velocities. On the other hand, the concentration of the particles across the section can be increased or decreased at different positions. This phenomenon is due to the formation of the primary phase which tends during its growth to push the particles to the interdendritic regions causing a heterogeneous variation in their concentration.

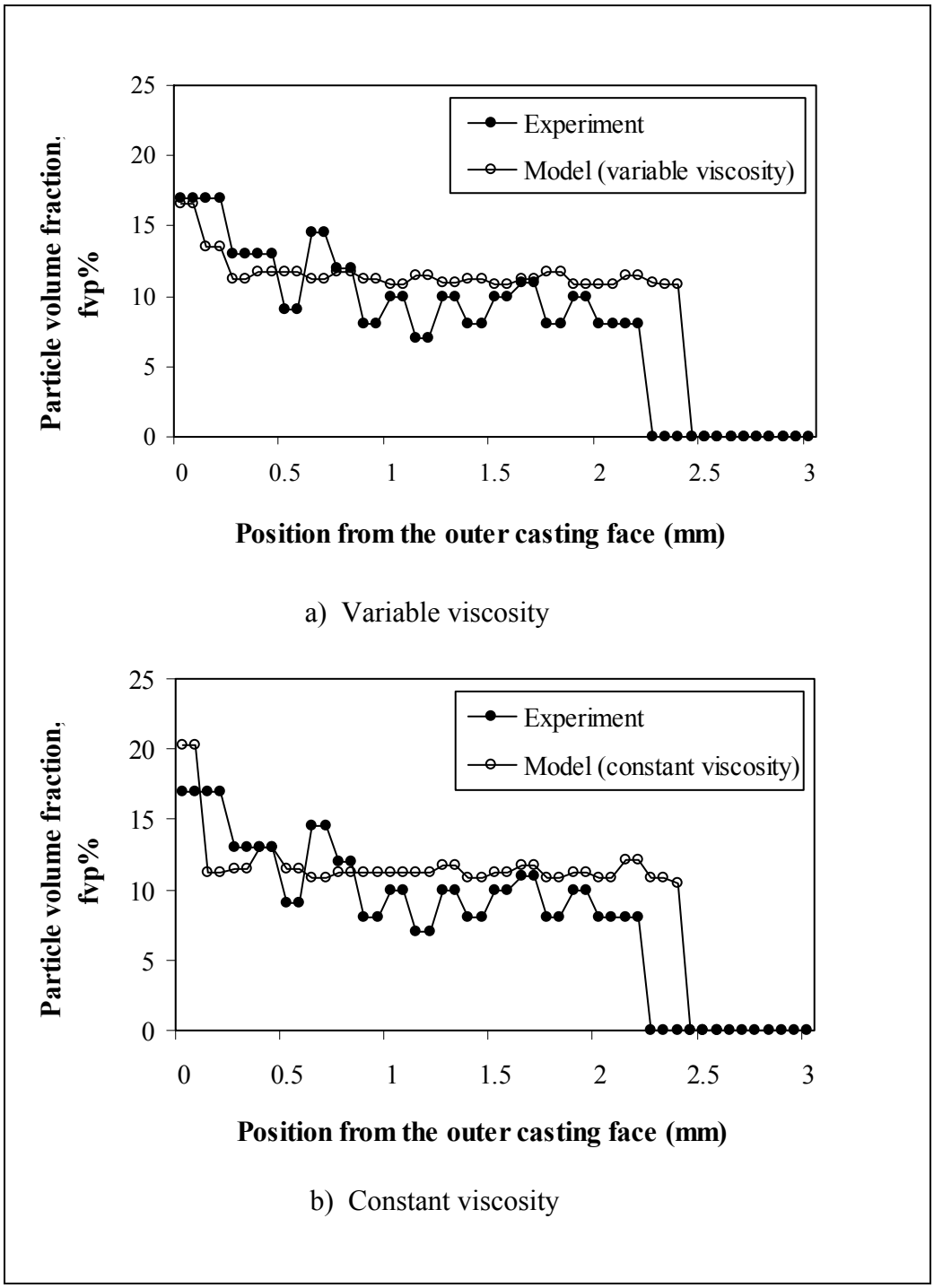

Figure 3. 12 Volume fraction of the particles across the section ($T_{metal, in}$ = 953 K, $T_{mold, in}$ = 623 K): a) variable viscosity, b) constant viscosity.

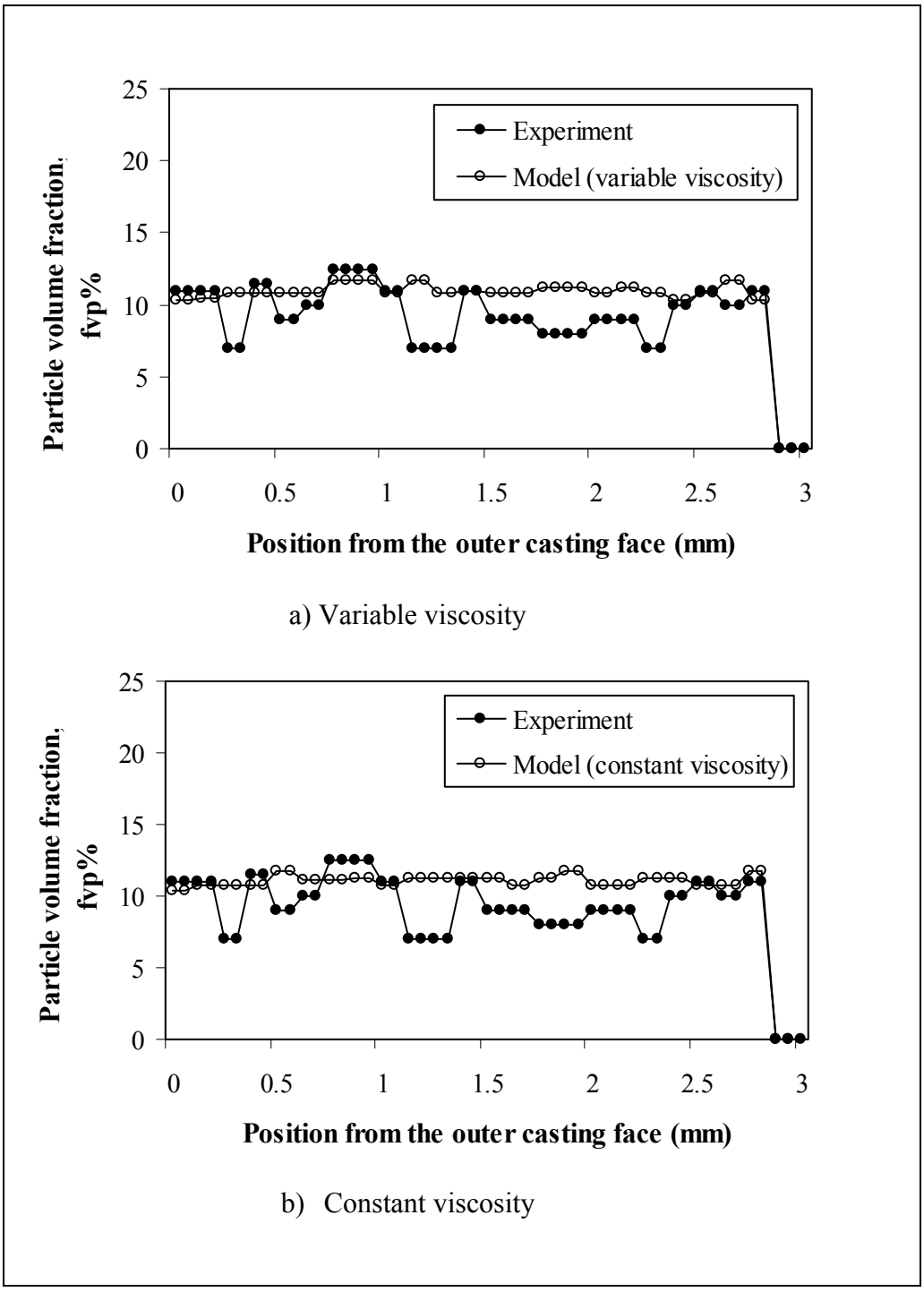

Figure 3. 13 Volume fraction of the particles across the section ($T_{metal,in}$ = 923 K, $T_{mold,\ in}$ = 303 K): a) variable viscosity, b) constant viscosity.

3.5.5 Particle segregation: influence of particle volume fraction variation

In our analysis, the influence of the initial particle volume fraction on the viscosity, and thereafter on the particle velocity and deceleration, was taken into account. On the other hand, as a first step, in order to even more clearly show the influence of the temperature change alone on the viscosity variation and particle velocity and segregation, the influence of the change in the particle volume fraction on viscosity and particle segregation, during centrifugation, was not considered. This allowed us to clarify the influence of the increase in viscosity on the particle velocity and segregation due to the decrease in the temperature alone without it being influenced by other phenomena, such as changes in the particle volume fraction. Thereafter, based on Eq. 3.22, the particle segregation across the casting section was recalculated after considering the influence of the variation in the particle volume fraction as a function of time and position on the apparent melt viscosity and particle velocity (Figs. 3.14, 3.15, and 3.16).

In comparing Figs. 3.14, 3.15, 3.16 with Figs. 3.10, 3.11, 3.12, which do not consider the influence of the variation in the particle volume fraction on the apparent melt viscosity and particle segregation, a small decrease in the particle volume fraction on the outer casting surface due to the increase in the particle volume fraction and apparent melt viscosity on this surface was observed. However, the volume fraction of the particles does not undergo a great change across the casting section. This effect may be explained by the high cooling rate that the distance traveled by the particles and their volume fraction across the section do not attain a high value before the solidification begins, which does not affect dramatically the apparent melt viscosity and particle segregation. However, the variation in the particles' volume fraction during the centrifugation process would have a more remarkable influence on the apparent melt viscosity and particles' segregation if the distance traveled by the particles and the change in their volume fraction across the casting section was greater than the results obtained in this study.

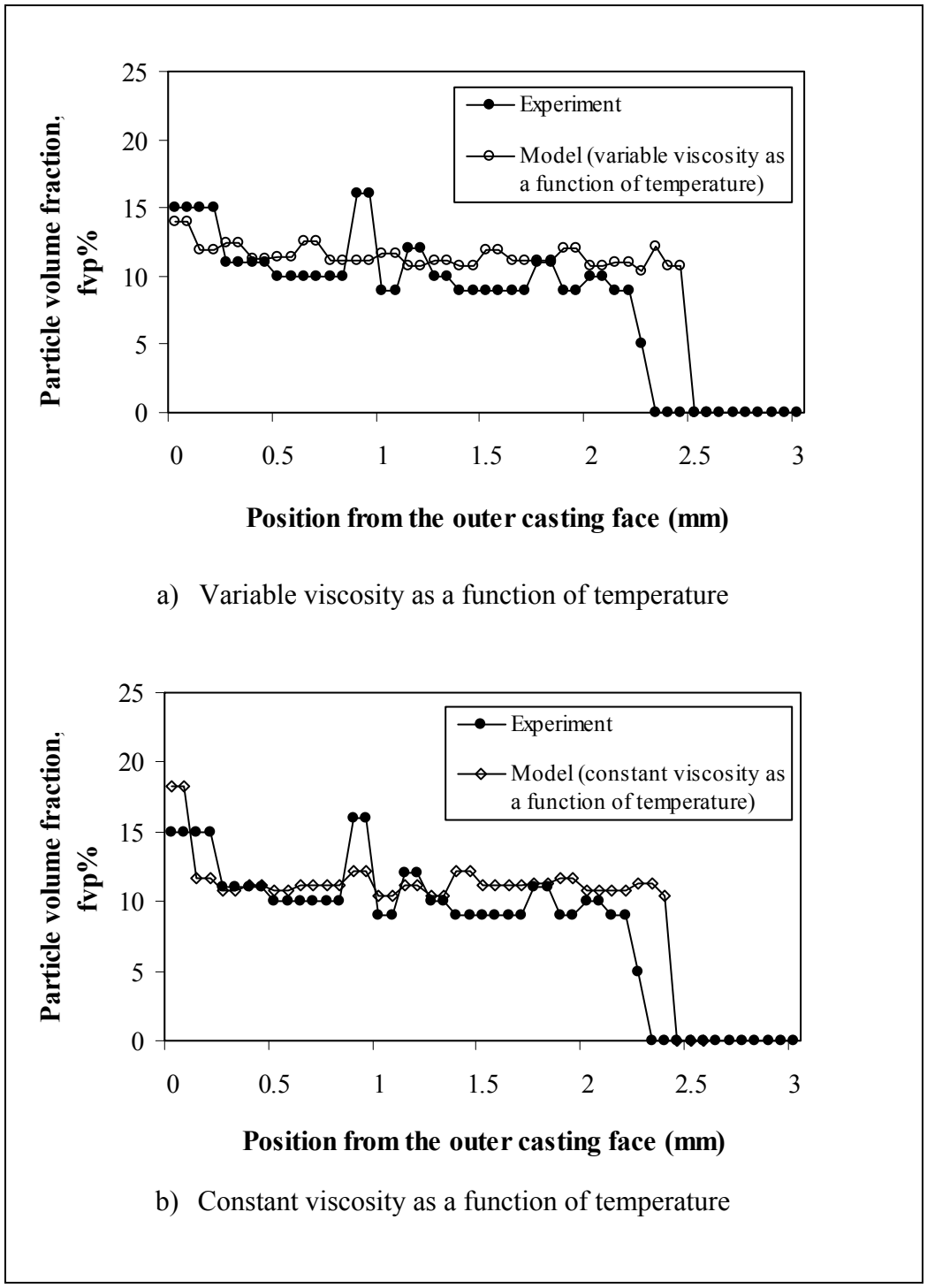

Figure 3. 14 Volume fraction of the particles across the casting section taking into account the influence of the variation in the particle volume fraction on the apparent melt viscosity and particle segregation ($T_{metal,in}$ = 973 K, $T_{mold,in}$ = 373 K).

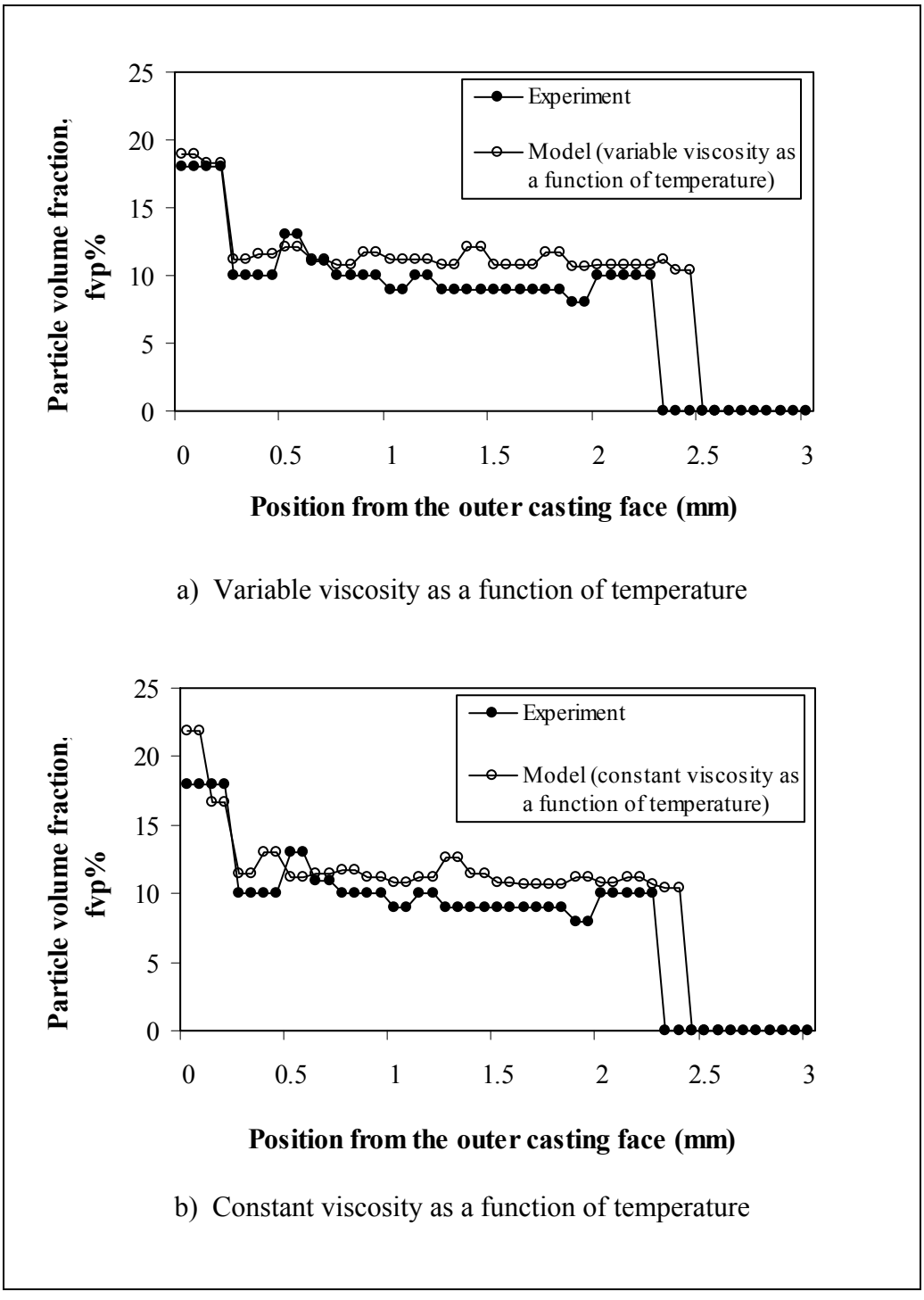

Figure 3. 15 Volume fraction of the particles across the casting section taking into account the influence of the variation in the particle volume fraction on the apparent melt viscosity and particle segregation ($T_{metal,in}$ = 973 K, $T_{mold,in}$ = 673 K).

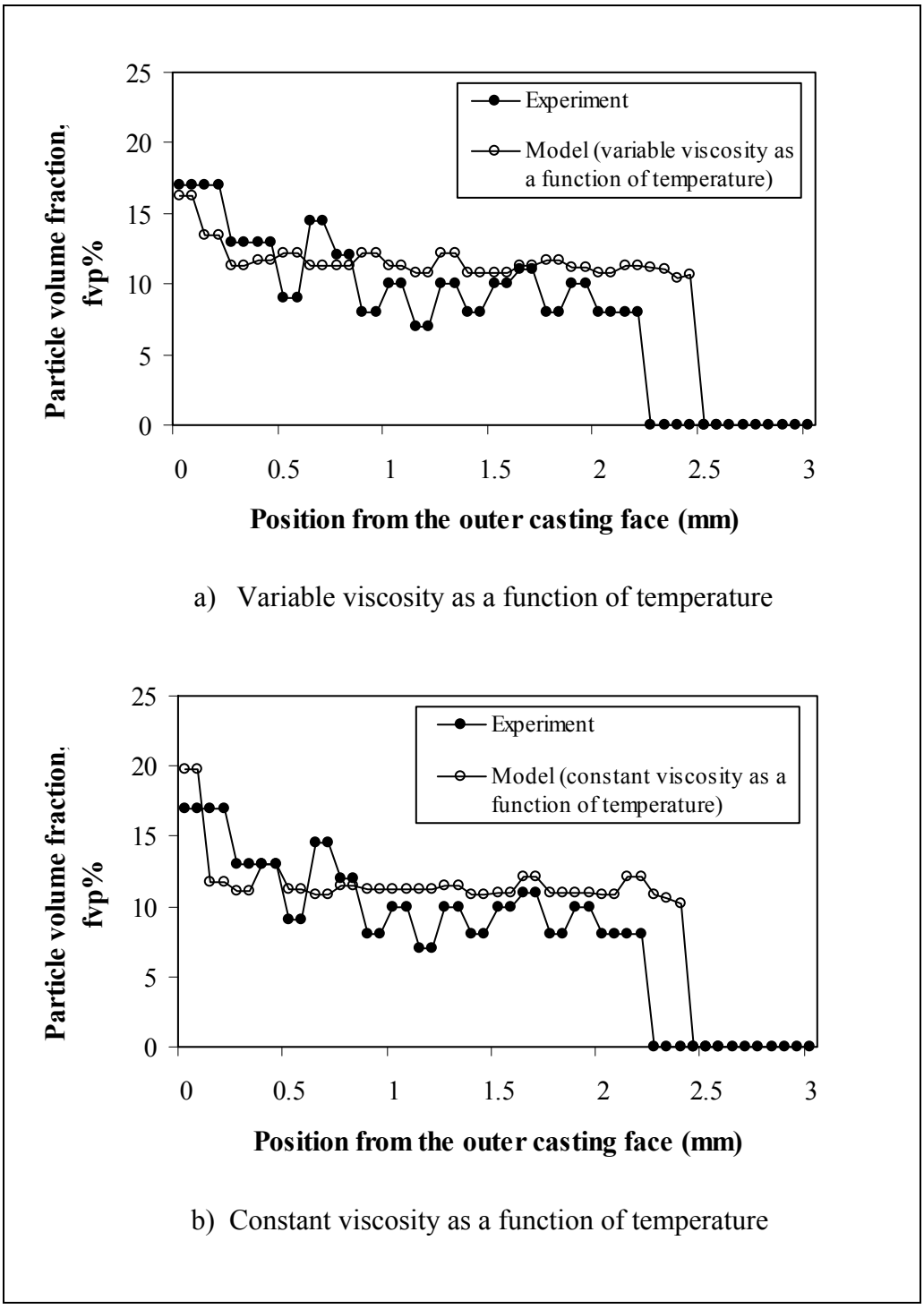

Figure 3. 16 Volume fraction of the particles across the casting section taking into account the influence of the variation in the particle volume fraction on the apparent melt viscosity and particle segregation ($T_{metal,in}$ = 953 K, $T_{mold,in}$ = 623 K).

3.6 Microstructure and distribution of particles

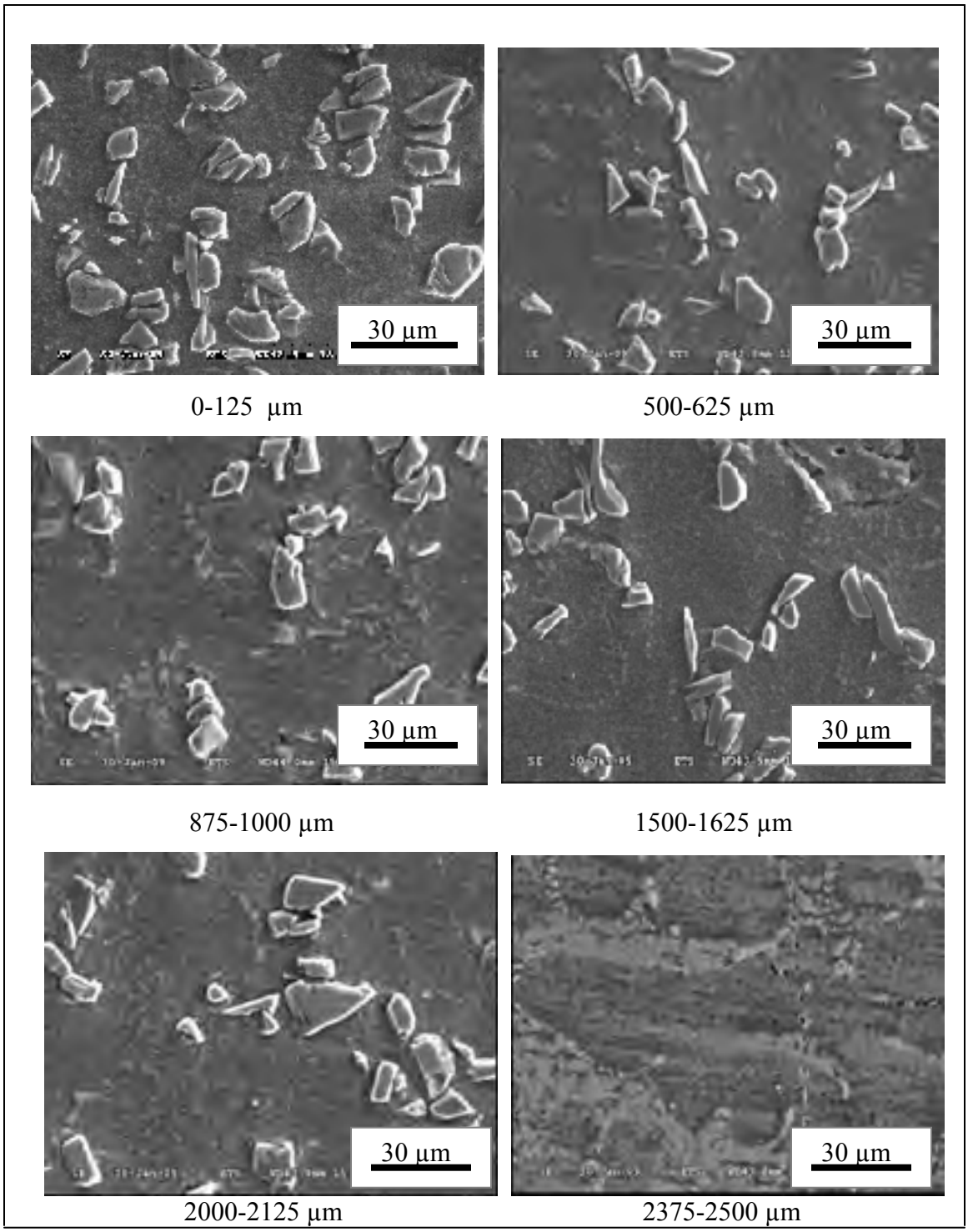

Figure 3. 17 Segregation of particles, $T_{metal,\ in}$ = 973 K, $T_{mold,\ in}$ = 673 K, (distances taken from the external casting surface).

Fig. 3.17 shows the segregation of particles at different locations from the external casting surface. It can bee seen on this figure the variation of the particles' volume fraction across the casting section. Furthermore, Fig. 3.18 taken with optical microscope shows the variation in the microstructure across the casting section. The dendrite size increases while advancing to the inner casting surface. In fact, the solidification speed at the inner casting surface is lower compared to that at the outer surface which is in contact with the mold. The decrease of the solidification speed and its variation across the section affects the formation of the primary phase. The lower the solidification speed the larger the dendrite size. The results agree with those of Rodriguez-Castro and Kelestemur (2002).

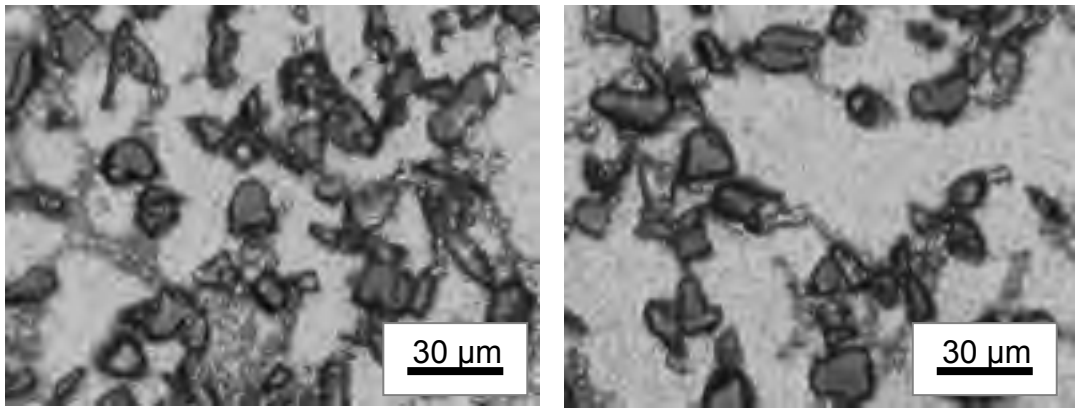

Figure 3. 18 Microstructure of Al/SiC composite, (distances taken from the external casting surface).

3.7 Discussions

The main interest of our work lies in its allowing us, when modeling the segregation of particles, to consider the evolution of the viscosity with temperature and cooling rate across the matrix, in addition to the change of the centrifugal radius during the displacement of the particle. This allows for a precise prediction of the volume fraction of the particles on the

outer/inner casting periphery. Furthermore, this work modeled the real variation in the particle velocity and deceleration during the centrifugation process, using Stokes' law at each discrete time interval for a particle moving at a constant velocity. The analysis done in this work illustrates the impact of the change in the centrifugal radius with the displacement of the particle and the increase in the viscosity with the decrease in temperature, on the dynamic and behaviour of particles during their segregation.

It was found in this work, while taking into account the variation of the centrifugal radius during centrifugation process that changes in the melt viscosity during the cooling process can have a significant impact on particle segregation and volume fraction through the matrix, depending on the initial pouring and mold temperatures and on the process parameters. Modeling of the velocity, deceleration/acceleration, displacement, and volume fraction of the particles, taking into account the change in temperature, cooling rate through the part section, and centrifugal radius, shows the effect of the variation in the viscosity on the segregation of the particles, and leads to results which better match their experimental counterparts on the outer casting surface. In contrast, modeling particle segregation with a constant viscosity can lead to a higher volume fraction than that obtained experimentally. This variation of the volume fraction of the particles is seen on the outer surface of the composite as well as through the matrix. Furthermore, the higher the initial pouring and mold temperatures, the higher the effect of the viscosity variation. This is explained by the increase of the cooling time. The higher the time required to extract superheat, the higher the effect of the viscosity on the segregation of the particles. The volume fraction of the particles on the outer casting surface stops increasing when the solidification begins, but continues to change through the matrix for a certain amount of time. This analysis is in line with the results found by Lajoye and Suéry (1988), who show that when the solidification of liquid metal begins very quickly, with no superheat to extract, the volume fraction of the particles on the outer surface of Al/SiC composite is low and very close to that obtained at the beginning of the segregation zone near the inner surface.

The volume fraction of the particles on the inner/outer surface and through the matrix should be controlled taking into account the impact of the cooling rate and the variation of the centrifugal radius and melt viscosity with time and position through the matrix. The fact that the increase in the initial pouring and mold temperatures increases the required time for the extraction of superheat allows particles to move across larger distances. Consequently, their volume fraction on the outer surface becomes higher.

3.8 Conclusions

- The discretization of Stockes's law over time, during centrifugal casting, allows a prediction of the real particles' velocity and displacement, which leads to a more precise determination of the particles' volume fraction, especially on the outer casting surface.

- In this work, variations in the centrifugal radius during the segregation of the particles are combined with the change in viscosity during the cooling process. It was found that the particle behavior varies with time and position whether the used centrifugal radius, viscosity, and therefore velocity of the particle are constants or variables.

- Modeling the particles' volume fraction variation across the casting section and on the outer casting surface, with a variable viscosity as a function of temperature produces results that are more accurate and closer to those obtained experimentally.

- Increasing the initial mold and pouring temperatures accentuates the effect of viscosity on particle segregation and increases the time required to extract superheat. This would favour higher volume fraction of particles on the outer casting surface, while the free-particle zone near the inner surface becomes larger. On the other hand, according to the parameters and conditions used in this work, and for low initial pouring and mold temperatures, the volume fraction of the particles on the outer casting surface is low and almost similar to that obtained near the inner surface.

CHAPTER 4

GENERAL DISCUSSION

4.1 Macrosegregation

It is known that the solidification of alloys is accompanied by a microsegregation of alloying elements due to the lack of diffusion and non-equilibrium nature of solidification. On the other hand, a macro-scale of segregation can appear through the matrix. This type of segregation is called macrosegregation, where the concentration of alloying elements and phases may vary substantially throughout the part section, thereby impairing its quality, affecting its properties, and limiting its size and productivity. Therefore, the importance of macrosegregation cannot be ignored when producing casting parts.

The degree of macrosegregation is influenced by the type and amount of alloying elements, ingot dimensions, solidification rate, and microstructure formation (columnar or equiaxed dendrites). The most relevant studies on macrosegregation have examined the macrosegregation of alloying elements such as aluminum in zinc-aluminum alloy ZA27 as well as tin and lead in bronze-tin alloy C92200, but studies on macrosegregation of phases and constituents, such as the eutectic, are very limited. Also, no data was found in the literature on the variation in the eutectic concentration from outer and inner surfaces to the center of the casting, and on its behavior in relation with the speeds of solidification fronts and their influence on the zone and position of the final solidification point.

Knowing that macrosegregation is an irreversible defect, the question is how far it is possible to control it in order to minimize its occurrence and its influence on castings' properties and on the process productivity. For a given alloy, the macrosegregation of eutectic is related to several conditions and parameters such as the morphology of the microstructure, the rate of solidification, and the movement of the solid phases and interdendritic liquid, under the influence of the solidification fronts, towards the zones of thermal contraction and

solidification shrinkage. Therefore, although the basic mechanism of macrosegregation is known, the modeling of eutectic macrosegregation during centrifugation is aimed to control and reduce its severity taking into account the experimental conditions and parameters, solidification mechanisms, zone of final solidification point, alloy characteristics, and segregation in order to determine and specify the way they affect the eutectic macrosegregation and their influence on its magnitude.

Based on the modeling and analysis and on the experimental data done in this work, we were able to define the macrosegregation of the eutectic, generated in thin-walled zinc alloy produced by centrifugal casting, as a normal segregation during which the interdendritic liquid moves under the influence of solidification fronts and primary solidifying phases to the final point of solidification. The experimental and theoretical results found in our study are in good agreement with the theory of the basic mechanism of macrosegregation phenomenon mentioned by Flemings (1974) for the normal segregation. Furthermore, it was found in our study that the decrease in the pouring and mold temperatures and the increase in solidification rate seem to reduce the rate of macrosegregation variation and its magnitude across the casting section. On the other hand, the control of the ratio between the speeds of the solidification fronts advancing from the inner and outer casting surface allows us to control the zone of the final solidification point and maximum eutectic concentration. Thus, to limit and decrease the rate of macrosegregation and the change in the eutectic concentration through the section, it is recommended that centrifugal casting be performed at the lowest possible pouring and mold temperatures and at the highest possible cooling rate that can be used, given the quality of the part surface.

In addition, it was found in our work that the zone of the final solidification point that was determined theoretically corresponds to the zone of maximum eutectic concentration found experimentally across the casting section. Therefore, depending on the conditions under which the part is used, and on its most constrained surface (resistance to abrasion and/or constraints on the inner and/or outer surface), the zone of maximum eutectic macrosegregation can be moved far from the constrained surface by controlling the ratio

between the speeds of solidification in the inner and outer surfaces. This control will thus permit a reduction in the risk of failure generated by the low ductility and toughness of the maximum eutectic concentration zone. Therefore, for increasing the service reliability of centrifugally cast parts and for improving their strength and quality, a control of macrosegregation across the casting section should be conducted based on the parameters, experimental conditions, solidification rate, and speed of solidification in both inner and outer casting surfaces.

4.2 Particles' segregation

Metal matrix composites can be produced by several techniques including gravity casting, powder metallurgy, centrifugal casting, squeeze casting, and die casting. However, for fabricating functionally graded composites, centrifugation is the most used technology, especially for hollow and cylindrical parts. The centrifugation technique permits us to vary and control the particles' segregation and their graduation degree across the casting section in order to obtain specific mechanical properties at the desired points of the section.

The modeling of particle segregation during centrifugal casting of MMC_P was conducted by several authors (Lajoye and Suery 1988; Raju and Mehrotra 2000; Rodriguez-Castro and Kelestemur 2002; Bonollo et al. 2003; and others) using Stokes' law, approximately, with constant centrifugal radius and viscosity regardless of change in the particles' velocity during their displacement and its impact on the particle volume fraction and segregation across the casting section. Using such approximation makes the prediction of particle segregation less precise and can lead to poorer quality parts. Therefore, in order to remedy this lack in the modeling and analysis of the particles' segregation, we discretized Stokes' law over time, and a mathematical modeling was done for each physical parameter that affects the particles' segregation (velocity, acceleration, displacement). This discretization allowed us to deduce more realistic particle behavior and velocity due to the change in the centrifugal radius and viscosity during the cooling process. This helped us achieve better control of the particles' segregation on the outer casting surface. During the modeling of the particles' segregation,

we calculated the distance traveled by the particle using equation 3.21, which is expressed in term of velocity and acceleration calculated by equations 3.11 and 3.17 while using Stockes' law discretized over time.

Lajoye and Suery (1988) have mentioned that the pouring temperature and the change in viscosity during the solidification process can affect the particles' velocity and segregation. Although this was neglected in their modeling, Lajoye and Suery found a good agreement between the theoretical and experimental results obtained. However, the value of the viscosity used was too high (0.0025 Pa.s), while the viscosity of the liquid metal does not exceed 0.002 Pa.s., even for a temperature that does not differ much from the liquidus temperature, taking into account the initial particles' volume fraction. Moreover, according to our modeling, the higher value of the viscosity increases the viscosity force in the opposite direction to the centrifugal force and reduces the particles' displacements for a given time of centrifugation. On the other hand, if the cooling time is short and the extraction of superheat is too fast, the influence of the change in the viscosity with temperature on the particles' segregation becomes smaller. In that case, the results obtained with constant and variable viscosities become almost similar. Therefore, the time of the superheat extraction and the value of the viscosity used have a major influence on the particles' segregation.

The results found in our study are supported with experimental data. The volume fraction of particles obtained experimentally through the casting section is compared with that obtained theoretically. The difference in the results obtained theoretically for constant and variable viscosities compared with those obtained experimentally is very clear; especially on the outer casting surface which constitutes the most critical place of a part subjected to a friction stress. Regarding the section of the casting away from the outer surface, this difference in the results is less pronounced because of the small increase in the particles' volume fraction far from the outer casting surface for the parameters and experimental conditions used in our study.

Furthermore, regarding the comparison between the theoretical and experimental results of particles' volume fraction, Watanabe *et al*. (1998) found a difference of about 30 %V

between the experiments and the theoretical results while using Stokes' law with a constant particle velocity. According to our results, the difference between the experimental and theoretical results, at a constant viscosity, varied from about 15%V to 25%V depending on the initial pouring and mold temperatures, while this difference varied from about 2%V to 5%V with variables viscosity and particle velocity. Thus, it is shown that using variable viscosity in modeling gives more accurate results that are very consistent with experimental data. On the other hand, the particles' concentration across the casting section was measured more than one time in order to determine the errors that could occur during measuring. The results showed experimental variations of particle volume fraction ranging from ±1%V to ±2%V, which are much less than the difference found between the theoretical and experimental results (15%V to 25%V). In addition, as mentioned in paragraph 3.2, the photos of the section, which were used to measure the particles' concentration, were obtained with a magnification of 500 times, which facilitated the easy cutting of the particles.

4.3 Repulsive force

Most authors have neglected the repulsive force during modeling of the particles' segregation. Panda *et al.* (2006) were one of the few authors to model the particles' segregation, taking into account the repulsive force caused by the solidifying interface. However, it was mentioned by these authors that their modeling is only an approximation, and their model is based on assumptions that are only partially valid. For example, in their work, the solidification front was considered to be planar, while it can also be cellular or dendritic depending on the rate of solidification. The authors also mention that it is very difficult to predict either cellular or dendritic morphology of the solidification front. Thus, the influence of the solidifying interface on the particles' segregation is not yet completely understood. Research on this subject continues until today. Therefore, as has been reported by most authors (Lajoye and Suery 1988, p. 16; Raju and Mehrotra 2000, p. 1629; Rodriguez-Castro and Kelestemur 2002, p. 1815; Bonollo *et al*. 2003, p. 51; and others), it was assumed in our work that the particles are not rejected by the solidifying interface. Furthermore, the solidification rate is supposed to be very high at the outer casting surface

because of the high heat transfer at the mold/metal interface and, as was found by Rodriguez-Castro and Kelestemur (2002, p. 1819), the high solidification rate produces finer microstructures and leads to a better distribution of reinforcement particles in the matrix. The particles are less rejected by the solidification front due to the relatively high speed between the particles and the solid-liquid interface, especially on the outer casting surface. Consequently, the particles are distributed homogenously near this surface. This has been observed in our results, where the particles' distribution was homogenous near the outer surface (Chapter 3, Figures 3.17 and 3.18).

4.4 Particles interaction

For large particles' volume fraction, interaction between particles occurs, thus reducing the particles' velocity. According to Lajoye and Suery (1988, p. 17) and Raju and Mehrotra (2000, p. 1629), it is assumed that the reduction in velocity due to the particles' interactions is characterized by an increase of the liquid's apparent viscosity. In our study, based on the work of Raju and Mehrotra 2000, the influence of the increase of apparent viscosity on the particle velocity was taken into account, using equations 3.9 and 3.10. Thus, according to Raju and Mehrotra, the influence of particles' interaction on particle velocity is considered, in our study, with the change in apparent melt viscosity.

4.5 Solidification

In order to model the heat conduction and the variation of the heat transfer between the mold and the metal during the cooling process, we conducted, using FLUENT, a numerical simulation of the cooling process that is based on the parameters and boundary conditions used in our experiments. We used FLUENT taking into account the mold's, metal's, and particles' thermophysical properties while using the rule of mixtures in determining the thermophysical properties of the composite, as has been conducted by several authors (Panda *et al*., 2006; Raju and Mehrotra, 2000; and others).

Our modeling was done through the implicit finite difference formulation for a transient one-dimensional unsteady state of solidification. A one-dimensional formulation of heat flow perpendicular to the mold wall was used because of the too-small thickness of the part section compared to its length (3mm/62mm). Thus, the cooling time in the radial direction is too small compared to that in the axial direction. Moreover, most authors have considered one-dimensional heat flow when modeling of solidification during centrifugation process (Lajoye and Suery 1988, p. 16; Kang *et al.* 1994, p. 247; Raju and Mehrotra 2000, p. 1626; Panda *et al*. 2006, p. 1676; and others).

Using FLUENT to model the heat transfer is a powerful and effective way to determine the variation of the temperature as a function of time and position through the part section. The experimental determination of the temperature variation in each segment across the section is very difficult. Almost all researches on the temperature variations across the casting section during the centrifugation process were conducted theoretically (Lajoye and Suery 1988; Kang *et al.* 1994; Watanabe *et al.* 1998; Raju and Mehrotra 2000; Panda *et al*. 2006; and others). In addition, Watanabe *et al.* (1998, p. 595) mentioned that using experimental techniques to determine the temperature distribution and solidification time through the centrifugal method is very difficult, since the mold rotates at a very high speed during solidification.

The modeling of the heat transfer using FLUENT was done taking into account the initial particle volume fraction (fv = 10 %V) and its influence on the thermophysical properties variation of the composite. However, in order to clearly analyze the influence of the change of the particle volume fraction on the temperature and cooling rate variation across the casting section, the modeling of the heat transfer was redone with fv = 20 %V for given initial mold and pouring temperatures (T_{metal} = 973 K, T_{mold} = 673 K).

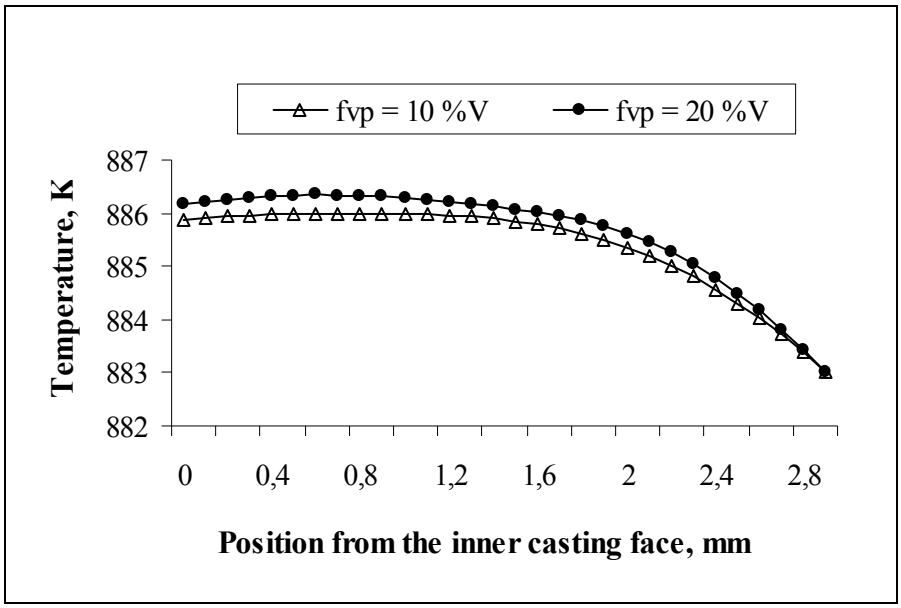

Figure 4. 1 Variation of the temperature across the casting section for different particle volume fractions (t = 0.57s).

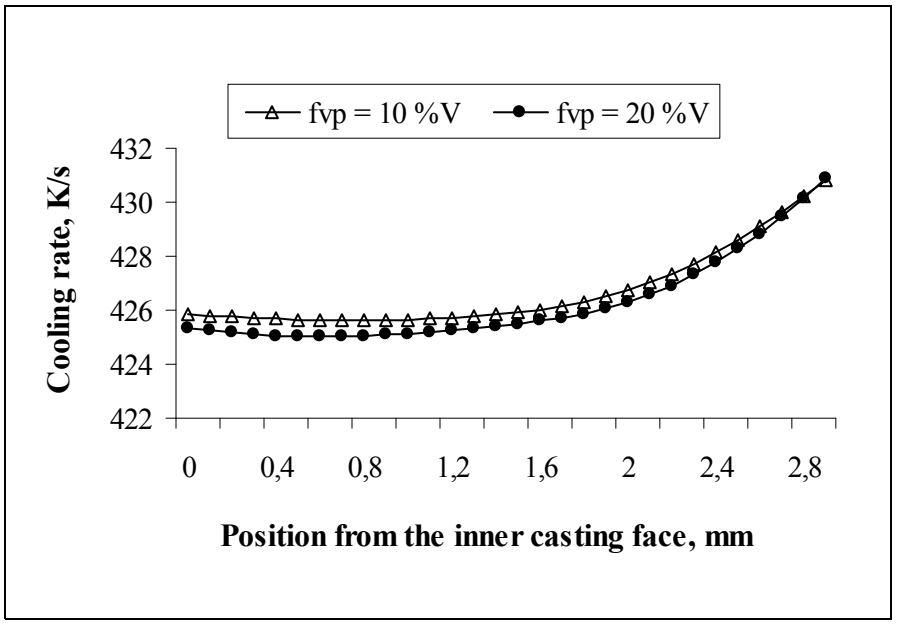

Figure 4. 2 Variation of the cooling rate across the casting section for different particle volume fractions (t = 0.57s).

Figures 4.1 and 4.2 show for the experimental conditions and parameters used in our study, the variation of temperature and cooling rates across the casting section for different particle volume fractions. It can be seen by these figures that, for a given time of cooling (0.57 s) necessary for the extraction of superheat across the section for given initial mold and pouring temperatures, the change in the particle volume fraction from fv = 10V% to fv = 20V% does not significantly affect the temperature and cooling rate variations across the casting section. The maximal difference in the cooling rate between the different particle volume fractions used is about 0.617 °C/s, which corresponds to a variation in temperature and cooling time of 0.35 °C and 0.002s respectively, for a total time of cooling of 0.57s. Thus, the time of superheat extraction during which the particles move is almost the same whether the particle volume fraction was 10%V or 20%V. Consequently, we assume, for the parameters and experimental conditions used in our study, that the increase in the particle volume fraction to fv = 20%V on the outer casting surface does not affect significantly the temperature variation and particles' displacement and segregation across the casting section during the extraction of superheat.

This analysis was done with a particle volume fraction of 20%V because according to our results, the maximum particle volume fraction obtained on the outer casting surface does not exceed 20%V.

4.6 Viscosity

The final behavior of the particles is a result of the competition between the increase in viscosity due to the reduction in temperature on the one hand, and to the increase in the centrifugal radius with the displacement of the particles on the other. In the case when the viscosity is constant, the particles move toward the outer casting surface with acceleration caused by the increase in the centrifugal radius alone, while they move with deceleration if a variation of the viscosity with temperature is taken into account. However, the change in the viscosity is also influenced by the variation in the particle volume fraction across the casting section. This was considered in our modeling using equations 3.9, 3.10, and 3.22. In fact, our

modeling was done in two steps. As a first step, the viscosity was modeled taking into account the variation of the temperature alone, which allowed us to clarify the influence of the temperature decrease on the viscosity and particle segregation without being influenced by another phenomenon such as the variation in the particle volume fraction. Thereafter, the segregation of the particles was modeled taking into account the variation of the viscosity as a function of temperature and particle volume fraction variations (Figs. 3.14, 3.15, 3.16). The results obtained for the two cases were compared and discussed which allowed us to observe a small reduction in the particle volume fraction on the outer casting surface due to the increase in viscosity with an increase in the particle volume fraction near this surface.

4.7 Time increment

In our study, the discretization of the particle velocity which is expressed by the Stokes' law is done over time, and Δt is used as a constant value. Although Δt is not a physical parameter, the choice of this parameter can influence the estimation of the particles' velocities during their segregation, the estimation of the total time of superheat extraction and the estimation of the particles' displacement during the cooling process. The smaller the time increment, the higher is the accuracy of the particle velocity discretization. Also, the smaller the Δt, the smaller will be the difference between the calculated temperature and that of the liquidus before the temperature falls in the mushy zone. A small Δt used in the modeling allows taking into consideration the change in temperature, during cooling for a longer and more precise time before the temperature drops in the mushy zone, given that the particles' displacement in the mushy zone is negligible. This allows, during the modeling of the particles' segregation for a given time of centrifugation, to consider the distance travelled by the particles for a total time of cooling corresponding better to the time of superheat extraction. Thus, a use of a small constant Δt gives more accurate results on the total distances travelled by the particles, which improves the prediction of the particles' volume fraction on the outer surface and across the section of the casting (appendix IV). In addition, Lajoye and Suery (1988, p.17) used Δt as the delay of superheat extraction and considered it

as a parameter that influences particles' volume fraction variation while using Stokes law with a constant particle velocity.

In our study, the analysis of Δt is not done in order to show its influence on the particles' segregation, but in order to justify the value of Δt used in the models. Thus, from this analysis, we come to the conclusion that Δt value should be as small as possible. For an average time of superheat extraction of 0.4 s, it was found that from $\Delta t = 0.005$ s and down, the variation of the particles' volume fraction on the outer casting surface becomes insignificantly affected by the variation of Δt and the small deviation of temperature of that of the liquidus one while using a constant Δt (appendix IV, Fig. IV. 1).

4.8 Modeling of particle volume fraction

While modeling the particles' segregation, Siva Raju and Mehrotra (2000) considered the variation in the time of the volume fraction of particles by ensuring the conservation of the total mass of particles at all times. In their approach, the volume of particles between two consecutive nodal points always remains the same, but the length of the segment varies with time. On the other hand, in the modeling of Panda *et al*. (2006), the nodes remain fixed at all times, and the variation of the particles' volume fraction in any particular segment, over time, is calculated by considering the particle movement in time.

In our modeling, we considered the variation of the particles' volume fraction with time by ensuring the conservation of the total particles' volume fraction through the matrix at all times and, thus, by ensuring the conservation of the total mass at time (i.e., Siva and Mehrotra's approach). Therefore, the initial particles' volume fraction through the whole casting matrix remains constant at all times, but it varies in each sub-volume, due to the particles' movement. This occurs while using Stokes's law and particle velocity, discretized over time, to determine the distance traveled by the particles (taking into account the variation in the viscosity and centrifugal radius during the centrifugation process).

Thus, the modeling of the particles' segregation and of the changes in their volume fractions across the section is based on the particles' movement and volume/mass conservation through the part section at any instant of time. The percentage of the volume fraction gained by given sub-volumes will be lost by other sub-volumes, and the initial particles' volume fraction throughout the whole matrix remains the same. Our formulation of the particles' segregation as a function of time and position is expressed analytically by equation 4.1.

$$fv_{V_i}^{ti} = fv_{V_i}^{t_0} + fv_{\rightarrow V_i}^{ts} - fv_{V_i\rightarrow}^{ts} + \sum_{i=0}^{n} \Delta fv_{V_{i+1}\,(fv(V_i+1)>52\%)}^{ts} \qquad (4.1)$$

Figure 4.3 schematizes several sub-volumes across the casting section. Each sub-volume contains an initial particle volume fraction of 10 %V, with particles distributed homogenously over its entire length. Based on the mass/volume conservation, the total particles' volume fraction, throughout the entire matrix at all times (t_i), should be equal to the initial particles' volume fraction at time t = 0; hence, the variation of the initial total volume fraction over time is zero ($df_v/dt = 0$). Thus, for a given time of centrifugation (t_i), the sum of the particles' volume fractions on all sub-volumes, divided by the number of sub-volumes, gives the initial volume fraction through the matrix (Eq. 4.2):

$$fv_{fin.matrix}^{ti} = \frac{\sum_{i=0}^{n} fv_{V_i}^{ti}}{N_{V_i}} = fv_{ini.matrix}^{t_0} \qquad (4.2)$$

where:

N_{Vi}: number of sub volumes;

fv_{vi}^{ti} : particles' volume fraction in sub volume V_i at time t_i ;

$fv_{ini.matrix}^{t_0}$: initial particles' volume fraction in the matrix;

$fv_{fin.matrix}^{t_0}$: final particles' volume fraction in the matrix.

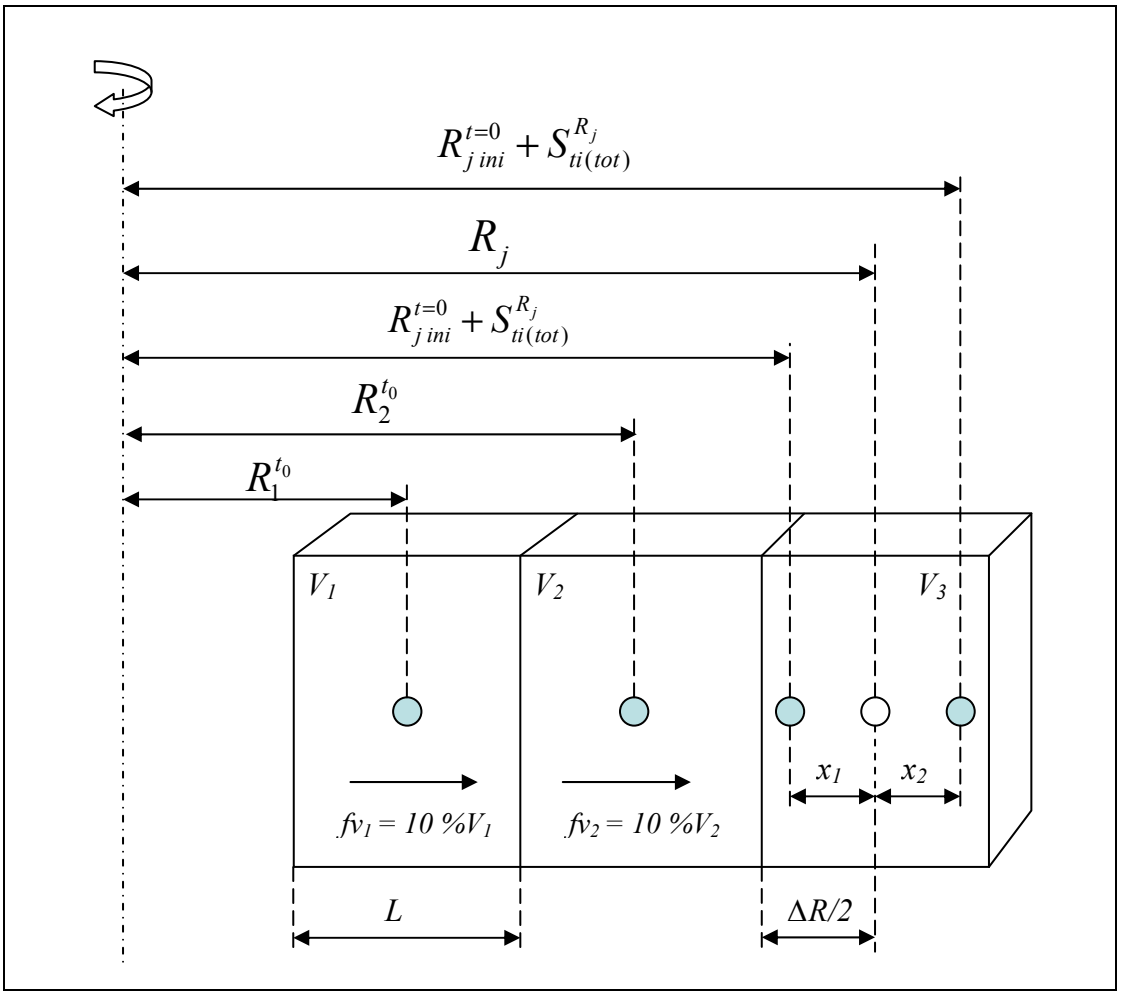

Figure 4. 3 Schematization of the particles' segregation analysis in a casting section consisting of several sub-volumes.

In the proposed modeling, nodal points are considered at the center of each segment. The distance (R_j) between the rotation axis and the volume fraction of a given sub-volume is determined from the center of the latter. Thus, the particle positions are considered at the nodal points. If, for a given time of centrifugation, a volume fraction *(fv)* moves to a distance x_1 or x_2 from the center of V_i (Fig. 4.3), then a percentage of the moved particles will be segregated in sub-volume V_{i-1} or V_{i+1}, respectively. Equation 4.3 expresses the volume fraction entering sub-volume V_i and the percentage of volume fraction *(fv)* that can be segregated in V_{i-1} or V_{i+1}, depending on its position relative to the R_j of V_i:

$$fv^{ts}_{\rightarrow V_i} = \left[\sum_{i,j=0}^{n} fv^{ts}_{V_i,ini\left(R_j-\Delta R/2<R^{t=0}_{j(ini.)}+S^{Rj}_{(ti)tot}<R_j\right)}\right] - \sum_{i,j=0}^{n}\frac{fv^{ts}_{V_i,ini}}{\Delta R}\cdot\left[R_j-\left(R^{t=0}_{j(ini.)}+S^{Rj}_{(ti)tot}\right)\right]+$$
$$+\left[\sum_{i,j=0}^{n} fv^{ts}_{V_i,ini\left(R_j<R^{t=0}_{j(ini.)}+S^{Rj}_{(ti)tot}<R_j+\Delta R/2\right)}\right] - \sum_{i,j=0}^{n}\frac{fv^{ts}_{V_i,ini}}{\Delta R}\cdot\left[\left(R^{t=0}_{j(ini.)}+S^{R_j}_{(ti)tot}\right)-R_j\right] \quad (4.3)$$

The analysis below, based on figure 4.3, shows the calculation of the percentages of a given volume fraction segregated at sub-volumes V_i and V_{i-1} when its position, after moving for a given centrifugation time, is at distance x_1 from R_j:

$$x_1 = R_j - \left(R^{t=0}_{jini} + S^{R_j}_{ti(tot)}\right) \quad (4.4)$$

In each radius increment, ΔR, there is a particle volume fraction of $fv_i=10\ \%V_i$. Accordingly, $\Delta R/2$ corresponds to $f_{Vi}/2$. Therefore, we can express the percentage of the volume fraction segregated in V_{i-1} as follows:

$$fv_{(Vi-1)} = \frac{f_{Vi,ini.}}{\Delta R}\cdot x_1 \quad (4.5)$$

$$\Rightarrow fv_{(Vi-1)} = \frac{f_{Vi,ini.}}{\Delta R}\cdot\left[R_j - \left(R^{t=0}_{jini} + S^{R_j}_{ti(tot)}\right)\right] \quad (4.6)$$

Since many sub-volumes exist throughout the matrix in many different positions in relation to the rotation axis, the particles can move to a given sub-volume V_i from different positions across the casting section, based on the distances they travel for a given time of centrifugation. Thus, we express equation (4.6) by equation (4.7), where *(i)* represents the sub-volumes and *(j)* represents the positions from the rotation axis:

$$fv_{(Vi-1)} = \sum_{i,j=0}^{n}\frac{f^{ts}_{Vi,ini.}}{\Delta R}\cdot\left[R_j - \left(R^{t=0}_{jini} + S^{R_j}_{ti(tot)}\right)\right] \quad (4.7)$$

This analysis demonstrates that for a particle volume fraction of 10 $\%V_i$ that moves to a position of x_1 from R_j of a sub-volume V_i, the percentage of the volume fraction segregated in the sub volume $V_{i\text{-}1}$ can be calculated. This percentage corresponds to equation (4.7), while the remaining parts of the *10* $\%V_i$ segregated in V_i correspond to expression (4.8), which comprises the first part of equation (4.3):

$$\left[\sum_{i,j=0}^{n} fv_{V_i,ini}^{ts}{}_{\left(R_j-\Delta R/2<R_{j(ini.)}^{t=0}+S_{(ti)tot}^{Rj}<R_j\right)}\right]-\sum_{i,j=0}^{n}\frac{fv_{V_i,ini}^{ts}}{\Delta R}\cdot\left[R_j-\left(R_{j(ini.)}^{t=0}+S_{(ti)tot}^{Rj}\right)\right] \tag{4.8}$$

The same analysis applies when the volume fraction moved to a sub-volume V_i is at a distance x_2 from R_j (Fig. 4.3)—except in that case, x_2 is written this way:

$$x_2=\left(R_{jini}^{t=0}+S_{ti(tot)}^{R_j}\right)-R_j \tag{4.9}$$

Thus, the percentage of the particles' volume fraction that is segregated in the sub-volume V_{i+1} can be calculated using equation 4.10:

$$fv_{(Vi+1)}=\sum_{i,j=0}^{n}\frac{f_{Vi,ini}^{ts}}{\Delta R}\cdot\left[\left(R_{jini}^{t=0}+S_{ti(tot)}^{R_j}\right)-R_j\right] \tag{4.10}$$

On the other hand, the percentage of the particles' volume fraction that is segregated in the sub volume V_i will correspond to expression (4.11), which is the second part of equation (4.3):

$$\left[\sum_{i,j=0}^{n} fv_{V_i,ini}^{ts}{}_{\left(R_j<R_{j(ini.)}^{t=0}+S_{(ti)tot}^{Rj}<R_j+\Delta R/2\right)}\right]-\sum_{i,j=0}^{n}\frac{fv_{V_i,ini}^{ts}}{\Delta R}\cdot\left[\left(R_{j(ini.)}^{t=0}+S_{(ti)tot}^{R_j}\right)-R_j\right] \tag{4.11}$$

Therefore, during centrifugation, the conservation of mass/volume is established between V_{i-n}, V_i, and V_{i+n}. The percentage of the volume fraction gained by given sub-volumes will be lost by others, and the mass/volume conservation is always maintained (see example below).

On the other hand, the particles' volume fraction leaving a sub-volume V_i, for a given time of centrifugation, is expressed by equation (4.12). This equation takes into account the initial particles' volume fraction in V_i at $t = 0$, plus the sum of volume fractions entering this sub-volume during centrifugation, providing that:

1. The temperature in the sub-volume V_{i+1} at centrifugal time $t_i+\Delta t$ is higher than the liquidus temperature, since the particle does not move in the mushy zone.

2. The volume fraction of particles in V_{i+1} is smaller than 52 %V since, according to Watanabe *et al.* (1998), that is the maximum particles' volume fraction that a given volume of liquid metal may contain for a simple cubic packing of SiC.

$$fv_{V_i\rightarrow}^{ts} = \left(fv_{V_i(ini.)}^{t_0} + \sum_{i=0}^{n} fv_{\rightarrow V_i}^{ti} \right)_{(fv_{V_{i+1}}^{ti+\Delta t} < 52\%,\ T_{V_{i+1}}^{ti+\Delta t} \geq T_L)} \tag{4.12}$$

The position of the particles' volume fraction after displacement for a given centrifugation time is given by equation (4.13). This equation takes into account the initial positions of the volume fraction at time $t = 0$ and the total distance it moves for a centrifugation time t_i.

$$R_{(fv)_j^{t_s}}\Big|_{j=0}^{n} = R_{(fv)_j^{t_0}}\Big|_{j=0}^{n} + \sum_{i,j=0}^{n} S_{(fv)_{R_j}}^{t_i} \tag{4.13}$$

Equation (4.13) is the same simplified expression used in equation (4.3):

$$R_{jini}^{t=0} + S_{ti(tot)}^{R_j} \tag{4.14}$$

Example

Let V_1, V_2, and V_3 be sub-volumes, each of 100 μm length and containing a particles' volume fraction of 10 $\%V_i$ (Fig. 4.3). The sub-volume V_3 is on the border of the mold; hence, this sub-volume can gain particles, but cannot lose any. The centrifugal radius to the inner wall of sub-volume V_1 is 2000 μm.

Suppose that for a given centrifugation time t_i, the volume fractions that are initially in the sub-volumes V_1 and V_2 move distances of 55 μm and 65 μm, respectively.

With:

R_1 = 2000 μm + 50 μm = 2050 μm

R_2 = 2000 μm + 150 μm = 2150 μm

$R_j = R_3$ = 2000 μm + 250 μm = 2250 μm

The initial particles' volume fraction throughout the whole matrix is:

$$fv_{ini} = (10\%V_1+10\%V_2+10\%V_3)/3 = \mathbf{10\ \%V} \tag{4.15}$$

The new volume fraction in the sub-volume V_3, for a given centrifugal time t_i, is calculated using equations 4.1, 4.3, 4.7, 4.10, and 4.12, taking into consideration that particles do not leave this sub-volume and that, based on the final position of the displaced volume fraction (Eq. 4.13), $x_2 = 0$ in both V_3 and V_2:

$$fv_{(V3)} = 10\ \% + 10\ \% - (10\%/100) \cdot [2250\ \mu m - (2150\ \mu m + 65\ \mu m)] - \tag{4.16}$$
$$- 0\ \% + 0\ \% + 0\ \% = \mathbf{16.5\ \%V}$$

The new volume fraction in the sub-volume V_2 is calculated using equations 4.1, 4.3, 4.7, 4.10, and 4.12, taking into consideration, based on the final position of the displaced volume fraction (Eq. 4.13), that $x_2 = 0$ in V_1 and V_2:

$$fv_{(V2)} = 10\ \% + 10\ \% - (10\%/100) \cdot [2150\ \mu m - (2050\ \mu m + 55\ \mu m)] - \quad (4.17)$$
$$- 10 + (10\%/100) \cdot [2250\ \mu m - (2150\ \mu m + 65\ \mu m] + 0\% = \mathbf{9\ \%V}$$

The new volume fraction in the sub-volume V_1 is calculated using equations 4.1, 4.3, 4.7, 4.10, and 4.12, taking into account that V_1 is the first sub-volume in relation to the distance from the rotation axis. Hence, V_1 can only lose particles. Moreover, based on the final position of the volume fraction (Eq. 4.13), $x_2 = 0$ in V_1:

$$fv_{(V1)} = 10\ \% + 0\ \% + (10\%/100) \cdot [2150\ \mu m - (2050\ \mu m + 55\ \mu m)] - 0\% - 10\ \% = \quad (4.18)$$
$$= \mathbf{4.5\ \%V}$$

Based on equation 4.2, the final particles' volume fraction throughout the whole matrix is:

$$fv^{ti}_{fin.matrix} = \frac{16.5\ \%V + 9\ \%V + 4.5\ \%V}{3} = 10\ \%V = fv^{t_0}_{ini.matrix} \quad (4.19)$$

Therefore, the final particles' volume fraction, obtained through the whole section, corresponds to the initial volume fraction *(fv_{fin} = 10 %V = fv_{ini}),* which indicates the volume/mass conservation at any instant of time. In addition, it may be noted that a small particles' displacement of 65 μm can have a significant effect on the particles' volume fraction in a given sub-volume. In comparison with the initial particles' volume fraction in the sub-volume V_3 (fv_{ini} = 10 %V), an increase of about 65% of fv_{ini} was produced in this sub-volume after the given particles' displacement.

The analysis shown above was conducted again, supposing that for a given centrifugation time t_i, the volume fractions that are initially in the sub-volumes V_1 and V_2 move distances of 30 μm and 35 μm, respectively. The results give the following volume fraction in each sub-volume:

$$fv_{(V3)} = 13.5\ \%V$$
$$fv_{(V2)} = 9.5\ \%V$$
$$fv_{(V1)} = 7\ \%V$$

The final particles' volume fraction throughout the whole matrix is:

$$fv^{ti}_{fin.matrix} = \frac{13.5\ \%V + 9.5\ \%V + 7\ \%V}{3} = 10\ \%V = fv^{t_0}_{ini.matrix} \tag{4.20}$$

Thus, an increase of about 35% of fv_{ini} was produced in sub-volume V_3 after the given particles' displacement.

According to the graph of the particle positions (Fig. 3.8), the difference in the distance traveled by a particle for constant and variable viscosities is small, less than 50 μm. However, according to the demonstration above, a small particle displacement can cause a significant variation in the particle volume fraction for a given sub-volume. In addition, the variation of the particles' volume fraction in a given sub-volume can be caused by the simultaneous segregation and displacement of particles from several positions across the casting section, thus increasing the influence of a small difference in the distance traveled by the particles on their volume fraction variation. Thus, a difference in the particle-traveled distance of less than 50 μm causes a change of the particles' volume fraction in each sub-volume across the casting section. On the other hand, the difference in the distance traveled by the particles is assumed to increase with the increase of the casting thickness and the time of superheat extraction, which can increase the difference in the particles' volume fractions for the results of constant and variable viscosities. Therefore, after this analysis, we can conclude that the reduction in particle velocity and displacement, due to the increase in viscosity during the cooling process, affects the particles' volume fraction on the outer casting surface and across the section.

GENERAL CONCLUSIONS

After having studied and modeled – during centrifugal casting – the macrosegregation of phases and the zone of maximum eutectic segregation through a part section of zinc-aluminum alloy ZA8 and, after studying and modeling the segregation of SiC particles in MMC_P while using Stokes' law discretized over time, we conclude the following:

- The phase macrosegregation generated during centrifugal casting of a thin-walled zinc alloy is a normal segregation during which the interdendritic liquid is pushed under the influence of solidification fronts, to fill the zones of shrinkage and thermal contraction corresponding to the zone of the last solidification point.

- Macrosegregation, and its rate of variation across the section, decrease with increases in the solidification speed.

- The zone of maximum eutectic segregation across the casting section can be controlled by controlling the ratio between the solidification fronts. Thus, the weak zone of the microstructure, where the toughness and ductility are low, may be driven away from the surface where the constraints are applied.

- Centrifugal casting produces a fine microstructure. The dendrites are equiaxed, which promotes normal segregation. Moreover, the structure of the eutectic can be granular or lamellar, depending on the speed of solidification. High-speed solidification promotes the formation of granular eutectic.

- The change in the liquid metal viscosity with the drop of temperature and the variation of the centrifugal radius with the displacement of the particle affect the particles' segregation and volume fraction especially on the outer/inner casting surface. The increase in viscosity during cooling process increases the force opposing the centrifugal

force, which can affect the distances traveled by the particles for a given time of centrifugation causing a change in their volume fraction.

- Modeling the particles' segregation with constant viscosity leads to a volume fraction of particles on the outer casting surface higher than that found experimentally, depending on the value of viscosity used, along with initial mold and pouring temperatures. In contrast, when the variation in viscosity is taken into account, the volume fraction of the particles – obtained theoretically – on the outer casting surface, better matches the results found experimentally.

- The initial mold and pouring temperatures, the time required for extracting the superheat, and the process parameters (rotation speed, diameter, and initial volume fraction of the particles, density difference between the particles and the matrix) play a principal role in the segregation and distribution of particles across the casting section.

RECOMMENDATIONS

In this thesis, the macrosegregation of phases has been studied. The zone of maximum eutectic macrosegregation through the matrix was modeled during the centrifugal casting of ZA8 zinc-aluminum alloy. In addition, we have studied and modeled, during the centrifugal casting of a functionally graded aluminum matrix composite (Al/SiC), the segregation of submicron particles while using – during the modeling – a dynamic viscosity and a variable centrifugal radius. As a result of this work we can recommend, for future research, the following points:

- Study the centrifugal casting of metal matrix composites reinforced by nano-metric particles. This study will allow verification of the centrifugal laws on such particle types, as well as analysis of the phenomenon of agglomeration for this size of reinforcement and its influence on the particles' volume fraction across the casting section.

- Change the composition of the composite matrix in order to segregate, on the inner casting surface, hard and resistant to wear particles with low density, such as boron carbide (B_4C), for example. This can be done by adding to the matrix dense addition elements, such as copper, to increase the density of the matrix relative to that of the particles and thus reverse the direction of the particle displacement.

- Study the influence of alloying elements, such as magnesium (Mg), on the macrosegregation of phases. Mg gives, with aluminum and zinc, phases at temperatures higher than that of the eutectoid transformation that occurs in zinc-aluminum alloys, which may be useful to limit macrosegregation.

- Optimize the segregation of particles and phases during the centrifugal casting of metal matrix composites in order to have better mechanical properties and decrease the possibility of failure.

APPENDIX I

COMPOSITION AND MECHANICAL PROPERTIES OF ZINC ALLOYS

Table I.1 Designation and composition of zinc casting alloys
(From ASM Handbook, vol. 15, 2008)

Alloy		Stand - ard	Composition(a), wt%								
Common designation	UNS No.	ASTM	Al	Cu	Mg	Fe	Pb	Cd	Sn	Ni	Zn
No. 3	Z33530	B 86	3.5–4.3	0.25	0.02–0.03	0.100	0.005	0.004	0.003	…	bal
No. 5	Z35531	B 86	3.5–4.3	0.75–1.25	0.03–0.08	0.075	0.005	0.004	0.003	…	bal
No. 7	Z33523	B 86	3.5–4.3	0.25	0.005–0.02	0.10	0.003	0.002	0.001	0.005–0.02	bal
No. 2	Z35541	B 86	3.5–4.3	2.5–3.0	0.020–0.050	0.100	0.005	0.004	0.003	…	bal
ZA-8	Z35636	B 86	8.0–8.8	0.8–1.3	0.015–0.03	0.075	…	0.004	0.003	…	bal
ZA-12	Z35631	B 86	10.5–11.5	0.5–1.25	0.015–0.03	0.10	0.004	0.003	0.002	…	bal
ZA-27	Z35841	B 86	25.0–28.0	2.0–2.5	0.01–0.02	…	0.004	0.003	0.002	…	bal
ACuZinc5	Z46541	B 894	2.9	5.5	0.04	0.075	0.005	0.004	0.003	…	bal

(a) Maximum unless range is given or otherwise indicated

Table I.2 Comparison of typical mechanical properties of zinc casting alloys
(From ASM Handbook, vol. 15, 2008)

Alloy and product forms	Ultimate tensile strength		0.2% offset yield strength		Elongation in 50 mm (2 in.), %	Hardness, HB	Fatigue strength		Young's modulus	
	MPa	ksi	MPa	ksi			MPa	ksi	GPa	10^6 psi
No. 2 (D)	358	52	…	…	7	100	58	8.5	…	…
No. 3 (D)	283	41	…	…	10	82	47.6	6.9	…	…
No. 5 (D)	331	48	…	…	7	91	56.5	8.2	…	…
No. 7 (D)	283	41	…	…	13	80	…	…	…	…
ZA-8 (S)	248–276	36–40	200	29	1–2	80–90	…	…	85.5	12.4
ZA-8 (P)	221–255	32–37	207	30	1–2	85–90	51.8	7.5	85.5	12.4
ZA-8 (D)	372	54	290	42	6–10	95–110	…	…	…	…
ZA-12 (S)	276–317	40–46	207	30	1–3	90–105	103.5	15	83.0	12.0
ZA-12 (P)	310–345	45–50	207	30	1–3	90–105	…	…	83.0	12.0
ZA-12 (D)	400	58	317	46	4–7	95–115	…	…	…	…
ZA-27 (S)	400–440	58–64	365	53	3–6	110–120	172.5	25	75.2	10.9
ZA-27 (P)	421–427	61–62	365	53	1	110–120	…	…	75.2	10.9
ZA-27 (D)	421	61	365	53	1–3	105–125	…	…	…	…

D: die cast;

S: sand cast;

P: permanent cast.

APPENDIX II

GENERAL PRPERTIES OF CERAMICS

Table II.1 General properties of the most used ceramics as a reinforcement (From N. Villar, 1996)

Ceramics	Density (g/cm^3)	Hardness (GPa)	Young's modulus (GPa)	Coefficient of thermal expansion (10^{-6} K^{-1})	Thermal conductivity ($W.m^{-1}.K^{-1}$)
Cr_3C_2	6.7	10-20	285	10	19
ZrO_2 stable	5.5 - 6	10 - 15	97-207	13.5	1.7
TiC	4.92	28-35	430	7-8.5	30-35
TiB_2	4.5 - 4.6	15 - 35	515 - 575	8.1	65 – 120
Al_2O_3	3.97	18-22	380-450	7-8	25-30 à 20 °C 5-10 à 1000 °C
SiC	3.2	20-30	420-450	4-6	10-40 à 1000 °C
Si_3N_4	3.18	8-20	304	3	9-30
Mullite	2.8	----------	145	6	5
B_4C	2.52	Knoop microhardness: 2800-3500	448	----------	92
BN	2.18	----------	----------	----------	----------
Graphite	2.2	35-85	1.5-35	0.1-20	1-500

APPENDIX III

DETERMINATION OF HEAT TRANSFER COEFFICIENTS

Heat transfer coefficient by forced convection (Poirier D. R. and Poirier E. J., 1991)

$$h_c = \frac{N_u \cdot K_{aire}}{L} \tag{III.1}$$

Nusselt number is given through the following equation:

$$N_{uL} = 0.664 \cdot R_{eL}^{1/2} \cdot Pr^{1/3} \tag{III.2}$$

Reynolds number for laminar flow is given through the following equation:

$$R_{eL} = \frac{L \cdot V \cdot \rho_{aire}}{\mu} \tag{III.3}$$

Where:

K_{aire} : air thermal conductivity, w/m· ºC; L : thickness, m; V : air velocity;

μ : air viscosity, kg/m·s; ρ_{aire} : air density, kg/m^3; Pr : Prandtl number.

Heat transfer coefficient by radiation (Poirier D. R. and Poirier E. J., 1991)

$$h_r = F \cdot \sigma \cdot \left(T^2 - T_{air}^2 \right) \cdot \left(T - T_{air} \right) \tag{III.4}$$

Where:

F : emissivity function ε (ε = F = 0.09 – aluminum; F = 0.28 - steel);

σ : Stefan-Boltzman constant, $5.67 \cdot 10^{-8}$ W · m^{-2} · k^{-4}.

APPENDIX IV

CONSTANT TIME INCREMENT

Figure III.1 shows the variation in the particle volume fraction (fv) on the outer casting surface as a function of Δt. In this figure, the variation of fv decreases and tends to reach a constant value with decreasing Δt. According to Fig. IV.1, the decrease in Δt below 0.005s for an average time of cooling of 0.4s will not change significantly the particles' volume fraction on the outer casting surface. The reduction in Δt, while using it as a constant value, reduces the gap between the last variation of the temperature above the liquidus and the liquidus which increase the time of particles displacement, improves the homogeneity of their distribution, and reduces the difference between the theoretical and experimental results on the outer casting surface (Figs. IV.2, IV.3, IV.4, IV.5).

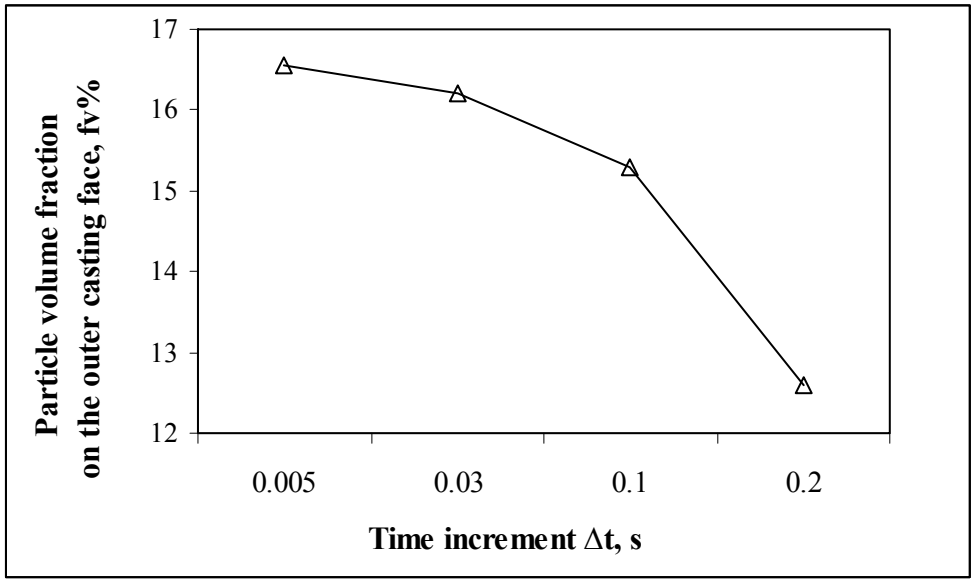

Figure IV. 1 Variation of the particles' volume fraction as a function of time increment (T_{metal} = 953 K, T_{mold} = 623 K).

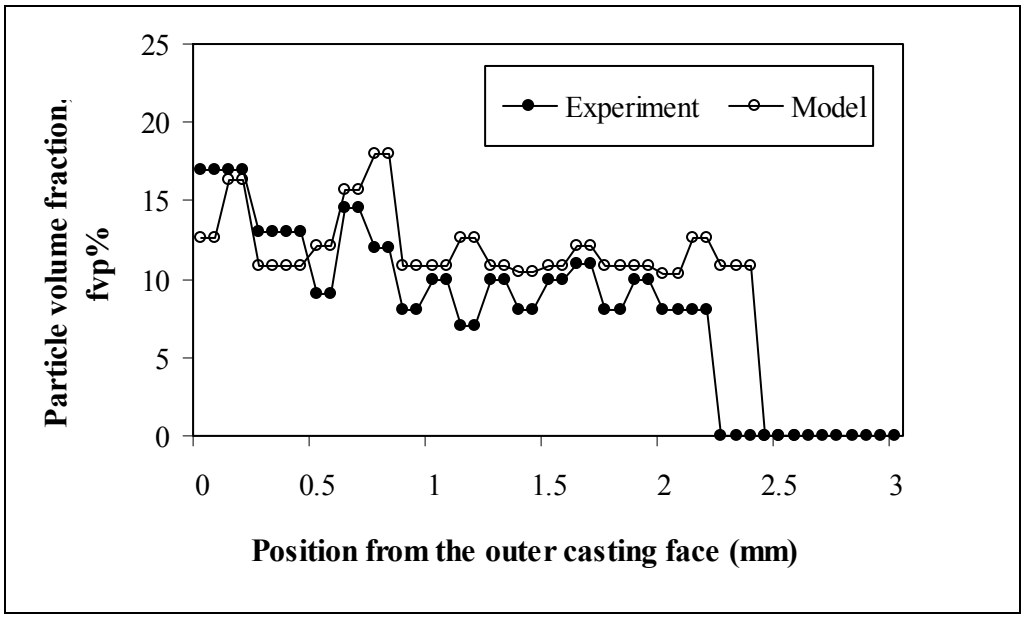

Figure IV. 2 Particle volume fraction variation for a time increment $\Delta t = 0.2$ s ($T_{metal} = 953$ K, $T_{mold} = 623$ K).

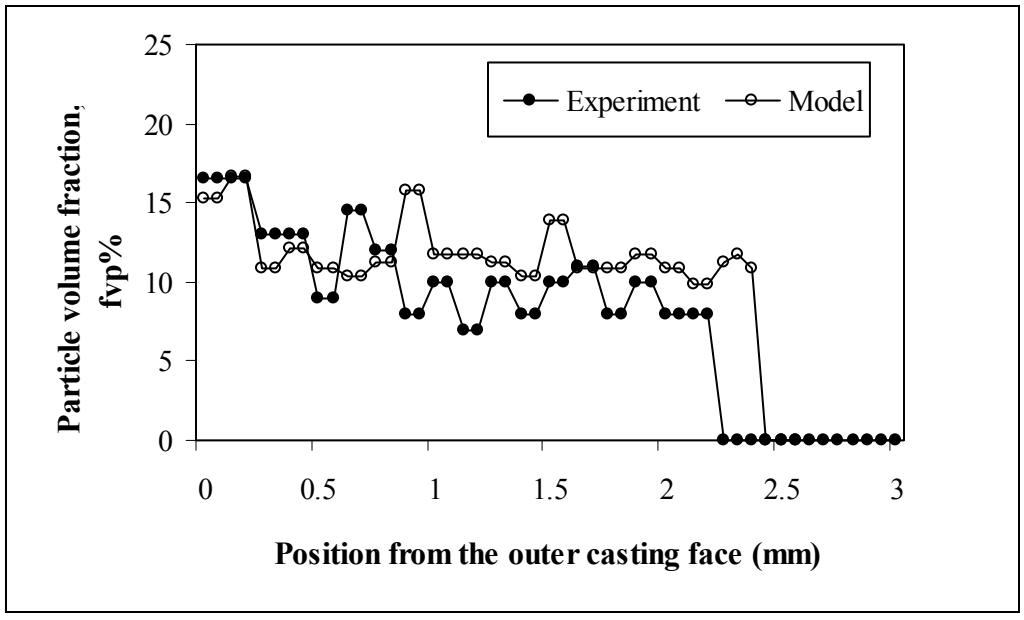

Figure IV. 3 Particle volume fraction variation for a time increment $\Delta t = 0.1$ s ($T_{metal} = 953$ K, $T_{mold} = 623$ K).

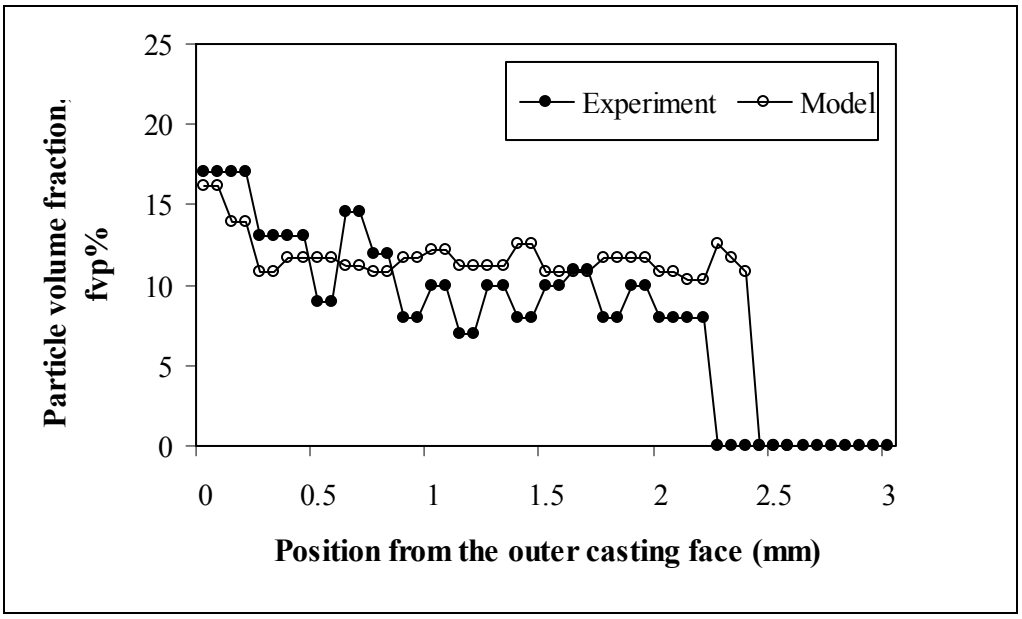

Figure IV. 4 Particle volume fraction variation for a time increment $\Delta t = 0.03$ s ($T_{metal} = 953$ K, $T_{mold} = 623$ K).

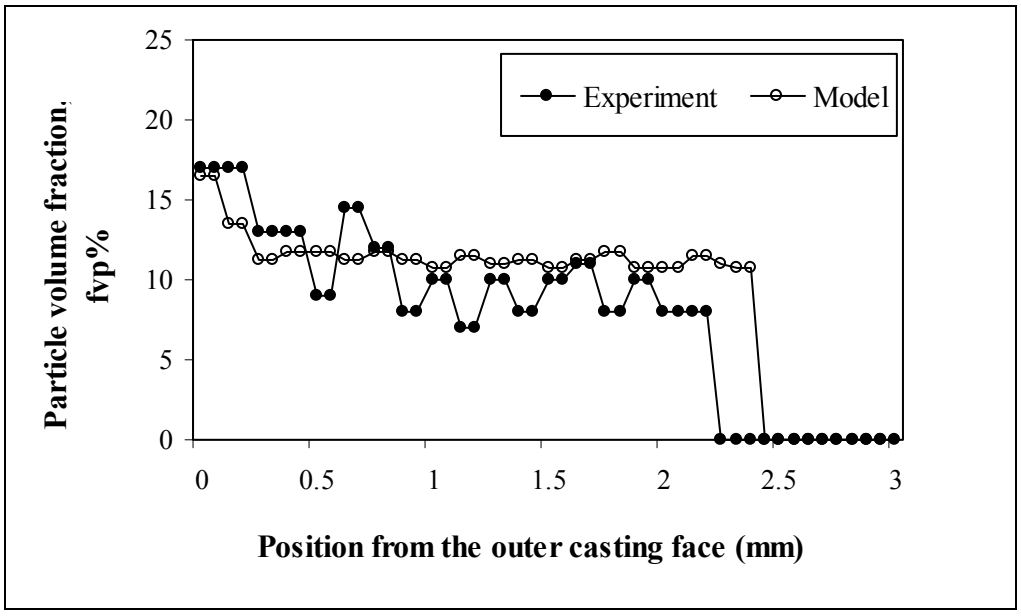

Figure IV. 5 Particle volume fraction variation for a time increment $\Delta t = 0.005$ s ($T_{metal} = 953$ K, $T_{mold} = 623$ K).

BIBLIOGRAPHY

Ares, A.E., Gassa, L.M., Gueijman, S.F., Schvezov, C.E., 2007. Correlation between parameters, structures, dendritic spacing and corrosion behaviour of Zn-Al alloys with columnar to equiaxed transition. Journal of Crystal Growth. vol. 310, p. 1355-1361.

Ares, E.E., Schvezov, C.E., 2007. Influence of solidification thermal parameters on the columnar-to-equiaxed transition of aluminum-zinc and zinc-aluminum alloys. Metallurgical and Materials Transactions. vol. 38A, p. 1485-1499.

ASM, handbook. 1988. *Casting*, vol. 15.

ASM, Handbook. 1973. *Metallography, Structure and Phase Diagrams*, vol. 8.

ASM. Handbook. 1979. *Properties and Selection: Nonferrous Alloys and Pure Metals*, vol.2.

Bonollo F., Moret A., Gallo S. et Mus C. 2004. Cylinder liners in aluminium matrix composite by centrifugal casting. Metallurgia Italiana, vol. 96, p. 49-55.

Britnell D. J. et Neailey K. 2003. Macrosegregation in thin walled castings produced via the direct squeeze casting process. Journal of Materials Processing Technology, vol. 138, p. 306-310.

Candan E. 2002. Effect of alloying elements to aluminium on the wettability of AL/SiC system. Turkish Journal of Engineering and Environmental Sciences. vol. 26, p. 1-5.

Çay, S, F., Kurnaz, C., 2005. Hot tensile and fatigue behaviour of zinc–aluminum alloys produced by gravity and squeeze casting. Materials and design. vol. 26, p. 479–485.

Chakrabarti A. K. 1996. Centrifugally cast ZA alloys. Foundry Management & Technology, vol. 124, p. 77-79.

Chen G., Tong M., et Zhu Z. 1999. Study on the macrosegregation of aluminum in centrifugal-cast ZA27 alloy. Materials Science and Engineering: Structural Materials: Properties, Microstructure and Processing, vol. A265, p. 306-309.

Chen W., Wang Q., Zhai C., Ma C., Zhu Y., He W. et Ding W. 2001. Microstructure and properties of in-situ Zn-Al-Si surface composites prepared by centrifugal casting. Zhongguo Youse Jinshu Xuebao/Chinese Journal of Nonferrous Metals, vol. 11, p. 416-423.

Cornie, J., Moon H. K. et Flemings M.C. 1990. A Review of Semi-Solid Slurry Processing of A1 Matrix Composites. *Proceedings of an ASM International Conference on Fabrication of Particulates Reinforced Metal Composites*, p. 63-78.

Epanchistov, O. G. 1972. Structure and properties of metals solidified under high pressure. Russian Casting prod, p. 34-37.

Fluent 6.2 documentation, L:/fluent.inc/help/index.htm

Forster M. F., Hamilton R. W., Dashwood R. J. et Lee P. D. 2003. Centrifugal casting of aluminium containing in situ formed TiB. Materials Science and Technology. vol. 19, p. 1215-1219.

Gao J. W. et Wang C. Y. 2000. Modeling the solidification of functionally graded materials by centrifugal casting. Journal of Materials Science and Engineering, vol.292, n 2, p. 207-215.

Garcia, A., Prates, M., 1978. Mathematical model for the unidirectional solidification of metals-1.Cooled molds. Metallurgical Transaction B. vol. 9B, p. 449-57.

Gomes, J. R.., Miranda, A. S., Rocha, L. A. et Silva, R. F. 2002. Effect of functionally graded properties on the tribological behaviour of aluminium-matrix composites. Key Engineering Materials, vol. 230-232, p. 271-274.

Grabowski A., Nowak M. et Sleziona J. 2005. Optical and conductive properties of AlSi-alloy/SiC composites: Application in modelling CO2 laser processing of composites. Optics and Lasers in Engineering. vol. 43, p. 233-246.

Hallam C. P. et Griffiths W. D. 2001. A model of the interfacial heat-transfer coefficient fort he aluminum gravity die-casting process. Metallurgical and Materials Transaction. vol. 35B, p. 721-733.

Halvaee A. et Talebi A. 2001. Effect of process variables on microstructure and segregation in centrifugal casting of C9200 alloy. Journal of Materials Processing Technology. vol. 118, p.123-127.

Hearn D. 2002. *Moulage par centrifugation*. Technique de l'Ingénieur AM 5210.

Ilegbusi, J. S. O. J. 1988. The engulfment of particles by an electromagnetically stirred melt. J Colloid and Interface Science, vol. 125 (2), p. 567-574.

Jung J. et Kang S. 2004. Advances in manufacturing boron carbide-aluminum composites. Journal of the American Ceramic Society, vol. 87, p. 47-54,

Kang C. G., Rohatgi P. K., Narendranath C. S. et Cole G. S. 1994. Solidification analysis on centrifugal casting of metal matrix composites containing graphite particles, ISIJ International. vol. 34, p. 247-254.

Kaptay G. 1996. Interfacial phenomena during melt processing of ceramic particle-reinforced metal matrix composites. Part I. Introduction (incorporation) of solid particles into melts. Proceedings of the 1995 2nd International Conference on Solidification and Gravity, Apr 25-28 1995. Materials Science Forum, vol. 215-216, p. 459-466.

Kirkwood, D.H., 1985. A simple model for dendrite arm coarsening during solidification. Material Science and Engineering. vol. 73, p. L1-4.

Kobashi M., Choh T., et Horibe Y. 1990. Effect of alloying elements on ZrC particulate dispersion in liquid aluminum. Nippon Kinzoku Gakkaishi/Journal of the Japan Institute of Metals, vol. 54, p. 933-940.

Lajoye L. et Suéry M. 1988. « Modelling of particle segregation during centrifugal casting of Al-matrix composites ». In *Proceedings of the International Symposium on Advances in Cast Reinforced Metal Composites.* Sep 26-30, Chicago, IL, USA, p. 15-20.

Lloyd D. J. 1989. Solidification microstructure of particulate reinforced aluminium/SiC composites. Composites Science and Technology, vol. 35, p. 159-179.

Liu Q., Jiao Y., Yang Y. et Hu Z. 1994. Theoretical analysis of particle distribution in gradient composite by centrifugal casting. Acta Metallurgica Sinica (English Edition), Series A: Physical Metallurgy & Materials Science, v 7, n 2, Sept, p. 107-113.

Ludmil B. D. et Jerzy. S. 2000. « A new model of solid particle segregation during centrifugal casting ». *Proceedings of a Symposium on State of the Art in Cast Metal Matrix Composites in the Next Millenium*. p. 23-44.

Ma, Y., Hao, Y., Yan, F-Y., Liu, H-J., 2004. « Microstructure analysis of ZA alloy rod directionally solidified by heated mold continuous casting ». *Proceedings of EPD Congress*, Charlotte, NC, United states, p. 261-268.

Maeng, D. Y., Lee J. H., Won C. W., Cho S. S., et Chun B. S. 2000. Effects of processing parameters on the microstructure and mechanical properties of modified B390 alloy in direct squeeze casting. Journal of Materials Processing Technology, vol. 105, p. 196-203.

Villar N., Masounave J. 1996. *Élaboration des composites à particules*. Technique de l'ingénieur, vol. M2448, p. 1-17.

Miliaev B. M. 1994. Détermination de la vitesse angulaire pendant la centrifugation verticale. Russie, p. 33-35.

Nadella, R., Eskin, D.G., Du, Q., Katgerman, L., 2008. Macrosegregation in direct-chill casting of aluminum alloys. Progress in Materials Science. vol. 53, p. 421–480.

Osorio, W.R., Garcia, A., 2001. Modeling dendritic structure and mechanical properties of Zn-Al alloys as a function of solidification conditions. Materials Science and Engineering. vol. A325, p. 103-111.

Panda E., Mazumdar D. et Mehrotra S. P. 2006. Mathematical modeling of particle segregation during centrifugal casting of metal matrix composites. Metallurgical and Materials Transactions A: Physical Metallurgy and Materials Science, vol. 37, p. 1675-1687.

Perrier, S. J. 2004. *Moulage des alliages d'aluminium.* Technique de l'ingénieur. vol. M3637, p. 17-21.

Poirier, D.R., Poirier, E.J., 1991. *Heat Transfer Fundamentals for Metal Casting*. TMS publication, Warrendale, PA, p. 19-43.

Poolthong N., Qui P., Nomura H., 2003. Primary particle movement and change of property of cast iron by centrifugal effect in semi-solid processing. Science and Technology of Advanced Materials. vol. 4, p. 481–489.

Qin X. H., Han W. X., Fan C. G., Rong L. J. et Li Y. Y. 2002. Research on distribution of SiC particles in aluminum-alloy matrix functionally graded composite tube manufactured by centrifugal casting. Journal of Materials Science Letters, vol. 21, n 8, p. 665-667.

Quaresma, J.M.V., Santos, C.A., Garcia, A., 2000. Correlation between unsteady-state solidification conditions, dendrite spacing, and mechanical properties of Al-Cu alloys. Metallurgical and Materials Transactions A. vol. 31A, p. 3167-3178.

Qudong W., Yongjun C., Wenzhou C., Yinhong W., Chunquan Z. et Wenjiang D. 2005. Centrifugally cast Zn-27Al-xMg-ySi alloys and their in situ (Mg2Si/ZA27 composites. Materials Science and Engineering A, vol. 394, p. 425-434.

Raju P S. S., Mehrotra S. P. 2000. Mathematical modeling of centrifugal casting of metal matrix composites., Materials Transactions, JIM. vol. 41, p. 1626-1635.

Rodriguez-Castro R. et Kelestemur M. H. 2002. Processing and microstructural characterization of functionally gradient Al A359/SiCp composite. Journal of Materials Science, vol. 37, p. 1813-1821.

Rohatgi, R. A. P. K. 1988. *Transfer of particles and fibres from gas to liquid during solidification processing of composites,* in ASM international, W. Univ. of Wisconsin-Milwaukee, USA, Ed., Sep 26-30 ed. Milwaukee, p. 61-66.

Scheed L., Pomie L. et Masounave J. 1997. Influence of particulate size on wear behaviour of aluminum metal matrix composite reinforced by silicon carbide particulates for

different sliding speeds. Intérêts technologiques et marchés potentiels des composites à matrice métallique. Paris. P. 162-169.

Stefanescu D. M., Moitra A., Kacar A. S. et Dhindaw B. K. 1990. Influence of buoyant forces and volume fraction of particles on the particle pushing/entrapment transition during directional solidification of Al/SiC and Al/graphite composites. Metallurgical Transactions A (Physical Metallurgy and Materials Science). vol. 21A, p. 231-239.

Velhinho A., Sequeira P. D., Braz Fernandes F., Botas J D. et Rocha L A. 2003. « Al/SiCp functionally graded metal-matrix composites produced by centrifugal casting: Effect of particle grain size on reinforcement distribution ». In *Proceedings of the Seventh International Symposium on Functionally Graded Materials.* Oct 15-18, Beijing, China, p. 257-262.

wang Z. w. N. et Weatherly G. C. 1990. « Aging charcteristics of SiC (particulate)/Al (A356) metal matrix composite ». In *Fabrication of particulates reinforced metal composites*, F. G. Hamel, Ed. Montréal, Québec, Canada, p. 145-152.

Watanabe Y., Yamanaka N. et Fukui Y. 1998. Control of composition gradient in a metal-ceramic functionally graded material manufactured by the centrifugal method. Composites Part A. (Applied Science and Manufacturing), vol. 29A, p. 595-601.

Yang, L. J. 2003. The effect of casting temperature on the properties of squeeze cast aluminium and zinc alloys. Journal of Materials Processing Technology, vol. 140, p. 391-396.

Zhang J., Wang Y. Q., Zhou B. L. et Wu X. Q. 1998. Functionally graded Al/Mg2Si in-situ composites, prepared by centrifugal casting. Journal of Materials Science Letters, vol. 17, n. 19, p. 1677-1679.

Zhang J., Fan Z., Wang Y. et Zhou B. 1999. Microstructural refinement in Al-Mg_2Si in situ composites. Journal of Materials Science Letters, vol. 18, p. 783-784.

Zhu Y. H., Lee W. B. et To S. 2003. Tensile deformation-induced phase transformation in cast Zn-Al-based alloy (ZnAl7Cu3). Materials Research Bulletin, vol. 38, p. 1851-1858.

Zuehlke M. W. H. B.2001. The hows and whys of centrifugal casting, p. 775-794.